Optical Parametric Oscillator based real-time trace gas analysis for bio-medical applications

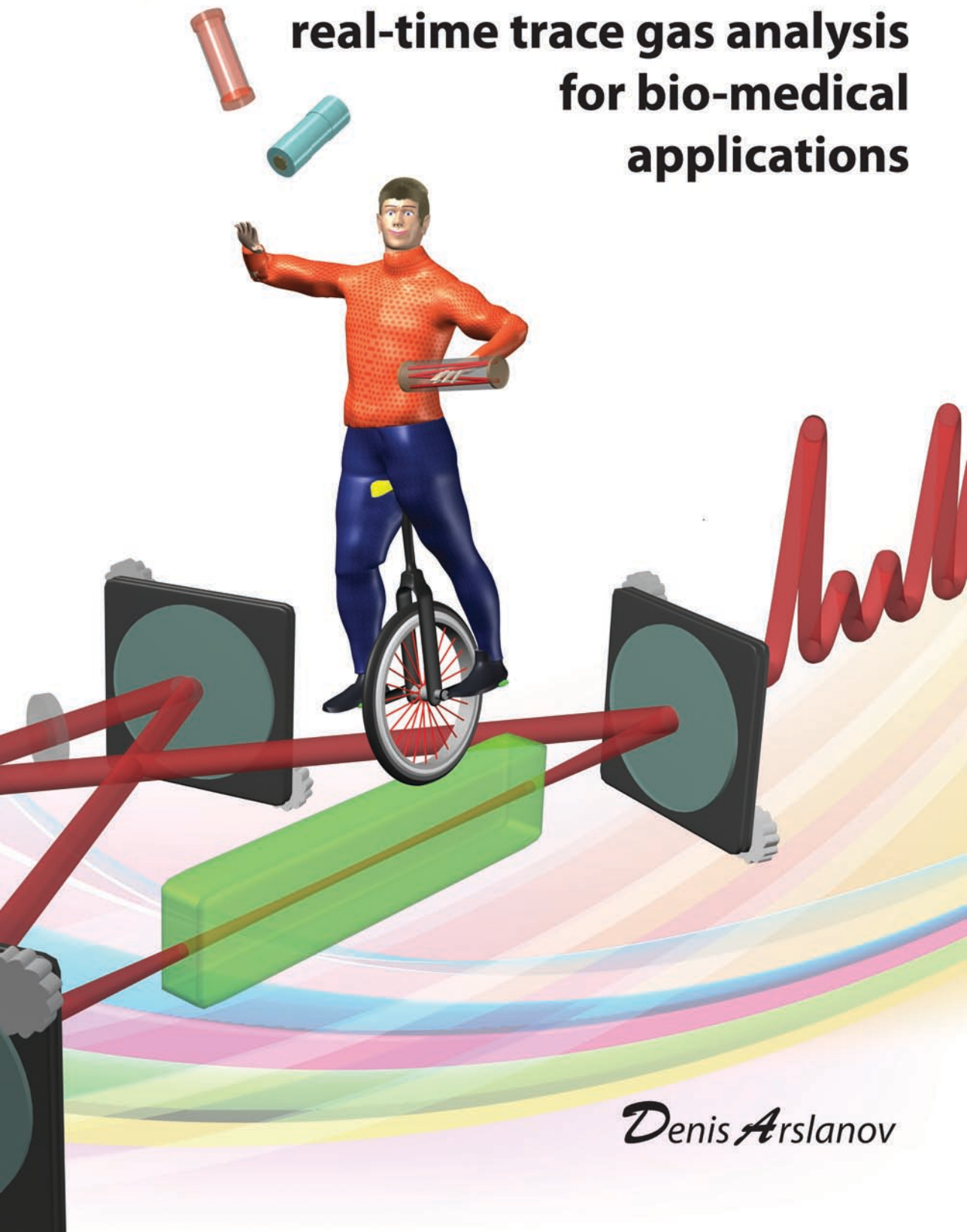

Denis Arslanov

Optical Parametric Oscillator based real-time trace gas analysis for bio-medical applications

The work described in this thesis was partly made possible by The Netherlands Organisation for Scientific Research NWO, the Dutch Technology Foundation STW and the European Commission under the programmes FP6-NESTA-0025042 'the Optical Nose' and the IOP Photonic Devices project PD-55

Optical Parametric Oscillator based real-time trace gas analysis for bio-medical applications

Proefschrift

ter verkrijging van de graad van doctor
aan de Radboud Universiteit Nijmegen
op gezag van de rector magnificus prof. mr. S.C.J.J. Kortmann,
volgens besluit van het college van decanen
in het openbaar te verdedigen op donderdag 15 november 2012
om 12.00 uur precies

door

Denis Arslanov

geboren op 29 december 1984
te Nizhnevartovsk (Rusland)

Promotor:	Prof. dr. D. H. Parker
Copromotoren:	Dr. F. J. M. Harren
	Dr. S. M. Cristescu
Manuscriptcommissie:	Prof. dr. W. L. Meerts (voorzitter)
	Prof. dr. K.-J. Boller (Universiteit Twente)
	Prof. dr. M. Ebahim-Zadeh (ICFO- Institute of Photonic Sciences, Barcelona, Spain)

Optical Parametric Oscillator based real-time trace gas analysis for bio-medical applications

Doctoral Thesis

to obtain the degree of doctor
from Radboud University Nijmegen
on the authority of the Rector Magnificus prof. dr. S.C.J.J. Kortmann,
according to the decision of the Council of Deans
to be defended in public on Thursday, November 15, 2012
at 12.00 hours

by

Denis Arslanov

Born on December 29, 1984
in Nizhnevartovsk (Russia)

Supervisor:	Prof. dr. D. H. Parker
Co-supervisors:	Dr. F. J. M. Harren
	Dr. S. M. Cristescu
Doctoral Thesis Committee:	Prof. dr. W. L. Meerts (chairman)
	Prof. dr. K.-J. Boller (University of Twente, Enschede, the Netherlands)
	Prof. dr. M. Ebahim-Zadeh (ICFO- Institute of Photonic Sciences, Barcelona, Spain)

"Realists do not fear the results of their study."
Fyodor Dostoevsky

Preaface

It has been a few weeks already since I finished writing the manuscript of my doctoral thesis. Now it is a good time to accomplish a final impulse- to acknowledge the people who have affected or influenced my scientific and private life during the last four years. Honestly saying, as an experimental physicist, I would rather prefer to spend more time in the lab doing real experiments than to describe everything I did on a paper. However, the alluring final aim is to be able to explain to everybody that what you are actually doing is challenging, but exciting and useful for the future. I always liked to be a great listener who still has a strong point, and, if necessary, to be able to convince someone to my side. Thanks to Rob Kieboom who taught me the Belbin's model during "The Masterclass Photonic Devices Entrepreneurship" courses organized by IOP Photonic Devices. Shortly after the first meeting he recognized the 'monitor' personality in me. That was actually confirmed later as the result of the test. I do not know whether this is good or bad. But at least his explanation fits with my understanding of the world. Moreover, to know something more is never a bad idea. It will be always beneficial to understand better who you are, what your strong points are and who your colleagues are. Shortly after, I examined my colleagues with the personality test too. That was really exciting to anticipate the results of the tests with my expectations. Thanks a lot to my daily supervisor Frans Harren. After having a great pleasure to work with him for a period of four years I can declare- he is the great boss. He always knows how to distribute the tasks between the members of the group. In additioin, he is always friendly and helpful. I appreciate a lot our work together.

Although we are a very international group, with people from all over the world (for a long time Frans Harren was the only one Dutch in the group), I could proudly say that we created a very cohesive and friendly working environment. One can gain so much useful information from others. It concerns mainly traditions, culture and food. Thanks to Zhichao Chen for the invitation to visit the real Chinese dinner with fried cucumbers, a dish made of mushrooms 'the black wood ear', chicken with potatoes braised in coca-cola and, of course, tea. Thanks for the Indian food to Ashim Saha, Gautam Sarma, Chandan Bishwakarma and Devasena Samudrala. Very special thanks to Julian Mandon

for sharing with me a piece of French cuisine. So many delicious French deserts I prepared during this time. Thanks for nice Brazilian food from Maria-Priscila de Castro. Of course a lot of different foods that has been eaten during our department's cultural evenings. Thanks for sharing with me the photography hobby to Gautam Sarma, Chung-Hsin Yang and Chandan Bishwakarma. Very special thanks to our 'marine admiral' Cor Sikkens for getting me inspired about sailing. And of course thanks to all the members of numerous department's sailing trips. Thanks for introducing me to squash to Marius Spunei and his wife Diana, Simona Cristescu and Sacco te Lintel Hekkert, with whom I played a lot. Later, I had a pleasure to play intensively with Julien Mandon, for whom I already was as a trainer. The revenge came to me in the 'Petong' (originally from French 'jeu de boules') from the master of the game- Julian Mandon.

The next paragraph I would like to devote to the languages. I must say this is not my strongest point. Nevertheless, I always like to investigate something new. After I got closely acquitted with the Polish language, I was surprized by the similarities between both Russian and Polish languages. In other words, in my opinion, it is similar to the pair of Dutch and German. Both of them sound quite close (I mean no offence to anyone) to each other, however, often words have different meanings. At this point I would like to emphasize that Russian and Polish languages have different alphabets: Cyrillic and Latin-based, respectively; and still they are so close, amazingly. Of course I will always remember former member of the group Aleksandra Laska-Oberndorf for the very nice conversations not only about science. Dziękuję bardzo za przyjacielskie rozmowy, dużo śmiechu oraz za nauke polskiego (Thank you very much for friendly conversations, a lot of laughs and for the teaching of polish). On a later stage, Denys Marchenko, a new PhD in our group has joined our 'Slavic' club where we held plenty of pleasant conversations: everyone tried to speak in his own language: Russian, Ukrainian or Polish, and others tried to understand (it happened quite well). We also had a couple of Polish guests Michal and Silvia, who helped in learning new Polish words. German language: I like it for its clarity and precision. Although, I was learning German at school, I could not speak it fluently when I arrived to start my PhD, because of the lack of communication in it. Thanks to Raymund Centeno, master student and lately PhD student of our group, who has endured my German. Ich möchte in Zukunft auch weiterhin meine Zeit der deutschen Sprache widmen, um mich auf demselben Niveau wie mein Englisch ausdrücken zu können (In the future I would like to dedicate my time to the German language in order to express myself on the same level as my English). Thanks to Julien Mandon, PostDoc of our group, who taught me the basics of the French language- totally new language for me. Merci pour la persévérance dont tu as fait preuve, mais si séduisant soit le français, il me reste encore beaucoup d'efforts à faire pour en maîtriser toutes les subtilités (Thank you for the patience you have shown; however, so beautiful French language requires a lot of effort from me to master all details). And, of course, I cannot miss the Chinese language, a completely different language. I was interesting in learning

it as well. Thanks to Zhichao Chen, Fuchun Liu, Bin Yan and Yuwei Jin. 中文是一很博大精深的言，我我最大的努力去好它。 (Zhōngwén shì yī mén hěn bódàjīngshēn de yǔyán, wǒ jiāng jǐn wǒ zuìdà de nǔlì qù xuéhǎo tā (I promise, I will try my best. But Chinese language is so difficult)) Very big thanks for the opportunity to speak in Russian with all my Russian-speaking friends here in Nijmegen: Dmitry Malik, Aleksandrda Kalashnikova, Kostya Vidma, Alexey Kimel, Andrey Kirilyuk, Sergei Semin, Anna Shipulina, Mikhail Akhukov, Maya Melnik, Alex Melnik, Denys Marchenko, Ruslan Subkhangulov, Dmitro Afanasiev, Sergei Semenov, Ilya Razdolsky, Sergei Marinchyuk, Agata Rakzhewska, Jonas Sweep, Raymund Centeno (I wish you best in mastering the Russian language) Katya Sokolova and many more. Спасибо вам всем! Рад, что не даете забывать родной язык (Thanks a lot to all of you! Glad that you don't give me the chance to forget the mother tongue). Although, I spent four years in the Netherlands, it is a shame that it is so difficult for me to learn the Dutch language. First of all, it is quite comfortable to live in the Netherlands with just English. Everyone can speak or at least understand English (during the whole period I met just a very few people with whom I had to use some other languages to communicate). Secondly, the hospitality of Dutch people and wish to help you makes them shift to English when they hear how you try to create a Dutch sentence with a foreign accent. I met plenty of times these situations. Maar in ieder geval begrijp ik nu Nederlands, spreken is moeilijker (But at least I can understand Dutch. Speaking is a bit more difficult). I have not to forget the English language, the main language of communication at the University. I would say that on a daily basis English is not the most difficult one; however, it needs a regular improvement. Thanks to Ben Webster and Phil Brown for a bunch of pronunciation requests.

Coming back to the everyday life, It is not a secret how hard it is to find a proper apartment to rent in Nijmegen. My current place is 5-th during my four years of stay here in Nijmegen. And this is, perhaps, the worst thing about the city. At this point I would like to thank Elena Crespo for giving me the opportunity to sub-rent her apartment when I came to Nijmegen. To my fortune, she was at a business trip to USA for a period of three months. This was enough to get used to the life abroad and to find some other place to live. Very big thanks for the furniture to Aleksandra Laska-Oberndorf, that she gave me for the first days after I moved to my totally empty, next apartment. The everyday life in Nijmegen will not be complete without bicycles. I knew how to cycle before, but I did it very rarely. Now I can admit, that the bicycle commuting is very convenient, especially here in the Netherlands. Nowadays, I am not even 'going shopping', but 'cycling shopping'. However, there are enough days to hate bikes. It is tedious to cycle under the rain, against the strong wind or in the snow, however, the public transportation designed in not the best way and age-old traditions of cycling let you no choice. Moreover, this helped me to learn the bicycle from the inside (how to repair the bike). I even got inspired and learned unicycling. Fantastic feeling! I can claim that everyone could face such a temptation. The desire leads to the dreams implementation,

whether it is Rubik's cube solving or juggling.

Nevertheless, PhD is mostly about the Science. Very often PhD students play roles of motors for the Sciences. They drive the experiments in the labs. They are educated and experienced; in addition, they have a very great dream-goal of a doctorate degree. I thank Marius Spunei for showing me the basics of OPO operation. Very big and special thanks to Simona Cristescu. Without her it would be difficult to run bio-medical applications. This is so important for us, physicists, to connect our research interests with attractive applications. Thanks to all the members and guests of our Trace Gas Research Group: Frans Harren, Simona Cristescu, Stefan Persijn, Aleksandra Laska-Oberndorf, Elena Crespo, Marius Spunei, Julien Mandon, Denys Marchenko, Devasena Samudrala, Raymund Centeno, Yuwei Jin, Noortje Creemers, Anne Neerincx, Phil Brown, Anelot Schuring, Charlotte Vroomen, Koen Swinkels; Antonio Cellini (for the tips about Italy), Francesco Spinelli (I remember how we took the wrong part of the train which brought us from Roermond to Heerlen instead of Maastricht), Michal Nosek and Silvia (for exchanging of words in Polish and Russian), Zenya Yordanova, Johanna Leenders, Svetlana Rampon, Christian Hermans ('chocolate guy'), Marco Kai, Brian Farneti ('tomato guy'), Maria-Priscila de Castro (pleasant work together on the OPO project, squash); people from another group of the Molecular and Laser Physics department: David Parker, Konstantin Vidma, Chung-Hsin Yang, Zahid Farooq, Mehrnoosh Mirzaei, Zhichao Chen, Afric Meijer, Andre Eppink, Gautam Sarma, Ashim Saha, Chandan Bishwakarma, Alexander von Zastrow, Jolijn Onvlee, Raymond Rammeloo, Sjoerd Vogels, Bas van de Meerakker. Of course people from other departments: Leo Meerts, Wim van der Zande, Rienk Jongma, Szymon Smolarek, Frans Spiering, Frans Wijnen, Arjan Donkerbroek. And many more people. Of course, I cannot miss the Technicians: Cor Sikkens, Peter Claus, Leander Gerritsen, Ruurd Lof, Arjan van Vliet; and Secretaries: Magda Speijers, Erna Gouwens, Ine Meijer.

A couple of more important issues I still have to describe. The first one is about skiing- how can skiing turn your life into a completely new route? When I came to Europe I knew how to do cross-country (or nordic) skiing and ice skating, as they are very popular in Russia. However, I have never tried alpine skiing. In fact, it appeared to be so naturally easy to me, that I liked it. Annually, for a few years, I organized the skiing trips. The tour of this year (January 2012) has changed my life totally. I met my fiancée Katya Sokolova. Now, thinking back, I realized that we actually could have met much earlier. We were born about 4500 km apart, but studied at the same Lomonosov Moscow State University and, moreover, at the same Physics Faculty, however we both independently found jobs in different groups at the Radboud University and met each other after a couple of years being in Nimegen on a skiing trip in the French Alpes. Do I believe in a destiny after that? At the end I would like to conclude my acknowledgements with thanking my school number 13 of Nizhnevartovsk city and the Lomonosov Moscow State University for the education provided and my Family- my parents Arslanova Nina

and Arslanov Danis, my sisters: Arslanova Anna and Zakharova Dina with her husband Zakharov Aleksander and my niece Viktoria, my brother Arslanov Aleksander, my grandmother (father's line) Arslanova Gaysha, my aunt Arslanova Lilya with my cousin Guzel and my uncle Arslanov Rustam and my grandfather (mother's line) Mincer Febus, Thank you so much!

Finally, I would like to thank again all for their support!

Denis Arslanov
Nijmegen, September 2012.

Contents

Chapter 1

Introduction

1.1 Methods of trace gas detection

Nowadays, the detection of gaseous compounds at low concentration level has become an attractive and promising field of research with a wide variety of applications within physics [1–9], environmental studies [1, 9–13], medicine [6–8, 14–21] and biology [9, 13, 22–24]. Different concentration levels may be considered as trace concentrations; however, in this thesis mostly sub-ppmv ($1 : 10^6$, parts-per-million by volume) and even sub-ppbv ($1 : 10^9$, parts-per-billion by volume) levels will be discussed. In this field of research a large amount of clinical and scientific studies have been performed during the last two decades [1, 2, 9, 15, 17]. Superior advantages of trace gas detection as diagnostic or monitoring tool are: non invasivity, safety and ease of sample collection. Nevertheless, the spectroscopy of gaseous media needs to be better studied. At present, the fundamental problems of trace gas detectors remain in the detection sensitivity of some Volatile Organic Compounds (VOCs), due to interference with other gases or high chemical reactivity. Other problems concern selectivity are due to the lack of the precise databases of volatiles and preparation, and storage of samples due to high chemical reactivity of some of the components [15, 16, 21].

There is a wide diversity of methods for trace gas detection ranging from gas chromatography [25], mass spectrometry [25], the electronic nose [20, 26, 27], chemiluminescence [20, 28], to various laser-based techniques [1, 2, 9, 17, 29]. As many gases have strong fingerprint absorption in the mid-infrared wavelength region, it is advantageous to use laser absorption spectroscopy in compare with other spectroscopic methods, which serves as an excellent approach for the highly sensitive detection of the VOCs. In addition, each molecule has its own unique absorption spectrum which makes laser-based

absorption spectroscopy an excellent method for selective detection in complex gas mixtures [1, 2].

It is generally known that gas chromatography and mass spectrometry techniques proved themselves to be a good workhorse for detection of large molecules. However, the equipment is usually bulky and expensive [25]. Although cheap, electronic noses cannot reach a high sensitivity, are in general slow, and sometimes have issues with selectivity [30]. Laser-based detection techniques deal commonly with the only one or few molecules detection at a very sensitive level when using narrow linewidth coherent sources, or multiple molecules detection using broadband lasers. The latter, however, leads to a poorer sensitivity. Although, there are laser-based spectroscopic schemes that allow measuring several gaseous compounds simultaneously, they are often expensive [18] and require several laser sources [31], or have a relatively slow wavelength tuning scheme [32]. To overcome these issues we built trace gas detectors based on Optical Parametric Oscillators (OPOs) pumped by a fiber amplified, multi-sections distributed Bragg reflector (DBR) diode laser, incorporated within a variety spectroscopic methods. The two OPOs used in this thesis emit light in the wavelength range between 2.8 to 3.8 μm,where a large amount of molecular end groups containing carbon atoms have characteristic absorbing wavelengths [2]. Both OPO sources have a narrow linewidth (2 MHz and 50 MHz) and produce continuous wave output powers up to 1.2 W. One OPO is able to scan the output wavelength in a mode-hop-free operation mode with a speed of up to 5 kHz over a 0.5 cm^{-1} range (however, slower scanning rates will cover a wider wavelength range: e.g. at 1 kHz 3 cm^{-1}, and 5 cm^{-1} at 100 Hz [8]) and is used mostly for real-time and fast processes. The second source is somewhat slower (scan speed up to 10 Hz for about 0.5 cm^{-1}), but it is more stable and is suitable to carry out long-term (over days and weeks) measurements.

1.2 Optical Parametric Oscillator

Non-linear generation of light has found widespread use in the field of sensitive trace gas sensing, due to its ability to generate frequencies in the near and mid-infrared wavelength range, where most of the molecules have their strongest ro-vibrational transitions. Although, this happened 50 years after the first demonstration of the optical parametric oscillator developed by Joseph Giordmaine and Robert Miller at Bells lab [33]; nowadays, mid-infra-red singly-resonant Optical Parametric Oscillators (SROs) are considered to be the most useful configurations for such sensitive gas sensing due to their high power ($\sim$Watt level) and ease of tunability [2] (see Chapter 3).

When light propagates through a crystalline medium, its electro-magnetic field generates a dielectric polarization wave:

$$\mathbf{P} = \varepsilon_0 \chi \mathbf{E}, \tag{1.1}$$

where ε_0 is the optical dialectric constant and χ is the optical susceptibility. Here, only the electric polarization wave is taken into account, because it has a much stronger effect than the corresponding magnetic polarization wave due to the larger value of the electric susceptibility. At low light intensities the induced polarization wave will travel together with the electro-magnetic wave through the medium (i.e. the induced polarization depends linearly on the electric field) because $\chi^{(1)} >> \chi^{(2)} >> \chi^{(3)}$ ... etc. In the materials with second and/or higher orders of susceptibilities $\chi^{(2)}$, $\chi^{(3)}$ with a high enough light intensity the polarization wave depends on the electric field in a non-linear way:

$$P = \varepsilon_0(\chi^{(1)}E + \chi^{(2)}E^2 + \chi^{(3)}E^3 + ...) \tag{1.2}$$

Suppose that an electro-magnetic wave consists of two waves with frequencies ω_1 and ω_2:

$$E = E_1\cos(\omega_1 t) + E_2\cos(\omega_2 t), \tag{1.3}$$

The first nonlinear term of the Eq. 1.2 would be:

$$\begin{aligned} P^{(2)} =& \varepsilon_0\chi^{(2)}E^2 = \\ \frac{\varepsilon_0\chi^{(2)}}{2}\{&(E_1^2 + E_2^2) + E_1^2\cos(2\omega_1 t) + E_2^2\cos(2\omega_2 t) + \\ &2E_1E_2[\cos((\omega_1+\omega_2)t)] + \cos((\omega_1-\omega_2)t)\}, \end{aligned} \tag{1.4}$$

Therefore, it contains second harmonics components $2\omega_1$ and $2\omega_2$ and sum and difference frequencies $(\omega_1 \pm \omega_2)$. This gives rise to nonlinear optical effects, such as frequency doubling, difference and sum frequencies generation.

Within the OPO process the pump photon is split into two other photons with different energies, the signal and idler frequency. Historically, the photon with highest energy is called signal and other is termed idler: $\omega_{signal} < \omega_{idler}$. Energy conservation law specifies the exact wavelengths at which signal and idler photons will be generated:

$$\omega_{pump} = \omega_{signal} + \omega_{idler} \tag{1.5}$$

However, not all the possible combinations under Eq. 1.5 of signal and idler photons will be amplified during nonlinear conversion, but those for which phase matching condition is fulfilled along:

$$\mathbf{k_{pump}} = \mathbf{k_{signal}} + \mathbf{k_{idler}} \tag{1.6}$$

The Eq. 1.6 relates the wave vectors of the pump, signal and idler beams and adds an additional condition to the ω_{signal} and ω_{idler} (determined by Eq. 1.5) which will be constructively generated. Those waves at wavelengths which comply with both of the Eq. 1.5 and Eq. 1.6 interact constructively lengthwise in the crystal. This can only be achieved when a phase mismatch is equal to zero: $\Delta\mathbf{k} = \mathbf{k_{pump}} - \mathbf{k_{signal}} - \mathbf{k_{idler}} = 0$; in other words, along the whole length of the crystal the induced polarization wave and the electric field

will be in phase. The efficient transfer of energy will take place only when a constant phase relationship between interacting waves along the crystal is achieved.

However, when a small mismatch is introduced ($\Delta\mathbf{k} = \mathbf{k_{pump}} - \mathbf{k_{signal}} - \mathbf{k_{idler}} \neq 0$), the phase difference between the polarization wave and the electric field grows during propagation through the crystal, reaching a value of π after a certain distance, which is called a coherent length L_c. The coherence length L_c depends on the crystal properties and the combination of signal and idler waves for a given pump beam wavelength and the incident conditions. From this distance a destructive interference starts to play a role. All the power which was transferred from the pump beam to the signal and idler beams now is returning back resulting in a total output power after two coherence lengths $2\times L_c$ ($2\times L_c$=Λ- the period of the crystal for a certain pair of signal and idler wavelengths) to be nearly or equal to zero. In total, over a long distance inside the crystal constructive and destructive interferences change each other.

Nevertheless, any pair of signal and idler photons within the transparency range of the crystal for which energy conservation law is fulfilled can be amplified. High conversion efficiencies could be obtained even when the phase matching condition does not occur. The technique of quasi-phase matching (QPM) resets the phase difference every time it reaches π. Thus, the polarization wave P and the electric field E are again in phase. This prevents a destructive interference and produces comparable power output as for the birefringent phase matched crystal. In addition, QPM has a few advantages over birefringent phase matching: it allows conversion to any signal and idler within the transparency range of the crystal, which is not always achieved under pure phase matching; and the beams propagate collinearly through the whole length of the crystal, avoiding a spacial mismatch of the interacting beams as for non-collinear injection; therefore, longer crystals can be used with a greater total conversion efficiency. Although quasi-phase matching was known for a long time, it took almost 30 years to build the first continuous wave, quasi-phase matched OPO in 1996 [34].

One of the methods to obtain QPM is periodic poling of nonlinear crystal materials. The process involves a spatial modulation of the nonlinear parameters of the crystal, so that the sign of nonlinear susceptibilities changes every coherence length. This results in a change of a sign of the induced polarization wave which radiates the idler wave. The most common technique for periodic poling is a domain structure inversion. In some of the crystals with ferroelectric properties the process can be manufactured by applying a high electric fields to electrodes placed on the surface of the crystal with a periodicity of Λ. The permanent reverse in a domain orientation occurs.

Nowadays, periodically-poled crystals are widely used in cw OPOs. In particular, periodically-poled lithium niobate (PPLN) crystals with periods as small as a few micrometers up to hundreds of micrometers are the most common for the mid-IR OPOs. With the advent of high power tunable pump lasers with narrow linewidth OPO became a workhorse for sensitive chemical sensing in the last decade. A variety of applications

profits from the ability of OPOs to cover a very wide spectral region [2].

1.3 Laser-based absorption spectroscopy

The Beer-Lambert law relates the transmitted optical power through the medium $P(\lambda)$ with the initial power $P_0(\lambda)$ at a given wavelength λ:

$$P(\lambda) = P_0(\lambda) \cdot e^{-N \cdot \sigma(\lambda) \cdot L}, \tag{1.7}$$

where N is the number density of absorbing molecules, $\sigma(\lambda)$ is the absorption cross section of the molecule and L is the path length. The product of N and $\sigma(\lambda)$ is called absorption coefficient:

$$\alpha(\lambda) = N \cdot \sigma(\lambda). \tag{1.8}$$

A desired detection limit of 1 ppmv (corresponding to a molecular density of 2.7×10^{13}molecules/cm^3 at 1000 mbar) results in an absorption coefficient of $\alpha = 2.7 \times 10^{-5}$cm^{-1} for a typical absorption cross section $\sigma(\lambda) = 10^{-18}$cm^2. In accordance with Eq. 1.7 an attenuation of transmitted power $P(\lambda)$ to the incident power $P_0(\lambda)$ even at a path length of L=1 m is

$$\frac{P_0(\lambda) - P(\lambda)}{P_0(\lambda)} = 2.7 \times 10^{-3}. \tag{1.9}$$

Although, this relative difference could be detected by means of a straightforward power detection scheme, the direct absorption nowadays is rarely used for a sensitive gas sensing, where ppbv or even sub-ppbv concentration levels are realized. To improve the detection limit several adjustments of the system might be applied:

1. folding an optical path inside a compact multipass cell configuration a path length enhancement of up to hundreds of times can be achieved;

2. by means of Wavelength Modulation Spectroscopy (WMS) or Frequency Modulation Spectroscopy (FMS) the detection of the signal is transferred to higher frequencies where electronic noise levels are orders of magnitude lower;

3. various cavity enhanced optical configurations for a creation of an effective optical path length in the range of few km on a table top setup, by use of highly reflective mirrors;

4. photoacoustic detection of acoustic waves created by de-excitation of molecules excited by light resulting in a sample heating and a pressure increase.

1.4 The scope of this thesis

This thesis provides noteworthy links between physics, biology and medicine. The focus of this study is to develop trace gas methods based on a singly-resonant, high output, continuous wave Optical Parametric Oscillator, which is capable of sensitive detection of gases emitted by metabolic processes and disorders occurring in plants, animals or humans. Apart from a high sensitivity and a good selectivity the spectrometer should also incorporate the possibility to realize the detection of larger molecules, to perform real-time measurements, such as real-time human breath analysis, and to maintain stable output wavelength and power over days or weeks for long-term measurements.

The thesis is organized as follows: an introduction to bio-medical applications with laser-based absorption spectroscopy is described in Chapter 2. This chapter will describe the importance of the volatile organic compounds (VOCs) that indicate some metabolic processes or their disorders that occur in plants and animals and how can be they measured with the laser-based spectroscopic methods. The chapter ends with the advantages and drawbacks of the method.

Chapter 3 reviews the applications of cw OPOs for sensitive molecular gas sensing. This shows the potential of OPO based infrared spectroscopy for environmental and bio-medical applications. The chapter focuses mostly on mid-infrared cw singly resonant OPOs (SROs), nowadays considered as the most useful configuration for sensitive molecular detection. There are many possible detection schemes described that use laser spectroscopy, each with their own advantages or disadvantages.

After the introductory chapters our first experiment is shown in Chapter 4. The chapter is devoted to the spectrometer based on Optical Parametric Oscillator incorporated with Wavelength Modulation Spectroscopy. The detector shows the ability of rapid (100 THz/s) and broad (up to 5 cm^{-1}) mode-hop-free tuning. The setup was used to detect ethane (C_2H_6) at 2996.7 cm^{-1} with a detection limit of 0.8 ppbv recorded in 1.3 s. A comparison between results using 1^{st}, 2^{nd} and 4^{th} harmonic derivative signal from wavelength modulation is described. In addition, a broad continuous tunability was demonstrated covering 35 cm^{-1} while recording absorption features of ethane, methane and water. The last capability clearly shows the ability to multi-component detection of several gases, simultaneously, which is a key feature in the bio-medical trace gas detection field of research.

Chapter 5 deals with the OPO-based Off-Axis Integrated Cavity Output Spectroscopy for rapid chemical sensing. The same OPO as used in Chapter 4 was incorporated with Integrated Cavity Output Spectroscopy (ICOS) in its off-axis configuration (OA-ICOS). The technique takes the advantage of extremely large effective path length inside the optical cavity created by a pair of highly reflective mirrors. In comparison with the results from Chapter 4 the improvement of detection limit in 16 times (50 pptv in compare with 800 pptv) has been achieved moreover in a much shorter time: 0.25 s. This results in a

Noise Equivalent Absorption Sensitivity (NEAS) of 4.8×10^{-11} cm^{-1}Hz$^{-1/2}$. The setup was also used to measure methane (CH_4) and water concentrations in exhaled human breath, in real time.

In Chapter 6 experiments which started in Chapter 5 continued, but with a more pronounced direction towards real applications such as real-time exhaled human breath analysis. The concentration dynamics of ethane were followed during free exhalation in multiple breath samples for non-smoking and smoking subjects over tens of minutes. It showed real-time multicomponent gas detection of ethane (C_2H_6), methane (CH_4) and water, and combined fast detection with a wide spectral coverage, as well as sub-second detection of larger molecules such as acetone in exhaled breath. The experiments show an important step forward in real-time, multi-component breath analysis.

Experiments with another OPO configuration that was built to enhance long-term wavelength and power stability for biological applications is described in Chapter 7. The OPO was incorporated with photoacoustic spectroscopy to ensure high sensitivity with robustness. Hydrogen Cyanide (HCN) was chosen as measurement gas, because it represents an important indicator of some processes in plants, bacteria or humans. However, HCN has not been studied very well yet due to its toxicity, high volatility and chemical reactivity. Most of the research carried out on HCN was performed using other methods. Here, OPO based photoacoustic technique was used. During experiments several difficulties were met that have been solved gradually to ensure a long-term continuous operation of the set-up over a period of several weeks, achieving a detection limit of 0.4 ppbv of HCN at 3287.2 cm^{-1}. The detector was successfully tested for HCN (hydrogen cyanide) emission from clover leaves, apple seeds, exhaled human breath and pseudomonas bacteria.

References

[1] A. Kosterev, G. Wysocki, Y. Bakhirkin, S. So, R. Lewicki, M. Fraser, F. Tittel, and R. F. Curl, "Application of quantum cascade lasers to trace gas analysis," *Appl. Phys. B*, vol. 90, no. 2, pp. 165–176, 2008.

[2] D. D. Arslanov, M. Spunei, J. Mandon, S. M. Cristescu, S. T. Persijn, and F. J. M. Harren, "Continuous-wave optical parametric oscillator based infrared spectroscopy for sensitive molecular gas sensing," *Laser and Photonics Rev.*, vol. DOI 10.1002/lpor.201100036, pp. 1–19, 2012.

[3] Y. He and B. J. Orr, "Detection of trace gases by rapidly-swept continuous-wave cavity ringdown spectroscopy: pushing the limits of sensitivity," *Appl. Phys. B*, vol. 85, no. 2-3, pp. 355–36, 2006.

[4] B. J. Orr and Y. He, "Rapidly swept continuous-wave cavity-ringdown spectroscopy," *Chem. Phys. Lett.*, vol. 512, no. 1-3, pp. 1–20, 2011.

[5] I. Galli, S. Bartalini, S. Borri, P. Cancio, D. Mazzotti, P. De Natale, and G. Giusfredi, "Molecular Gas Sensing Below Parts Per Trillion: Radiocarbon-Dioxide Optical Detection," *Phys. Rev. Lett.*, vol. 107, no. 27, pp. 270802–1–4, 2011.

[6] F. Adler, M. J. Thorpe, K. C. Cossel, and J. Ye, "Cavity-enhanced direct frequency comb spectroscopy: Technology and applications," *Annu. Rev. Anal. Chem.*, vol. 3, pp. 175–205, 2010.

[7] D. D. Arslanov, K. Swinkels, S. M. Cristescu, and F. J. M. Harren, "Real-time, subsecond, multicomponent breath analysis by Optical Parametric Oscillator based Off-Axis Integrated Cavity Output Spectroscopy," *Opt. Express*, vol. 19, no. 24, pp. 24078–24089, 2011.

[8] D. D. Arslanov, S. M. Cristescu, and F. J. M. Harren, "Optical parametric oscillator based off-axis integrated cavity output spectroscopy for rapid chemical sensing," *Opt. Lett.*, vol. 35, no. 19, pp. 3300–3302, 2010.

[9] S. M. Cristescu, S. T. Persijn, S. T. L. Hekkert, and F. J. M. Harren, "Laser-based systems for trace gas detection in life sciences," *Appl. Phys. B*, vol. 92, no. 3, pp. 343–349, 2008.

[10] C. Stroud, S. Madronich, E. Atlas, B. Ridley, F. Flocke, A. Weinheimer, B. Talbot, A. Fried, B. Wert, R. Shetter, B. Lefer, M. Coffey, B. Heikes, and D. Blake, "Photochemistry in the arctic free troposphere: Nox budget and the role of odd nitrogen reservoir recycling," *Atmosph. Environ.*, vol. 37, no. 24, pp. 3351–3364, 2003.

[11] J. A. De Gouw, S. T. L. Hekkert, J. Mellqvist, C. Warneke, E. L. Atlas, F. C. Fehsenfeld, A. Fried, G. J. Frost, F. J. M. Harren, J. S. Holloway, B. Lefer, R. Lueb, J. F. Meagher, D. D. Parrish, M. Patel, L. Pope, D. Richter, C. Rivera, T. B. Ryerson, J. Samuelsson, J. Walega, R. A. Washenfelder, P. Weibring, and X. Zhu, "Airborne Measurements of Ethene from Industrial Sources Using Laser Photo-Acoustic Spectroscopy," *Environ. Sci. Technol.*, vol. 43, no. 7, pp. 2437–2442, 2009.

[12] A. Kosterev and F. Tittel, "Chemical sensors based on quantum cascade lasers," *IEEE J. Quantum Elect.*, vol. 38, no. 6, pp. 582–591, 2002.

[13] T. A. Dueck, R. de Visser, H. Poorter, S. Persijn, A. Gorissen, W. de Visser, A. Schapendonk, J. Verhagen, J. Snel, F. J. M. Harren, A. K. Y. Ngai, F. Verstappen, H. Bouwmeester, L. A. C. J. Voesenek, and A. van der Werf, "No evidence for substantial aerobic methane emission by terrestrial plants: a C-13-labelling approach," *New Phytol.*, vol. 175, no. 1, pp. 29–35, 2007.

[14] S. Kharitonov and P. Barnes, "Exhaled markers of pulmonary disease," *Am. J. Respir. Crit. Care Med.*, vol. 163, no. 7, pp. 1693–1722, 2001.

[15] T. H. Risby and S. F. Solga, "Current status of clinical breath analysis," *Appl. Phys. B*, vol. 85, no. 2-3, pp. 421–426, 2006.

[16] T. H. Risby and F. K. Tittel, "Current status of midinfrared quantum and interband cascade lasers for clinical breath analysis," *Opt. Eng.*, vol. 49, pp. 111123–1–14, 2010.

[17] C. Wang and P. Sahay, "Breath Analysis Using Laser Spectroscopic Techniques: Breath Biomarkers, Spectral Fingerprints, and Detection Limits," *Sensors*, vol. 9, no. 10, pp. 8230–8262, 2009.

[18] M. J. Thorpe, D. Balslev-Clausen, M. S. Kirchner, and J. Ye, "Cavity-enhanced optical frequency comb spectroscopy: application to human breath analysis," *Opt. Express*, vol. 16, no. 4, pp. 2387–2397, 2008.

[19] M. Gianella and M. W. Sigrist, "Infrared Spectroscopy on Smoke Produced by Cauterization of Animal Tissue," *Sensors*, vol. 10, no. 4, pp. 2694–2708, 2010.

[20] J. Mandon, M. Hogman, J. F. M. Merkus, J. van Amsterdam, F. J. M. Harren, and S. M. Cristescu, "Exhaled nitric oxide monitoring by quantum cascade laser: comparison with chemiluminescent and electrochemical sensors," *J. Biomed. Optics*, vol. 17, no. 1, 2012.

[21] W. Miekisch, J. Schubert, and G. Noeldge-Schomburg, "Diagnostic potential of breath analysis - focus on volatile organic compounds," *Clin. Chim. Acta*, vol. 347, no. 1-2, pp. 25–39, 2004.

[22] E. Crespo, H. de Ronde, S. Kuijper, A. Pol, A. H. J. Kolk, S. M. Cristescu, R. M. Anthony, and F. J. M. Harren, "Potential biomarkers for identification of mycobacterial cultures by proton transfer reaction mass spectrometry analysis," *Rapid Commun. Mass Spectrom.*, vol. 26, no. 6, pp. 679–685, 2012.

[23] L. A. J. Mur, J. Mandon, S. M. Cristescu, F. J. M. Harren, and E. Prats, "Methods of nitric oxide detection in plants: A commentary," *Plant Science*, vol. 18, 2011.

[24] S. M. Clarke, S. M. Cristescu, O. Miersch, F. J. M. Harren, C. Wasternack, and L. A. J. Mur, "Jasmonates act with salicylic acid to confer basal thermotolerance in Arabidopsis thaliana," *New Phytol.*, vol. 182, no. 1, pp. 175–187, 2009.

[25] B. Buszewski, M. Kesy, T. Ligor, and A. Amann, "Human exhaled air analytics: Biomarkers of diseases," *Biomed. Chromatogr.*, vol. 21, no. 6, pp. 553–566, 2007.

[26] V. H. Tran, H. P. Chan, M. Thurston, P. Jackson, C. Lewis, D. Yates, G. Bell, and P. S. Thomas, "Breath Analysis of Lung Cancer Patients Using an Electronic Nose Detection System," *IEEE Sens. J.*, vol. 10, no. 9, pp. 1514–1518, 2010.

[27] A. D. Wilson and M. Baietto, "Advances in Electronic-Nose Technologies Developed for Biomedical Applications," *Sensors*, vol. 11, no. 1, pp. 1105–1176, 2011.

[28] A. Artlich, B. Jonsson, M. Bhiladvala, P. Lonnqvist, and L. Gustafsson, "Single breath analysis of endogenous nitric oxide in the newborn," *Biol. Neonate*, vol. 79, no. 1, pp. 21–26, 2001.

[29] G. Berden and R. Engeln, *Cavity Ring-Down Spectroscopy: Technology and Applications*. Wiley, 2009.

[30] A. D. Wilson and M. Baietto, "Applications and Advances in Electronic-Nose Technologies," *Sensors*, vol. 9, no. 7, pp. 5099–5148, 2009.

[31] J. H. Shorter, D. D. Nelson, J. B. McManus, M. S. Zahniser, S. R. Sama, and D. K. Milton, "Clinical study of multiple breath biomarkers of asthma and COPD (NO, CO_2, CO and N_2O) by infrared laser spectroscopy," *J. Breath Res.*, vol. 5, no. 3, SI, pp. 037108–1–12, 2011.

[32] G. N. Rao and A. Karpf, "External cavity tunable quantum cascade lasers and their applications to trace gas monitoring," *Appl. Opt.*, vol. 50, no. 4, pp. A100–A115, 2011.

[33] J. A. Giordmaine and R. C. Miller, "Tunable coherent parametric oscillation in $LiNbO_3$ at optical frequencies," *Phys. Rev. Lett.*, vol. 14, no. 24, pp. 973–976, 1965.

[34] W. Bosenberg, A. Drobshoff, J. Alexander, L. Myers, and R. Byer, "Continuous-wave singly resonant optical parametric oscillator based on periodically poled $LiNbO_3$," *Opt. Lett.*, vol. 21, no. 10, pp. 713–715, 1996.

Chapter 2

Introduction to biomedical applications with laser spectroscopy

2.1 Introduction

In contrast with fundamental science for trace gas detection, where the main goal is to achieve the best sensitivity regardless price, size of required equipment, acquisition time spent, or amount of energy consumed, in field applications there are many more restrictions. The detector should be operable by a non-skilled personnel, a hand-held device is preferable, the price should be affordable in the case of mass production, dust and moisture protection level is needed for "field" measurements, the device should benefit from low power consumption, real-time or fast detection is needed often in applications, such as exhaled human breath analysis. However, for most of the applications the extremely low concentrations such as ppqv (parts-per quadrillion per volume, $1 : 10^{15}$) [1] and microsecond time scale [2] are not required [3]. There is no dispute, one can sacrifice sensitivity in favor of other criteria.

Another general complexity when working with real applications such as detection of volatile organic compounds (VOCs) from plants, insects, the environment, or for exhaled breath, is the interference between compounds. Water is the well known 'obstacle' in the field of trace gas detection: the water absorption spectrum in the infrared is very dense and, although, the absolute cross section values are usually much lower than the ones of the molecules of interest, the concentration of water in the gas sample is high [4].

One has to consider a typical concentration of water in air at the percentage level, and several percent in exhaled breath. In addition, even in regions where there is no direct interference with water absorption lines, there often exists an influence of water in terms of adding a non-linear background in the system. This happens, e.g., due to a shoulder of a strong water line far away. It is very important to consider also that water is a very sticky molecule: it impairs the response time of the detector while waiting for water removal from the system. One can also consider, for instance, the influence of carbon dioxide which typically presents in ambient air at the level of 390 ppmv [5] and at the level of 4-6 % in exhaled human breath [3]. Methane is present in ambient air at level of 1.7-1.9 ppmv [6].

2.2 Importance of trace gas detection for medicine and biology

When VOCs emissions from plants or animals are analyzed, one can extract some information on the presence of unique components or the change in the concentration level of some of the compounds due to biological processes or metabolic disorders. These components, called indicators, play a role in understanding the physiology of the biological species: plant-plant communication [7], plant-insect interaction [8], early stage disease diagnostics [3], etc.

Consider breath analysis as an example of such diagnostics. There are more than 1000 different gas compounds found in exhaled human breath. Any molecule with a high enough vapor pressure present in the blood can be transport into the respiratory system via alveolar-capillary junctions in the lungs or vice versa. The concept of gas exchange governs the ability of breath analysis to be a diagnostic tool [3, 9]. The origins of VOCs in blood, and therefore in breath, are from endogenous production, or due to exogenous sources such as digestion of food and beverages, via the skin, through inhalation; or produced by extraneous cells such as viruses, bacteria, fungi. Diseases and metabolic disorders can influence a human body in the production of some gas compounds that are either absent in a healthy body or present at different level of concentration. The production of new gas compounds can appear as a consequence of the presence of a viral, fungal or bacterial infection; however, in most cases the differentiation between healthy and diseased people is made by the concentration change of a gas or gas complex.

However, there are a number of known indicators which are related to certain diseases or metabolic disorders. For example, acetone (C_3H_6O) is related to lung cancer, diabetes, dietary fat losses, congestive heart failure and brain seizure; ethane (C_2H_6) is related to lipid peroxidation and oxidative stress; methane (CH_4) is associated with intestinal problems and colonic fermentation [9, 10]. However, the biochemistry of the formation process is not always understood. Moreover the differentiation between healthy and diseased states is impeded by additional factors such as age, gender, race, habits, and due

to historical reasons (where the person has been during last days, what kind of food was consumed and air inhaled).

The examples shown demonstrate clearly the importance of trace gas detection for Life Science applications in biology and medicine. Novel detection techniques may be incorporated in the analysis when it brings specific information about the process: detecting new compounds, assign other indicators, correlate gasses together as group to become a hallmark for a certain process; simplification of the detection by reducing, time, effort and cost. No doubt, real time trace gas detection will compete with conventional methods since the analysis can be done quickly and decisions can be made sooner.

2.3 Its potential for the future

Despite some drawbacks, laser-based absorption spectroscopy for trace gas detection is a fast developing field of research, due to the ease of sample collection, the simplicity of sample preparation, reproducibility, sensitivity, selectivity, and speed of measurements. In recent years, with the fast development of high power, narrow linewidth, widely tunable lasers over the complete infrared wavelength region, the sensitivity and selectivity of gas detection has improved the fast detection of complex gas mixtures. The diversity of the employed spectroscopic methods can satisfy the individual requirements for each application in Life Science. Miniaturization and integration of photonic elements onto a chip is underway and soon the generation of laser light and light via non-linear processes will be offered in hand-held devices.

References

[1] I. Galli, S. Bartalini, S. Borri, P. Cancio, D. Mazzotti, P. De Natale, and G. Giusfredi, "Molecular gas sensing below parts per trillion: Radiocarbon-dioxide optical detection," *Phys. Rev. Lett.*, vol. 107, pp. 270802–1–4, 2011.

[2] B. Bernhardt, A. Ozawa, P. Jacquet, M. Jacquey, Y. Kobayashi, T. Udem, R. Holzwarth, G. Guelachvili, T. W. Haensch, and N. Picque, "Cavity-enhanced dual-comb spectroscopy," *Nat. Photon.*, vol. 4, no. 1, pp. 55–57, 2010.

[3] T. H. Risby and F. K. Tittel, "Current status of midinfrared quantum and interband cascade lasers for clinical breath analysis," *Opt. Eng.*, vol. 49, pp. 111123–1–14, 2010.

[4] L. S. Rothman, I. E. Gordon, A. Barbe, D. C. Benner, P. F. Bernath, M. Birk, V. Boudon, L. R. Brown, A. Campargue, J.-P. Champion, K. Chance, L. H. Coudert, V. Dana, V. M. Devi, S. Fally, J.-M. Flaud, R. R. Gamache, A. Goldman, D. Jacquemart, I. Kleiner, N. Lacome, W. J. Lafferty, J.-Y. Mandin, S. T. Massie, S. N. Mikhailenko, C. E. Miller, N. Moazzen-Ahmadi, O. V. Naumenko, A. V. Nikitin, J. Orphal, V. I. Perevalov, A. Perrin, A. Predoi-Cross, C. P. Rinsland, M. Rotger, M. Simeckova, M. A. H. Smith, K. Sung, S. A. Tashkun, J. Tennyson, R. A. Toth, A. C. Vandaele, and J. V. Auwera, "The hitran 2008 molecular spectroscopic database," *J. Quantum Spectrosc. Radiat. Transf.*, vol. 110, pp. 533–572, 2009.

[5] http://www.esrl.noaa.gov/gmd/ccgg/trends/global.html.

[6] M. Rigby, R. G. Prinn, P. J. Fraser, P. G. Simmonds, R. L. Langenfelds, J. Huang, D. M. Cunnold, L. P. Steele, P. B. Krummel, R. F. Weiss, S. O'Doherty, P. K. Salameh, H. J. Wang, C. M. Harth, J. Muehle, and L. W. Porter, "Renewed growth of atmospheric methane," *Geophys. Res. Lett.*, vol. 35, no. 22, pp. L22805–1–6, 2008.

[7] I. Baldwin, R. Halitschke, A. Paschold, C. von Dahl, and C. Preston, "Volatile signaling in plant-plant interactions: "Talking trees" in the genomics era," *Science*, vol. 311, no. 5762, pp. 812–815, 2006.

[8] G. A. Howe and G. Jander, "Plant immunity to insect herbivores," *Annu. Rev. Plant Biol.*, vol. 59, pp. 41–66, 2008.

[9] C. Wang and P. Sahay, "Breath analysis using laser spectroscopic techniques: Breath biomarkers, spectral fingerprints, and detection limits," *Sensors*, vol. 9, no. 10, pp. 8230–8262, 2009.

[10] B. Buszewski, M. Kesy, T. Ligor, and A. Amann, "Human exhaled air analytics: Biomarkers of diseases," *Biomed. Chromatogr.*, vol. 21, no. 6, pp. 553–566, 2007.

Chapter 3

Continuous wave Optical Parametric Oscillator based infrared spectroscopy for sensitive molecular sensing

Abstract

Over the past 10 years, with the advent of new crystals designs and a new generation of pump lasers, continuous-wave (cw) optical parametric oscillators (OPOs) have developed into mature monochromatic light sources. Nowadays, cw OPOs can fulfil a wide variety of criteria for sensitive molecular gas sensing. It can access the mid-infrared wavelength region, where many molecules have their fundamental rotational-vibrational transitions, with high power. This high power combined with wide wavelength tuning and narrow linewidth creates excellent conditions for sensitive, high-resolution spectroscopy. OPOs combined with robust methods, such as photoacoustic spectroscopy and cavity-enhanced spectroscopy, are well suited for field measurements and remote-sensing applications. The wide tunability of cw OPOs allows detection of larger molecules with broad absorption band structures, and its fast scanning capabilities allow rapid detection of trace gases, the latter is a demand for life-science applications. After a short introduction about the

This work has been published in:
D. D. Arslanov, M. Spunei, J. Mandon, S. M. Cristescu, S. T. Persijn, and F. J. M. Harren, "Continuous-wave optical parametric oscillator based infrared spectroscopy for sensitive molecular gas sensing" Laser Photonics Rev., **DOI10.1002/lpor.201100036** 1–19 (2012).

physical principle of cw OPOs, with its most recent physical developments, this review focuses on sensitive molecular gas sensing with a variety of spectroscopic applications in atmospheric and life sciences.

3.1 Introduction

In 1965, five years after the demonstration of the first laser, Joseph Giordmaine and Bob Miller developed the optical parametric oscillator (OPO) at Bell Labs [1]. While lasers found almost directly widespread use in the field of gas sensing (see, e.g., [2, 3]), this only happened for OPOs thirty years later [4]. Its initial slow development was caused by the fact that OPOs were far from being a workhorse. Lack of proper nonlinear crystals with a sufficiently high damage threshold, the unavailability of good pump lasers, and the need for skilled operators restricted their usefulness in applications. The advent of new crystals like periodically poled lithium niobate (PPLN) and a new generation of (fiber) pump lasers have changed this situation. Nowadays, OPOs are commercially available from many suppliers covering the visible, near- and mid-infrared and (recently) part of the ultraviolet wavelength region, using the pulsed and continuous-wave (cw) regimes [5].

Here, we will mainly focus on mid-infrared cw singly resonant OPOs (SROs), nowadays considered as the most useful configuration for sensitive molecular detection. For chemical sensing there are many possible detection schemes that use laser spectroscopy, each with their own advantages or disadvantages. OPO-based gas spectroscopy relies on the use of cw and pulsed OPOs. OPOs have proven to be excellent sources for spectroscopy within Doppler-free spectroscopy that relies on the reliable tuning characteristics and narrow linewidth of OPOs [6–8]; Photoacoustic spectroscopy that utilizes the power of OPOs in the infrared [9–11]; Cavity ring- down spectroscopy that benefits from the narrow linewidth attainable by cw OPOs [12, 13], and frequency/wavelength modulation spectroscopy that profits from the ease of modulation for certain types of OPOs [14, 15]. In this work, a number of these schemes are demonstrated and evaluated, and applications in atmospheric, medical and life sciences are presented.

For trace-gas sensing, OPOs have to be developed in the mid-infrared wavelength region between 2.5 and 25 μm, as many molecules possess their unique vibrational transitions in this 'fingerprint' wavelength region (see Table 3.1 for the 2.5-5 μm region). This wavelength region is widely dominated by Fourier transform infrared spectrometry (FTIR) to uniquely identify molecular gases. The development of mid-infrared laser sources associated with the strong fundamental rovibrational molecular transitions present in this region has offered remarkable opportunities for highly sensitive detection of these molecules. Thus, by combining selectivity (unique identification) with sensitivity (by using sensitive spectroscopic methods) state-of-the-art trace detection of molecu-

Table 3.1: *Some molecular (end) groups and their characteristic absorbing wavelength regions in the 2.5-5 μm range (2000-4000 cm^{-1}).*

Molecular end group	Spectral range (cm^{-1})	Molecular end group	Spectral range (cm^{-1})
$>CH_2$/–CH_2	2960–2850	>P–H	2440–2350
–CHO	2900–2700	–POOH	2700-2560
>O–CH_3	2850–2810	–C≡C–	2260–2150
–O–CH_2–O	2790–2770	–C≡N	2260–2200
>N-CH_3	2820–2780	–N=C=O	2275–2250
–C≡CH	∼3300	–N_3	2160–2120
>C=CH_2	3095–3075	–N=C=N–	2155-2130
>C=C–H	3040–3010	>C=C=O	∼2150
–OH	3650–3590	–N=C=S	2140–1990
>NH/=NH	3500–3300	R–S–C=N	2175–2140
–S–H	2600–2550		

lar gases is achievable.

Many molecular gases are involved in chemical processes in industry or atmosphere, but also in biological processes, in agriculture, biology or medicine, and nowadays within security and public safety. There is an increasing demand for novel monitoring techniques to detect all kinds of molecular gas species. OPOs are provided with a relatively broad continuous tuning range when they are based on quasiphase-matched materials; since they combine this with high power levels (∼ 1W cw) and narrow linewidth, they represent an excellent source for sensitive spectroscopic gas analysis.

3.2 Physical basics of optical parametric oscillators

In an optical parametric process the pump photon (ω_p) is split into two parts, forming two new photons with different energies (Fig. 3.1). The generated photon with the highest energy is termed signal (ω_s), and the other photon is termed idler (ω_i). The energy conservation has to be considered for the generated pair of photons, but is not sufficient to determine which frequencies will be amplified. In addition to that, destructive interference between the photons needs prevention. This gives rise to a second restriction, the phasematching condition [16, 17]. In bulk crystals birefringence is used to offset the dispersion and it satisfies the phasematching condition for specific wavelength combinations. Altering the propagation direction in such crystals (angle tuning) changes the selected frequency combination. Changing the crystal temperature may also change the refractive indices n_{idler}, n_{signal} and n_{pump} resulting in temperature tuning.

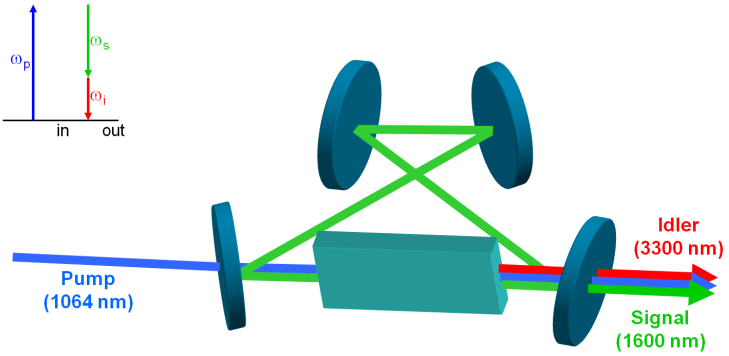

Figure 3.1: *Singly resonant optical parametric oscillator (SRO) configuration generating mid-infrared light. For this singly resonance case, all mirrors are highly reflective for the signal wavelength, while transparent for the pump and idler.*

Instead of trying to match the phase velocity of the pump laser and the parametrically generated signal and idler beams throughout the entire bulk crystal, an alternative way is quasiphase matching (QPM), which was devised independently by Armstrong et al. and Franken and Ward in 1962 and 1963, respectively [16, 17]. The invention of QPM reduces the effect of the destructive interference by resetting the phase difference between the polarization wave and the pump wave. This can be achieved by periodically inverting the generated polarization wave, which is done by domain inversion in the crystal, thereby changing the sign of the nonlinear coefficient [18]. The poling period of such a crystal can be made as small as a few micrometers and up to hundreds of micrometers. Although, QPM only partially compensates for the phase mismatch this does not mean that overall conversion efficiency will be low in QPM.With birefringent phase-matching, the idler, signal and pump waves will often have different paths inside the crystal, limiting the range in which the beams overlap. Within QPM the waves propagate collinearly, resulting in a maximum overlap between the waves. This means that very long crystals can be used with an effective interaction zone over their full length. Another advantage of QPM is that very high nonlinear coefficients can be used. With birefringent phase matching, the propagation direction through the crystal is determined by the angle required for phase matching. Generally, this means that the crystal direction with the highest nonlinear coefficient cannot be used. With QPM, this problem does not exist, resulting in the use of much higher nonlinear coefficients. Furthermore, with QPM it is also possible to use nonlinear crystals that are not birefringent but have a very high nonlinear coefficient, such as GaAs and ZnSe.

In 1965 the first birefringent phase-matched OPO was reported using a 5-mm long lithium niobate crystal [1]. Even though the principle of QPM was already known at

this time, it took almost 30 years before Bosenberg et al. [19] built the first continuous-wave, quasi phase matched, SRO in 1996, using a PPLN crystal with a single poling period. PPLN is a good material to use for quasiphase matching, due to its high nonlinear coefficient combined with a wide transparency range. The poled structure of PPLN can be engineered with a photolithographic mask, which makes it easy to produce a single crystal with several poling periods. Currently, crystals are available with as many as nine different poling periods. When such multiple-grating crystals are used, the operation wavelength range of an OPO can be significantly increased.

Even though PPLN has many advantages, it also exhibits several undesirable properties such as a weak photorefractive damage resistance. Due to high intensities photoexcited electrons generate a charge distribution, known as a spacecharge field that can cause damage of the crystal. In addition, the refractive index of the crystal changes in regions where the space-charge field is the strongest. Both can be prevented by using doped materials; nearly stoichiometric crystals doped with over 1.8 mol.% MgO showed no measurable photorefractive damage to intensities as much as 8MW/cm^2 at 532 nm [20]. Dopants like Mg, In or Zn increase the photoconductivity of the crystal and render advantages such as three orders of magnitude higher threshold damage and reduced lensing, resulting in better power and temperature stability, and room-temperature operation of the crystal. This last property extends the temperature tuning range within a single period considerably as compared to undoped PPLN [13]. Some of the limitations of PPLN can be overcome by the use of other kinds of ferroelectric materials, such as $LiTaO_3$, and $RbTiOAsO_4$, while orientation-patterned GaAs has recently gained a lot of interest [21].

With the advent of high-power tunable pump lasers for OPOs and the availability of better optical coatings the wavelength coverage of OPOs has extended considerably in the recent years. These aspects, together with lowering the oscillation threshold and continuous, mode-hop-free tuning, will be discussed in more detail.

3.3 Singly resonant OPOs

3.3.1 Efficient tuning of the cw OPO

Due to energy conservation, a widely tunable pump frequency will generate widely tunable signal and idler frequencies. With pump tuning, very wide idler tuning ranges can be obtained, because the well-developed tuning methods in pump sources can be transferred within an OPO to the idler frequency. Using this principle as one of the first, Klein and coworkers [22] developed a single-frequency SRO, directly pumped by a tunable InGaAs diode laser. Tuning the pump output around 925 nm resulted in coarse tuning of the idler wavelengths from 2.03-2.29 μm; they achieved 56 GHz continuous pump tuning for the idler wave. Van Herpen et al. [23] combined wide pump tuning with a high power SRO. Here, tuning of the idler frequency was achieved by longitudinal mode-hop tuning of the

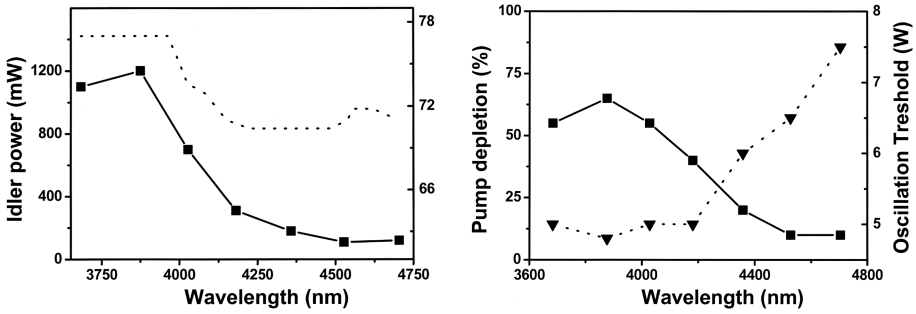

Figure 3.2: *OPO idler tuning with a multigrating crystal. The left panel shows the idler power (solid curve), which correlates strongly with PPLN transparency (dotted curve). The right panel shows the pump depletion (solid curve) and oscillation threshold (dotted curve) as function of the idler wavelength with 11W of pump power [26].*

pump source (free spectral range 100 MHz). In this way an idler frequency scan of 100-150 GHz could be obtained. Recent advances show that fiber lasers are very promising for wide pump tuning. Lindsay and coworkers [24] obtained 110 GHz continuous tuning using a fiber-amplified DBR laser. In addition, using a fiber-based source Henderson and Stafford [25] achieved 60 GHz of continuous mode-hop-free tuning by applying a voltage to a piezoelectric transducer attached to the fiber.

3.3.2 Widening the wavelength coverage

Most continuous-wave SROs are based on PPLN. PPLN shows stronger absorptions at wavelengths longer than 4 μm and therefore powerful pump lasers are required. For instance, van Herpen and coworkers [26] used an 11W Nd-YAG laser at 1064 nm to generate 120mW at 4.7 μm (see Fig. 3.2). Recently, a record high idler wavelength of 5.32 μm was reported for an OPO pumped by a 20-W cw Yb:YAG disk laser operating at 1030 nm [27]. This value was limited by the minimum QPM period length of 24.4 μm of the crystal that was available. In the future, one can expect even longer wavelengths as the output power of the main pumping lasers (disk and fiber lasers) continues to increase.

3.3.3 Continuous, mode-hop-free tuning

One of the main advantages of cw OPOs compared with other cw laser systems is their wide tunability. This total tuning range is achieved by combining the available poling periods and crystal temperatures, next to pump tuning coverage. Besides, OPOs are able to perform continuous wave, mode-hop-free tuning over a large wavelength range, which is important for high-resolution spectroscopy; in this way accurate positions of molec-

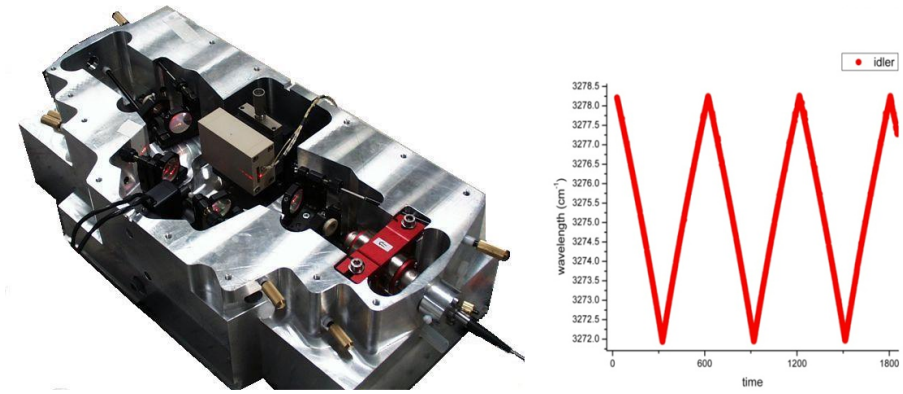

Figure 3.3: *Left panel: Continuous-wave mode-hop-free tunable optical parametric oscillator. Right panel: Wide mode-hop-free idler tuning over 180GHz by tuning of the seed laser.*

ular gas absorption lines can be determined. Mode-hop-free tuning can be achieved by combining pump tuning, tuning of the intracavity elements and changing the OPO cavity length. Arslanov et al. citeArslanovApplPhysB2011 demonstrated a SRO that is can be tuned mode-hop free over 5 cm^{-1}. For this, a 80-mW multisection DBR diode laser was used (linewidth 40 MHz, 1082 nm). Amplified in a Yb-doped fiber amplifier it generated 7.5W power to pump the OPO. Tuning of the OPO was performed in three steps. The first step was selecting an appropriate poling period of the PPLN crystal to roughly adjust the idler frequency at a wavelength between 3 and 4 μm. Then, by changing the crystal temperature the output wavelength can be changed within a 200 cm^{-1} range; thirdly a fast, 5 cm^{-1} range, mode-hop-free tuning can be achieved with the diode DBR pump laser. The latter is achieved by synchronously sweeping the current through resistive heaters of the DBR and the phase sections of the multisection diode laser. Mode-hop-free tuning or the absence of multimode operation of the idler is confirmed by the absence of discontinuities or broadened absorption lines, respectively, in the measured gas absorption spectra. The OPO itself is housed in a solid aluminium monoblock designed to ensure good long-term frequency stability (Fig. 3.3, left panel). Here a mode-hop-free tuning for the idler is shown over 6 cm^{-1} (Fig. 3.3, right panel).

Recently, the group of Zondy and coworkers [28] even demonstrated a 500-GHz mode-hop-free tuning around 3 μm. In their SRO the cavity length is shielded against acoustical perturbations causing mode hops by servoing its length to a stable confocal Fabry-Perot resonator using the FM/AM modulation spectroscopy.

3.3.4 Decreasing the oscillation threshold

To miniaturize OPOs and make them suitable for "field" applications, decreasing oscillation threshold is a primary concern. For many years the typical threshold pump power for oscillation of a continuous-wave SRO operating around 3 μm was 1.5-3.5W. Henderson and Stafford [25] could lower this value to 780mW using a long PPLN crystal of 80 mm. The Buse group showed that the threshold can be further reduced by using so-called 'hybrid pumping' in which, next to a coherent pump laser an incoherent laser is used to pump a piece of doped glass inside the cavity. In this way a threshold $<$ 100mW (of coherent light) was obtained [29]. Recently, they showed that only a threshold as low as 6mW is needed thanks to a completely new design based on whispering-gallery modes [30].

3.3.5 Broadband near- and mid-infrared OPOs

Recently, there is a growing interest in broadband, femtosecond OPOs for chemical sensing. Spectrometers based on broadband sources and with near/mid-infrared cameras allow massive parallel detection of gas species. In recent years there has been a rapid progress in the mid-infrared wavelength region, due to maturing laser technology in the near-infrared. An example is the high-power OPO-based frequency comb developed by the group of Jun Ye at the University of Colorado, with its continuous tunability from 2.8 to 4.8μm [31]. Their OPO was synchronously pumped by a 10-W femtosecond Yb-fiber laser centered at 1.07 μm. Its operation in the mid-nfrared wavelength region with a simultaneous bandwidth up to 300 cm^{-1} and an idler power of 1.5W generates an enormous potential for sensitive gas analysis. This potential was realized in 2010 when this OPO was used as a broadband source and coupled with a Fourier transform spectrometer [32]. Detection limits at the (sub) part per billion levels (ppbv, 1 : 10^9) were obtained for gases like methane, ethane, isoprene, formaldehyde and nitrous oxide using a 36-m multipass cell.

3.4 Molecular gas sensing via spectroscopy

Nowadays, gas-phase spectroscopy is very common in a wide variety of fields. Next to chemistry and physics it is involved in the research of living organisms ranging from biology to medical sciences. There are various ways of utilizing gas sensors, and each application requires a different set of demands. Some applications require very high sensitivity for one specific gas compound, while others benefit more from a sensor that can monitor a wide range of gases. A high time resolution is often desirable, as well as selectivity, robustness, and little or no need for sample preparation. To some extent, these characteristics can be combined within a single device, but often compromises

have to be made. Established methods of gas detection such as chemiluminescence and gas chromatography meet some of these requirements, but not all. For example, gas chromatography has a limited sensitivity and also sample preparation is needed. Often, the gas sample needs to be preconcentrated on a solid sorbent, which prohibits online measurement.

Laser-based absorption spectroscopy performs well in terms of sensitivity and selectivity, besides the fact that it allows online measurements. Its high sensitivity and selectivity are due to several factors. First, the narrow linewidth of lasers gives a high spectral power density as compared to broadband light sources. Especially for continuous-wave (cw) lasers this linewidth is typically much narrower than the molecular absorption lines. This causes the total laser intensity to be attenuated by the gas sample, instead of only a small fraction, as in the case of broadband sources. In addition, scanning over absorption lines improves the selectivity and helps to distinguish the target molecule from interfering compounds and background signals. The selectivity is further enhanced by the unique spectral absorption features of the molecules in the mid-infrared wavelength region. These 'fingerprint' absorption spectra correspond to rovibrational transitions features unique for each molecule; it probes the internal structure of the molecule, whereas other methods, such as mass spectrometry, only assess a global property of the investigated compound. Thus, in the infrared fingerprint wavelength region (2.5-25 μm) molecules have their characteristic, strong, absorption lines. Combined with highly sensitive spectroscopic methods, gases can be detected at sub-ppbv levels. Here, a number of these spectroscopic methods will be compared. Also, applications will be shown for a variety of gases.

3.4.1 Photoacoustic spectroscopy

The photoacoustic (PA) effect was discovered by A. G. Bell in 1880 [33]. Early photoacoustic instruments had limited sensitivities due to the use of blackbody radiators as the source. This situation changed when lasers became available. As early as 1971, an excellent detection limit of 10 ppbv was obtained for methane using an infrared He-Ne laser, operating at 3.39 μm [34]. Current state-of-the-art photoacoustic spectrometers use high-power lasers in combination with sensitive microphones or piezoelectric transducers and reach sub-ppbv detection sensitivity. Their robustness and real-time capabilities were recently shown in airborne measurements over industrial sources [35].

Photoacoustic spectroscopy is based on the detection of acoustic waves, formed after the absorption of modulated radiation (Fig. 3.4) [37]. When a gas absorbs light, the temperature of the gas increases; the gas expands adiabatically and generates a pressure increase. By turning the light off, the temperature and pressure drop. Thus, the modulated light generates a pressure wave at the same frequency as the modulation frequency (i.e. sound). This sound can be amplified in an acoustic resonator and is detected by a

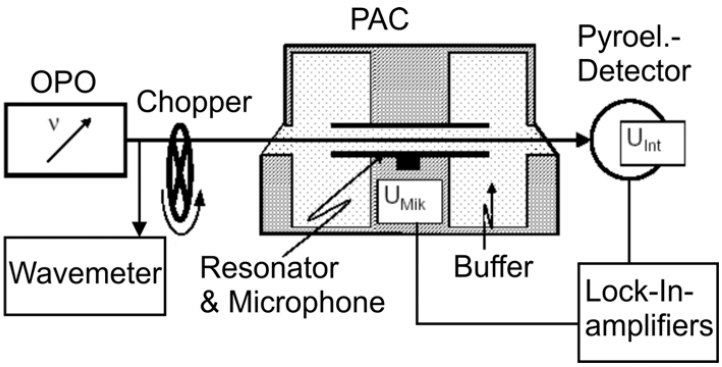

Figure 3.4: *Continuous-wave OPO-based photoacoustic spectrometer with a classical microphone. The generated sound in the cell is amplified by an acoustical resonator in its first longitudinal mode [36].*

microphone; the latter is connected to the resonator at a point where the pressure standing pressure wave has its maximum amplitude.

For small absorptions the strength of the photoacoustic signal is given by:

$$S = P \cdot R \cdot p_a \cdot \alpha, \tag{3.1}$$

with P the laser power, R the cell response, p_a the partial pressure of the absorbing gas and α the absorption coefficient. This equation shows the photoacoustic signal is linearly dependent on the concentration of absorbing molecules and the laser power. Therefore, high-power sources like OPOs yield the highest sensitivities. Since photoacoustic spectroscopy is an indirect detection technique, calibrated gas samples are needed to obtain absolute concentrations. Photoacoustic spectroscopy with OPOs has been applied to liquids, solids and gases. Here, we restrict ourselves to the application of trace-gas measurements.

Before the invention of high-power cw OPOs with PPLN crystals, pulsed OPOs were first used in the mid-infrared wavelength region for molecular spectroscopy. Already, in 1991, Haub et al. [38] used an injection seeded OPO with a BBO crystal (idler pulse energy 12 mJ) and recorded the photoacoustic absorption spectrum of acetylene gas in the nearinfrared at 10382.3 cm^{-1}. Using a commercial nanosecond pulsed OPO and difference frequency generation Bohren and Sigrist [39] covered the mid-infrared wavelength region between 2.5-4.5 μm. They were able to record different gases (methanol, ethanol, isopentane, benzene and toluene) and a mixture of 6 gases (methane, methanol, ethanol, isopentane, benzene and toluene) at atmospheric pressure in the region between 2850 and 3090 cm^{-1} at ppmv levels. Operating a pulsed OPO, Costopoulos et al. [40] developed a photoacoustic setup for measurements of N_2O around 3492 cm^{-1} and achieved a detection limit of 60 ppbv. Later, they used this OPO, with the grazing-incidence grating

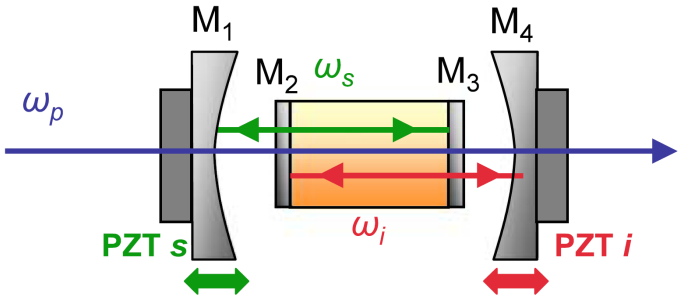

Figure 3.5: *Scheme of the entangled cavity doubly resonant OPO (ECOPO) with doublepass pump beam [11].*

for improving spectral resolution, to obtain a sensitivity of 1.2 ppbv for methane at 2948 cm^{-1} [41]. Recently, Berrou et al. [11] used tunable, narrow line width (<100 MHz), pulsed (8 ns) OPO radiation over the 3.8-4.3 μm spectral range at a multikilohertz repetition rate and 100W peak power (Fig. 3.5) for the photoacoustic detection of different greenhouse gases (CO_2, N_2O, SO_2 and CH_4). For N_2O, the sensitivity was estimated to be of 200 ppmv with a 300-ms integration time. This result shows that pulsed OPOs can be made miniaturized and that reasonable detection limits can be achieved. Due to the pulsed operation, resulting in high peak power, nonlinear absorption and a lower duty cycle, detection limits never reached extreme levels. On the other hand, broad scanning capabilities and smaller footprints are in advantage for pulsed OPOs.

3.4.2 Photoacoustic spectroscopy with cw OPOs

The first continuous-wave OPO photoacoustic setup was demonstrated by Kühnemann et al. [42] in 1998. Using a cw OPO with an output power of 100mW operating in the 2.3-4 μm range a detection limit of 0.5 ppbv was obtained for ethane (C_2H_6) with a scan time of 10 s. Later, van Herpen et al. citeHerpenApplPhysLett2002 used the combination of a SRO with photoacoustic spectroscopy for trace-gas detection of ethane. To measure at a specific absorption line, e.g. of ethane at 2996.9 cm^{-1}, the OPO was tuned to the centre of the absorption peak by adjusting the PPLN crystal to the proper period and rotating the solid intracavity etalon. This was followed by a 24-GHz of continuous tuning of the pump laser source over the entire absorption peak. Using a Lorentzian fit with a linearly decreasing background a detection limit of 0.01 ppbv (SNR = 1) was found, which results in a detection sensitivity of 3×10^{-10} cm^{-1} (scan time 40 s, Fig. 3.6).

In addition, the same authors were able to detect CO_2 emissions from small insects under atmospheric conditions [43]. For this, the OPO was made tunable in the 3.9-4.8 μm

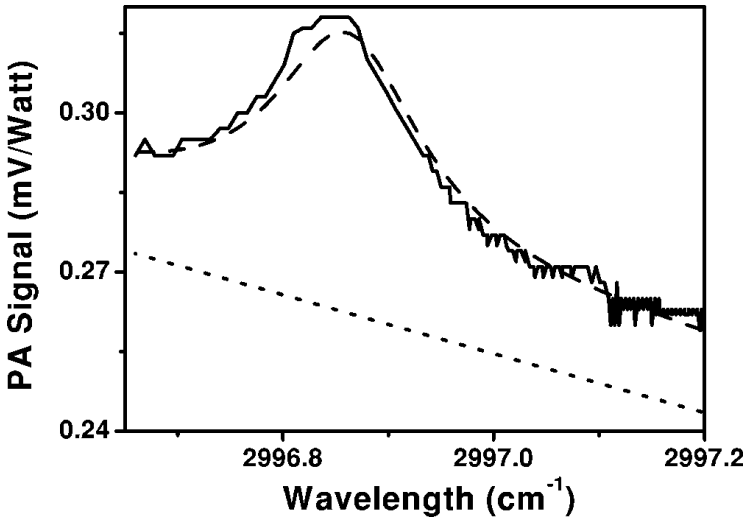

Figure 3.6: *Photoacoustic signal of the ethane absorption line at 2996.9cm^{-1} for a mixture of 0.4 ppbv ethane in nitrogen. A Lorentzian fit (dashed line) with a linearly decreasing background (dotted line) has been plotted through the experimental data (solid line). Evidently, there are the microphone noise (5 mV/Hz$^{1/2}$) and the high background signal (0.3 mV/W). Due to the wavelength-dependent background signal it is hard to use solely the peak value of the absorption at this ethane concentration, but the Lorentzian fit is able to find the background signal very well [9].*

infrared wavelength region, covering the strong rotational-vibrational absorption band of CO_2 at 4.23 μm. With this system it was possible to detect CO_2 with a sensitivity of 7 ppbv using 20mW OPO power. They demonstrated in real-time CO_2 in exhaled breath of a single ant (*Lasius niger*) and individual fruit flies (*Drosophila melanogaster*, Fig. 3.7) [43].

Another application of OPO photoacoustics was the monitoring of isotope methane ($^{12}CH_4$ and $^{13}CH_4$) emissions by plants. The study was provoked by an earlier study published in Nature [44] containing the finding that terrestrial plants can produce a large amount of methane in aerobic conditions. In collaboration with other research groups the research group of Harren re-examined this finding using an independent test performed on OPO spectroscopy [45]. For this study ^{13}C labelled plants were grown under controlled conditions in a hermetically sealed plant growth chamber (3.5 m^3) specifically designed for atmospheric isotope labelling. When investigating possible methane emission it is preferable to use ^{13}C labelled plants, since the natural background concentration of ^{13}C-methane is 20 ppbv compared to 1.7 ppmv of ^{12}C-methane. Methane shows a very pronounced absorption spectrum around 3000 cm^{-1} that is dominated by the strong ν_3

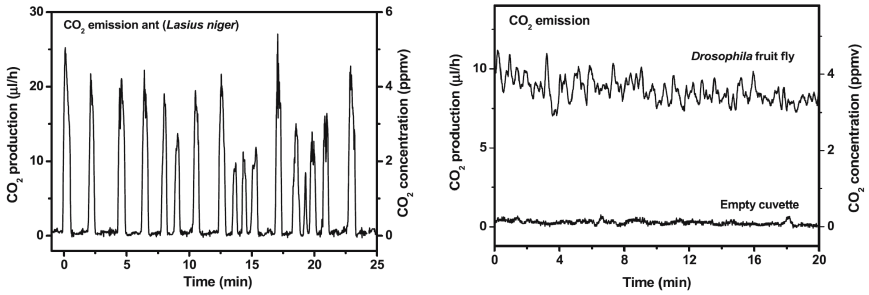

Figure 3.7: *Left panel: Real-time CO_2 emission of a small ant (Lasius niger, weight 3.7 mg). Analysis of the ants' respiration shows a periodic release of CO_2, on average every 90 s. Right panel: CO_2 release of a fruit fly (Drosophila melanogaster, weight 1.4 mg). The comparison of the CO_2 trace from the fruit fly with the background (without fly) shows that the CO_2 release does not drop to zero. The accuracy of the CO_2 detection shows that the CO_2 peaks vary in amplitude and frequency [43].*

band, and in which the band centres of $^{12}CH_4$ and $^{13}CH_4$ are shifted 10 cm^{-1} among each other. Figure 3.8 depicts a measurement of a ^{13}C-methane enriched sample and the comparison with a spectral simulation. The result of this study was that there is no evidence for substantial aerobic methane emission by terrestrial plants [45].

The studies above all relied on "classical photoacoustics" in which a microphone is the sensing element. In recent years, two new important developments have been announced, both focusing on the novel sensing elements. Kosterev et al. [46] introduced quartz-enhanced photoacoustic spectroscopy (QEPAS), where a small quartz tuning fork is used as a resonant element to detect the acoustic signal. The quartz tuning fork is inexpensive as it is mass produced for electronic watches and clocks in which it serves as a frequency standard. As it resonates, the piezoelectric quartz generates a pulsed current that is used to keep track of the passage time. The resonant frequency of the most widely used fork is 32 kHz. The QEPAS response (S) to optical absorption is described by:

$$S = k\frac{\alpha \cdot l \cdot C \cdot P \cdot Q}{f \cdot V}, \tag{3.2}$$

where α is the absorption coefficient of the gas species, l is the resonator length, C is the concentration of the gas, P is the power, f is the QEPAS sound frequency, V is the resonator volume and k is a constant describing other system parameters. The Q is a parameter of the quartz tuning fork and typically ranges from 10^4 to 10^5, depending on the carrier gas and the gas pressure. As compared to conventional photoacoustic spectroscopy, QEPAS has a high immunity to the background acoustic noise, because the ambient noise has a $1/f$ dependence and is very low above 10 kHz; the other advantage

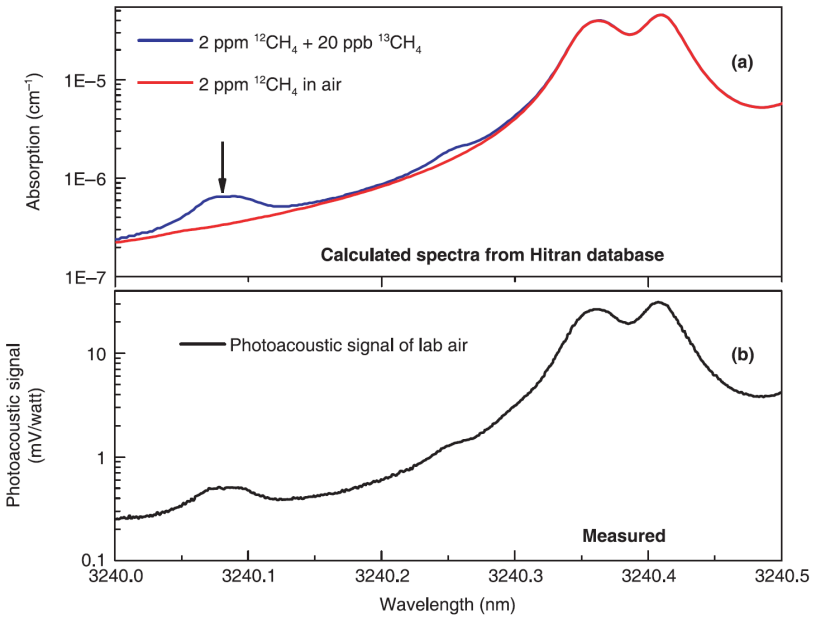

Figure 3.8: *Methane spectra. (a) Spectra calculated from the Hitran database (http:// cfa-www.harvard.edu/Hitran/). The arrow indicates the ^{13}C-methane peak used for the measurements. (b) Measured photoacoustic spectrum of laboratory air [45].*

is that there is a very small gas sampling volume ($\sim$1mm^3).

Most QEPAS studies reported to date have been performed using a wavelength modulation and 2–f detection to suppress the background signal. For gas detection the laser beam is focused between the prongs of the quartz tuning fork, which can be difficult to align. Ngai and coworkers [47] locked the idler wavelength of the OPO at an ethane absorption peak and verified the linear response of the QEPAS signal at different ethane concentrations (100 ppbv–20 ppmv) and different power levels. The detection limit for ethane was determined to be 13 ppbv (20 s averaging), corresponding to a normalized noise equivalent absorption coefficient of 4.4×10^{-7} cm^{-1} W/Hz$^{1/2}$.

Another recent development has been made on the use of a silicon cantilever as sensing element [48]. This method has already been successfully applied with different types of lasers reaching excellent sensitivities. A noise equivalent sensitivity of 1.7×10^{-10} cm^{-1} W/Hz$^{1/2}$ was achieved with this sensing element. Therefore it is thought that combining cantilever-based PAS with OPO systems will lead to subppbv detection limits for many gases.

Scientists at Sandia National Laboratory (USA) developed a broadly tunable, cw

Nd:YAG-pumped, intracavitytuned OPO as source for a field-portable photoacoustic spectrometer dedicated to monitoring VOCs in chemical sensing [49]. The device was able to measure broadly absorbing VOCs such as n-butyl acetate, methylamyl ketone, methylethyl ketone, isopropyl acetate, and toluene in the range of 1 ppmv in the presence of water interferences (of the order of 1 per cent).

With a 2.5-W Nd:YAG laser at 1064 nm Müller et al. [36] pumped a SRO reported on a possibility to use a cw dual-cavity OPO for building a transportable photoacoustic spectrometer in the wavelength region of 3.1-3.9 μm. The mode-hop tuning in steps of 450MHz is performed by tuning the intracavity etalon over 52 GHz, which is sufficient to resolve the pressure-broadened spectral lines at atmospheric pressure. The available idler power for photoacoustics of about 70 mW allowed the authors to reach a minimum detectable absorption coefficient of 3.2×10^{-9} cm^{-1} integration time, corresponding to the detection limit of 0.11 ppbv and 0.25 ppbv for ethane and ethylene, respectively.

3.4.3 Cavity ring-down spectroscopy

The development of cavity ring-down spectroscopy (CRDS) started in 1988 with a paper published by O'Keefe and Deacon [50] in which they adapted a technique to characterize high-reflective mirrors, and used this to measure the small absorption by gases in the visible region. A short laser pulse is coupled into the cavity and is reflected back and forth. Each time the light is reflected a small amount (1 – R) leaks out, leading to an exponential decay of the pulse energy in the cavity. This small amount is measured with a fast detector and recorded using a fast data acquisition card. The high sensitivity in CRDS results from the long path lengths of typically several kilometres that can be obtained. CRDS is based on the measurement of the exponential decay of light within the cavity rather than the absolute absorbance [51]. The temporal behaviour of the intensity $I(t)$ is given by:

$$I(t) = I_0 \cdot e^{-t/\tau} \text{ with } \tau(\nu) = \frac{d}{c[(1-R)+\alpha(\nu)d]}, \tag{3.3}$$

With I_0 the initial intensity falling on the detector and τ, the decay constant, is called the ring-down time, and is defined as the 1/e decrease of the exponential signal. The ring-down time can be written as a function containing the reflectivity of the mirrors (R), the distance between the mirrors (d), and $\alpha(\nu)$ the absorption coefficient. The ring-down time for an empty cavity, τ_0 for which $\alpha(\nu) = 0$, depends mainly on mirror losses and various optical phenomena like scattering and refraction. In the visible and near-infrared ring-down times up to a few hundred microseconds can be reached while in the mid-infrared, decay times are more modest ($<$13 μs) as the reflectivity is typically less than 99.99%. The absorption coefficient can be calculated from both ring- own times of an

empty cavity and filled with an absorber, and is given by:

$$\alpha(\nu) = \frac{1}{C\left(\frac{1}{\tau(\nu)} - \frac{1}{\tau_0(\nu)}\right)}, \tag{3.4}$$

Absolute densities can be determined by comparing the ring-down time in a nonabsorbing medium, such as nitrogen, with the ring-down time in the absorbing medium under investigation. The sensitivity is set by the accuracy at which these ring-down times can be determined. There are several factors that influence the accuracy: spatial characteristics of the laser beam, mode matching with the cavity, data acquisition card resolution and detector noise. The use of fast data acquisition cards and software is important to read the high amount of data and fit the decays. A major advantage of CRDS is that intensity fluctuations of the laser do not add to the noise in the final spectrum, as the ring-down time is independent of the initial light intensity I_0.

For pulsed lasers the bandwidth is sufficiently wide so that light will always couple into the cavity. For narrowband, continuous-wave lasers the laser frequency or cavity length must be tuned to mode-match the laser frequency to the cavity mode of the absorption cell and, thus, couple light into the cavity. Modulating the cavity length is normally done by using a piezoactuator attached to one of the mirrors. Typically, at least one free spectral range is covered in the scan so that a resonance in each period is guaranteed. When the light intensity inside the cavity exceeds a certain threshold, an acousto-optical modulator (AOM) turns off the OPO beam, followed by a measurement of the ring-down decay (Fig. 3.9). In a typical setup operating around a wavelength of μm the background ring-down time τ_0 has a maximum value of $\sim$13 μs, for a cavity length d= 50 cm and a mirror reflectivity R = 99.98%, which gives an absorption path of approximately 4 km.

3.4.4 OPO-based cavity ring-down spectroscopy

There are numerous research groups actively involved in the development and application of CRDS. The current state-of-the art is well described in a recent book by Berden and Engeln [52]. Here, we only refer to OPO-based instruments and applications for molecular gas sensing.

Van Zee et al. [53] were the first to apply a pulsed OPO for CRDS. Using an injection-seeded pulsed OPO with a bandwidth of about 115MHz and a short 10.5 cm ringdown cavity, they recorded the absorption spectra of the ^{P}Q(9) transition of the A-band of molecular oxygen ($\sim$13 100 cm^{-1}) by simultaneously scanning the OPO and the cavity length. An excellent noise-equivalent absorption coefficient of 5×10^{-10} cm^{-1}Hz$^{-1/2}$ was demonstrated, with a standard deviation for repeated measurements of the line strength better than 0.3%. Using a commercial pulsed OPO Morville et al. [54] recorded the collision-induced absorption band of oxygen at low temperatures in an 84-cm long cavity. This OPO was pumped by a frequency-tripled YAG laser with a pulse

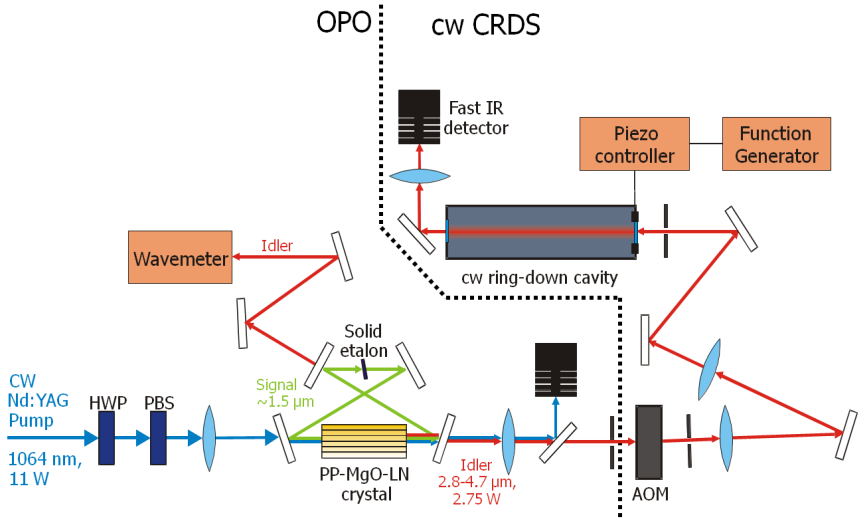

Figure 3.9: *SRO pumped by a cw-Nd:YAG laser used for cw cavity ring-down spectroscopy. The CRD cell is scanned by a piezo actuator over its free spectral range. If the OPO frequency is matching one of the cavity modes of the cell the transmitted light rises above threshold, after which the AOM turns off the OPO beam and the ring-down event is recorded.*

energy of several hundred microjoules, tunable from 400 to 700 nm and a large spectral width of the laser from 5-10 nm.

In 2002 Popp et al. [55] reported the first cw-CRDS trace-gas detector employing a pump-resonant SRO. They reached for ethane a 300 pptv (part per trillion volume, $1{:}10^{12}$) detection limit with an integration time of 16 s. Later, von Basum et al. [56] improved the performance of this system. The OPO was changed from a common-cavity design to one with two independent cavities for the pump and signal, which led to much wider frequency tunability. With the pump cavity locked to the laser by use of a Pound–Drever–Hall scheme, the idler beam is rapidly modulated in frequency. As a result, the ring-down cell is periodically excited, which led in their experiments to a high data rate of 1.4 kHz. An impressive 0.5 pptv ethane detection limit was obtained for 3 min integration time at 2997 cm^{-1}. They also demonstrated the detection of several gases by measuring ethane, methane and water in human breath within a 1 cm^{-1} spectral range, which shows the high potential of an OPObased CRDS for a transportable, ultrasensitive trace gas analyzer for environmental and medical studies.

Using a continuous-wave SRO, Ngai et al. [13] measured traces of CH_4 and C_2H_6 with CRDS. They used a cw-OPO pumped by a single frequency master oscillatorpower amplifier MOPA at 1064 nm, which could be tuned continuously over 48 GHz. A detec-

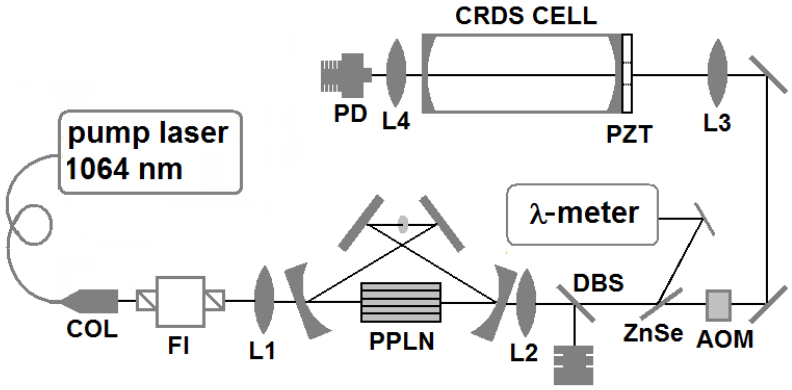

Figure 3.10: *Pump laser light is coupled into the OPO via a collimator (COL), Faraday isolator (FI) and AR-coated focusing lens (L1). The output of the OPO is collimated using an uncoated CaF_2 lens (L2). Signal and residual pump are separated from the idler using a dichroic beam splitter (DBS). Part of the idler beam is directed to a wavelength meter using a ZnSe window placed near the Brewster angle. The idler is guided through an acousto-optic modulator (AOM), and via mode- atching optics (L3) coupled into the ring-down cavity. Length of the cell is modulated at 35 Hz using a ring piezo-electric transducer (PZT). Light emerging from the cell is focused with a lens (L4) on a fast photodetector (PD) [57].*

tion limit of 0.16 ppbv was obtained for CH_4 using the absorption peak at 3221 nm (3105 cm^{-1}) in 200 s with a spectral resolution of 0.001 cm^{-1} and 0.07 ppbv for C_2H_6 over the absorption peak at 3337 nm (2997 cm^{-1}) in 60 s and a spectral resolution of 0.01 cm^{-1}.

The wide tunability of OPOs makes them especially suitable to measure the broad absorption patterns of larger molecules such as ethanol, propane or acetone. Under atmospheric conditions, the spectra of these molecules do not exist out of well-isolated lines but of broad absorption bands spanning typically 100 cm^{-1}. Using a cw-OPO tunable from 2693 nm to 3505 nm, Persijn et al. [57] developed a CRDS-based OPO spectrometer for sensitive and quantitative measurements. This setup has been used for trace-gas detection and also for purity analysis of gases. As a pump source for the OPO a DFB single-frequency fiber laser is used centered at 1063.9 nm with an output power of 7W and a laser linewidth better than 70 kHz. The laser can be tuned thermally over 45 GHz, or via applying a tensile strain to the fiber over 53 GHz using a multilayered piezo. The combined tuning range is 90 GHz (Fig. 3.10).

The system was used in VSL, the Dutch Metrology Institute for purity analysis of gases. For this, gas mixtures were prepared gravimetrically in cylinders, or via dynamic generation using diffusion tubes. The results were compared with data from the Hitran [58], NIST [59] and PNNL [60] databases. An example of benzene is given in Fig. 3.11

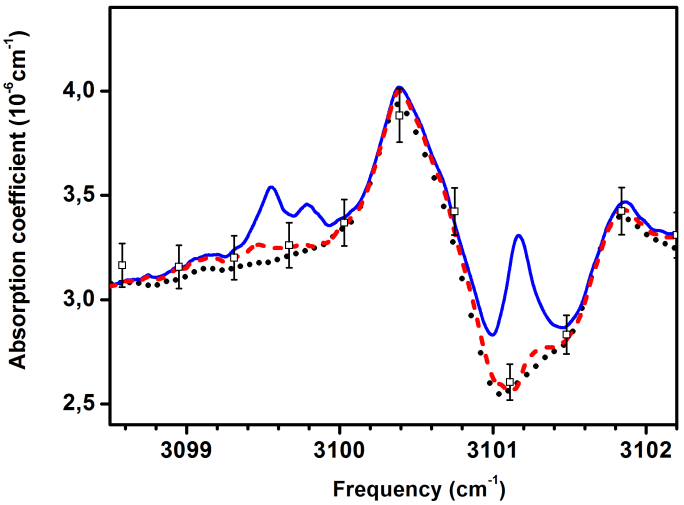

Figure 3.11: *Measurement of 1.00 µmol/mol benzene (solid blue line) and after subtraction of water vapor interference (dashed red line). Spectra from PNNL (black dots) and NIST (black squares including expanded uncertainty) databases are shown for comparison.*

for the Q-branch region at 3100 cm^{-1}, and as can be seen a good agreement is observed with the PNNL and NIST databases.

A problem arises when gas sensing is extended to larger, more complex molecules, which represent the majority of VOCs. At room temperature, these molecules exhibit broad and complex absorption patterns. Because of their lack of symmetry, these molecules tend to have a high degree of vibrational and rotational freedom, resulting in complex spectra consisting of a multitude of overlapping lines. This complicates the spectral identification considerably and it also effectively decreases the state density, i.e. detection sensitivity. One way to tackle this problem is using a supersonic planar jet expansion. Supersonic slit jet expansions, both cw and pulsed, are well known in the field of molecular spectroscopy. A planar expansion combines a Doppler-free environment with a relatively large absorption path length and low final rotational temperatures. The adiabatic cooling compresses the population distribution of a complex species into the lowest quantum states. Broad, complex, and overlapping absorption patterns thus become distinctive with linewidths that are principally determined by the residual Doppler broadening. Relatively short scans over tenths of wave numbers are sufficient to unambiguously identify and quantify multiple compounds with high sensitivity (ppbv- range) and short time scales. Using this approach, Ngai et al. [61] recorded the CH stretching

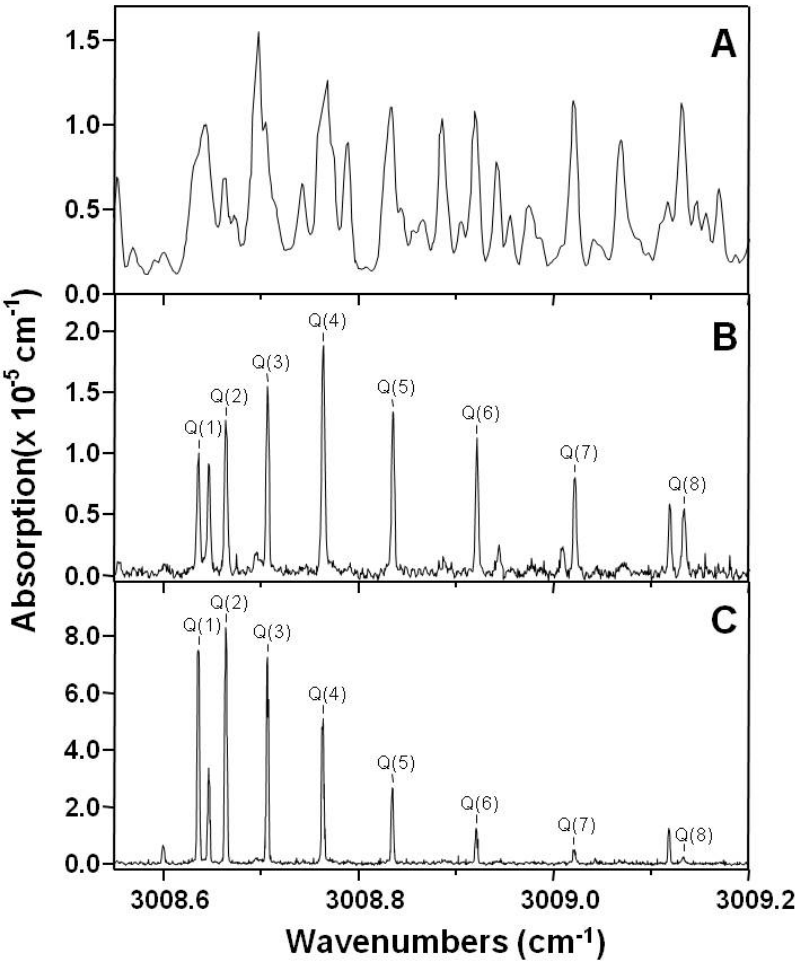

Figure 3.12: *Continuous-wave CRD spectra of the CH stretch fundamental region of methanol: (A) 125 ppmv methanol in 10 mbar laboratory air without jet, (B) an expansion of 60 ppmv methanol in a 525 l /h laboratory air flow, and (C) an expansion of 1250 ppmv methanol in 25 l /h air mixed with 500 l /h argon. For each data point 16 ring-down events were averaged over a data acquisition time of 1 s [61].*

region of methanol in a continuous jet at 10 mbar (Fig. 3.12). With a total optical path length of 180m in the planar jet, a detection limit for methanol in an air expansion was determined at 70 ppbv, corresponding to a minimum detectable absorption of 2.2×10^{-8} cm^{-1} (over 90 s).

The same setup was used [62] to measure in planar plasma the rotationally cold spectrum of formyl cation, HCO^+, in the CH-stretching region. The transitions observed

here were first recorded in 1983 in discharge cells using phase-sensitive detection and have been used ever since for testing new discharge techniques [63]. Using this detection method (CRDS in jet), it is possible to obtain absolute densities of the different species once the absorbance is available. The authors showed that direct absorption methods (cw-CRDS) could be used as an alternative method and would be suited to quantify reaction dynamical aspects in the expansion. Using this setup they obtain an average density of roughly 2×10^{10} HCO^+/cm^3. This setup allows the online probing of densities of different reaction products, by intersecting the plasma at different distances from the nozzle orifice.

3.4.5 Cavity-enhanced absorption spectroscopy

An alternative for cavity ring-down spectroscopy was developed independently in 1998 in two different groups by O'Keefe [64] and Engeln et al. [65]: integrated cavity output spectroscopy (ICOS) also named cavity-enhanced absorption spectroscopy (CEAS). Rather than via a decay time as in CRDS, this approach enables absorption spectra to be obtained by means of the integration of the transmitted light intensity. Light is enabled passing through the high-finesse optical cavity, either by oscillating the cavity length [66] or by antimode matching the laser with the cavity such that the laser couples to a large number of transverse cavity modes [67]. Very high effective optical path lengths can be obtained and the technique provides detection sensitivities comparable to CRDS.

The amplitude of the E-field transmitted through an optical cavity can be expressed as [68]:

$$E_t = \frac{E_0 e^{i\omega t} t_1 t_2 e^{-\alpha L/2}}{1 - r_1 r_2 e^{-\alpha L} e^{i\delta}}, \tag{3.5}$$

where E_0 and E_t are the incident and transmitted electrical fields, t_1, t_2, r_1, and r_2 the transmission and reflection coefficients for each mirror, ω the frequency of the light, α the absorption coefficient (in cm^{-1}), L the cavity length and δ the phase shift that the wave acquires in a round trip. For identical mirrors the transmitted intensity through the cavity will be:

$$\frac{I_t}{I_0} = \left|\frac{E_t^2}{E_0^2}\right| = \frac{T^2 e^{-\alpha L}}{1 + R^2 e^{-2\alpha L} - 2Re^{-\alpha L}\cos\delta} = \frac{T^2 e^{-\alpha L}}{(1 - Re^{-\alpha L})^2} \cdot \frac{1}{1 + F\sin^2(\delta/2)}, \tag{3.6}$$

in which $R = r^2$ and $T = t^2$ and $R + T = 1$. The second part of the last equation is the well-known Airy function used in multiple-beam interference with the coefficient of finesse: $F = 4R/(1-R)^2$. In the case of optimal transmission $\delta = 2\pi m$ with m an integer, we get:

$$\frac{I_t}{I_0} = \frac{(1-R)^2 e^{-\alpha L}}{(1 - Re^{-\alpha L})^2}. \tag{3.7}$$

For various reflectivities and absorption strengths this equation is shown in Fig. 3.13.

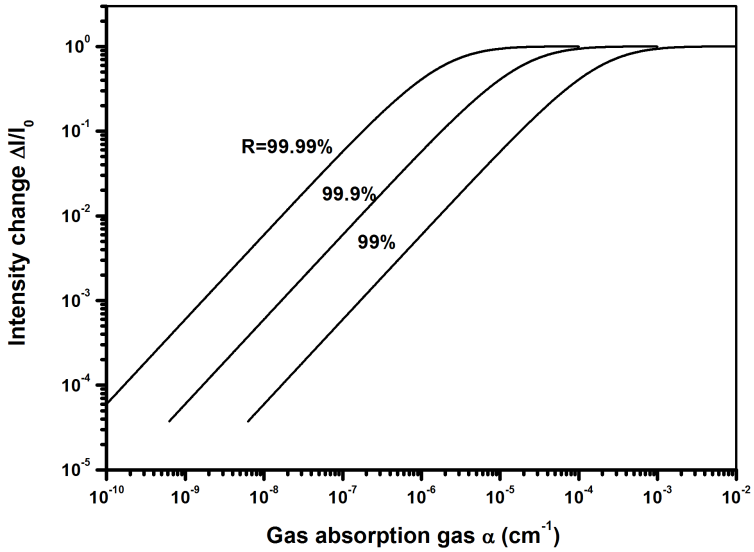

Figure 3.13: *The intensity change $\Delta I/I_0$ of the transmitted light beam through an optical cavity (with length L = 30 cm and mirror reflectivity R) is shown as a function of the absorption strength α for various mirror reflectivities. $\alpha = \sigma \times N$ with σ the absorption cross section at a specific wavelength (in cm^2) and N the density of the molecular gas (in $1/cm^3$). Data are results of Eq. 3.7.*

Figure 3.13 shows that even small changes in absorption result in rather large changes in the total transmitted signal. It also shows that for relative strong gas absorptions (e.g. 10^{-4} cm^{-1}) 99% mirrors can be sufficient (and cost effective) as compared to mirrors with a high reflectivity. Depending on the noise-reduction schemes a $\Delta I/I_0$ of 10^{-3}–10^{-4} is achievable; more advanced modulation schemes (such as wavelength modulation) are able to observe 10^{-5}.

As compared to CRDS, ICOS does not require active frequency-locking schemes, which results in simple alignment routines and more robust gas-detection cells for trace gases sensing. Although developed for pulsed laser systems, ICOS is ideally suited for continuous-wave lasers especially when off-axis ICOS configurations were developed. In off- axis integrated cavity output spectroscopy (OA-ICOS) multiple reflections are within the optical cavity before the light beam returns to its entry position [67]. Off-axis paths through optical cavities are well understood [69, 70]. This condition is dictated by the curvature and spacing between mirrors forming the cavity. For a spherical two-mirror

cavity, the stability condition is defined by:

$$0 < (1 - d/R_1)(1 - d/R_2) < 1, \tag{3.8}$$

where d is the mirror spacing and R_1 and R_2 are the mirror curvatures. The multiple reflections appear on the mirror surfaces as a series of spots in an elliptical pattern for spherical mirrors, or in a Lissajous spot pattern for astigmatic mirrors, which can further lengthen the re-entrant condition. The per-pass rotation θ is determined by the geometry of the cavity:

$$\cos\theta = 1 - d/R, \tag{3.9}$$

assuming the same reflectivity R for both mirrors. For a certain conditions the number of passes can approach infinity. OA-ICOS is effectively lowering the FSR of the cavity by effectively increasing the cavity length, which results in a dense mode structure [67, 71]. In a successful off-axis alignment, many cavity modes exist underneath every molecular transition and the laser linewidth should be broad with regard to the FSR of the cavity, but narrow with regard to the molecular line. Even narrow-band lasers link to many cavity modes simultaneously, which gives alignment robustness at the cost of transmitted power (see Fig. 3.14).

One big advantage of OA-ICOS is, as compared with CRDS, that neither the time evolution of every individual ring-down event has to be monitored nor that mode matching is needed between the laser frequency and the FSR. The potential drawback of the OA-ICOS approach is the significantly lower transmission power through the cavity compared with resonant-coupling methods. Therefore, high-power sources such as OPOs are rendered to be most suitable, usually, having an output cw power at Watt level [24, 72–74].

Despite the advantages that OPOs have over other mid-IR coherent sources, such as high power, narrow linewidth and broad tunability, not until 2010 was ICOS combined with an OPO [75]. The high output power of an OPO (>1W) gives superiority in use of OA-ICOS. The authors demonstrated that 50 pptv ethane (C_2H_6) in nitrogen, at 2997 cm^{-1}, can be recorded in just 0.25 s. In addition, they showed real-time breath sampling of methane and water with the time resolution of 0.1 s (Fig. 3.15).

3.4.6 Wavelength modulation spectroscopy

One of the most straightforward and simple methods to do laser spectroscopy is direct absorption spectroscopy. One can enhance the sensitivity by enlarging the path length up to hundreds of meters in a multiple-pass cell, using mirrors to fold the optical path. There are two basic conventional designs of multiple pass cells, developed by White [76] and Herriott and Schutte [70]. By incorporating wavelength modulation spectroscopy in such setups an order of magnitude better sensitivity can be achieved [77, 78].

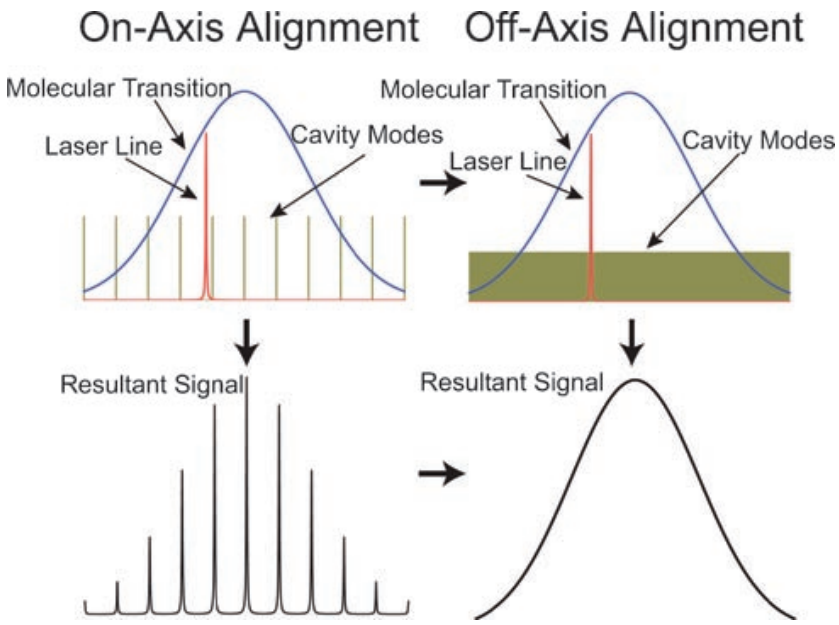

Figure 3.14: *Mode spectra shown here contrast the on-axis mode structure with the off-axis mode structure, showing how the free spectral range effectively collapses. The lower panels illustrate the resultant signals from each alignment. In a successful off-axis alignment, many cavity modes should exist underneath every molecular transition, and the laser line width should be broad with regard to the free spectral range of the cavity but narrow with regard to the molecular line [71].*

In practice, modulation spectroscopy can be divided into two approaches. The first is WMS, in which the modulation frequency is much lower than the absorption linewidth of the molecular transition; detection is performed at the modulation frequency ($1f$), or the higher harmonics ($2f$, $3f$, etc.). This typically corresponds to modulation frequencies from a few kHz to a few MHz. On the other hand, there is frequency modulation spectroscopy (FMS) that applies for modulation frequencies comparable to or higher than the spectral feature of interest (100MHz to GHz) [79, 80].

Due to the ease of diode laser frequency modulation, WMS has been widely applied in diode laser spectroscopy. Only in 2006 was WMS described for the first time in combination with an OPO [14]. One of the reasons could be that modulating the wavelength of the OPO is not as easy as in diode laser spectroscopy, for which injection current modulation is used.

When the laser is modulated around its center frequency ω_L at a frequency ω_m with modulation amplitude $\delta\omega$, the instantaneous frequency is $\omega = \omega_L + \delta\omega\ cos(\omega_m t)$. The intensity of the radiation transmitted through the absorption cell can then be expressed

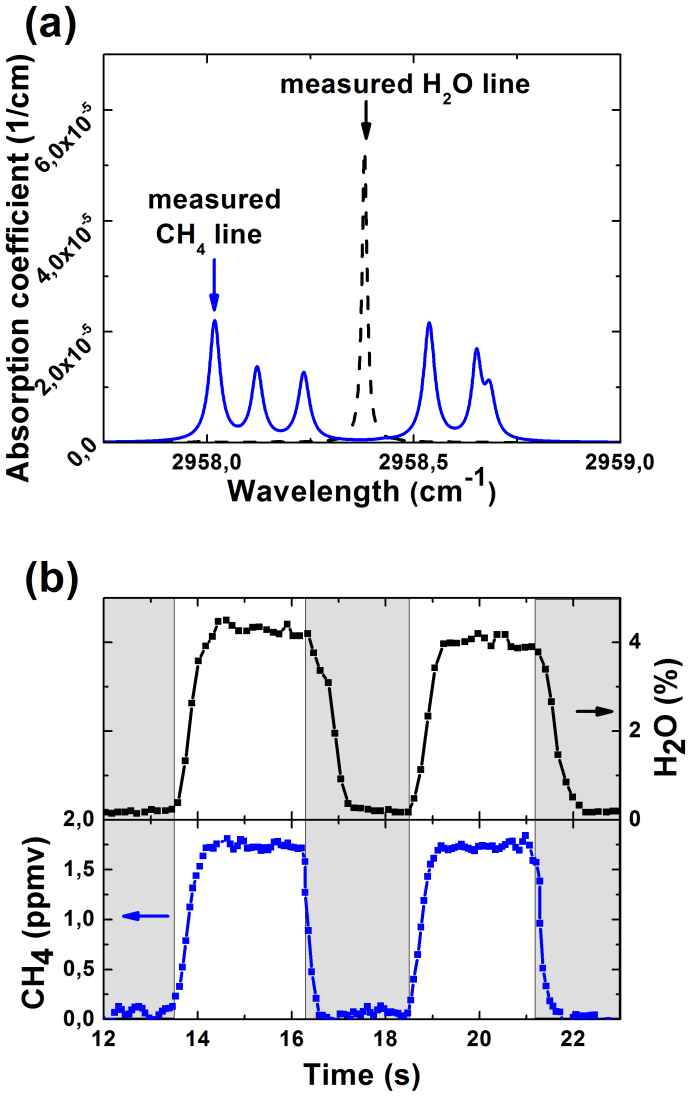

Figure 3.15: *Panel (a): Spectra simulated for 1cm path length and a pressure of 250 mbar of 1.7 ppmv of methane (solid curve) and 2% of water (dashed curve) based on the HITRAN 2008 database. (b) Dynamics of water (upper graph, right scale) and methane (lower graph, left scale) concentration measured in exhaled human breath, in real time. White sections correspond to exhalation, gray to inhalation [75].*

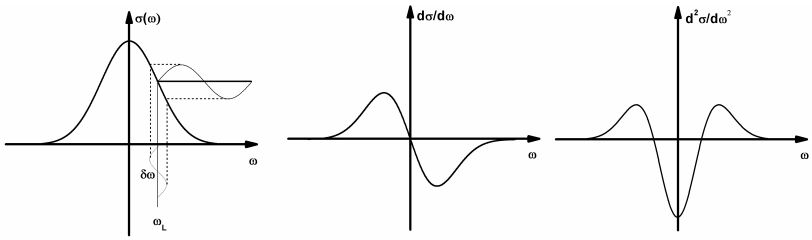

Figure 3.16: *Wavelength modulation spectroscopy of an absorption peak. When the modulated laser frequency at ω_L probes the absorption feature, part of the wavelength modulation is converted into an amplitude modulation, which is subsequently detected with a fast photodetector. Phase-sensitive detection with a lock-in amplifier of the first and second harmonics result in a WMS signal that is proportional to the first and second derivatives, respectively.*

as a Fourier series expansion:

$$I(\omega_L,t) = \sum_{n=0}^{\infty} A_n(\omega_L) cos(n\omega_m t), \tag{3.10}$$

where $A_n(\omega_L)$ $(n > 0)$ are the individual harmonic components, which can be measured with a lock-in amplifier. In the limit of low absorbance $(\sigma N \ll 1) A_n(\omega_L)$ becomes:

$$A_n(\omega_L) = \frac{2I_0 NL}{\pi} \int_0^{\pi} -\sigma(\omega_L + \delta\omega\, cos(\theta)) cos(n\theta) d\theta. \tag{3.11}$$

Thus, each harmonic component is directly proportional to the species concentration N. A special case occurs when the modulation amplitude $\delta\omega$ is much smaller than the absorption linewidth. In this case, a Taylor series expansion Each harmonic component is directly proportional to the derivative of $\sigma(\omega)$. The last is roughly proportional to the absorption signal, which is proportional to the species concentration (Fig. 3.16).

Due to the high modulation frequency for wavelength modulation and frequency modulation the noise at these frequencies is extremely low. This gives the advantage to achieve a factor 10 higher $\Delta I/I_0$ ratios per cm path length (10^{-5}) than other direct absorption methods (10^{-4}).

Ng et al. [81] were the first to combine WMS with an OPO for wavelength-modulated photoacoustic spectroscopy. In addition, Lindsay et al. [14] demonstrated the full potential of OPO-based WMS and FMS, their optical configuration is shown in Fig. 3.17. The idler output of the OPO (wavelength 3.1 μm) was passed through a 90-cm long absorption cell containing a dilute mixture of methane in nitrogen. For WMS, a 50-kHz modulation was applied to the DBR laser; a typical result is shown in Fig. 3.18, demonstrating spectra at both the modulation frequency ($1f$) and its second harmonic ($2f$). The authors clearly demonstrated that a SRO pumped by a fiber-amplified diode laser

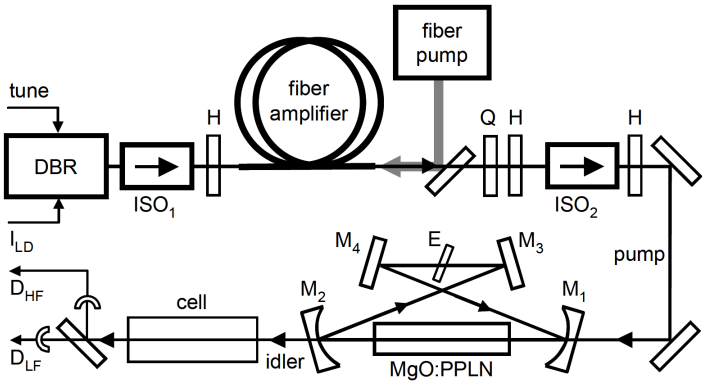

Figure 3.17: *Optical configurations for OPO-based WMS and FMS experiments. DBR: multisection distributed Bragg reflector diode laser, ISO_1: 60 dB isolator, ISO_2: 30 dB isolator, Q and H: quarter- and halfwave plates, M_{1--4}: OPO cavity mirrors, E: intracavity etalon, tune: tuning input to DBR laser, I_{LD}: DBR laser injection current supply, D_{HF}: fast mid-IR detector output, D_{LF} : slow mid-IR detector output [14].*

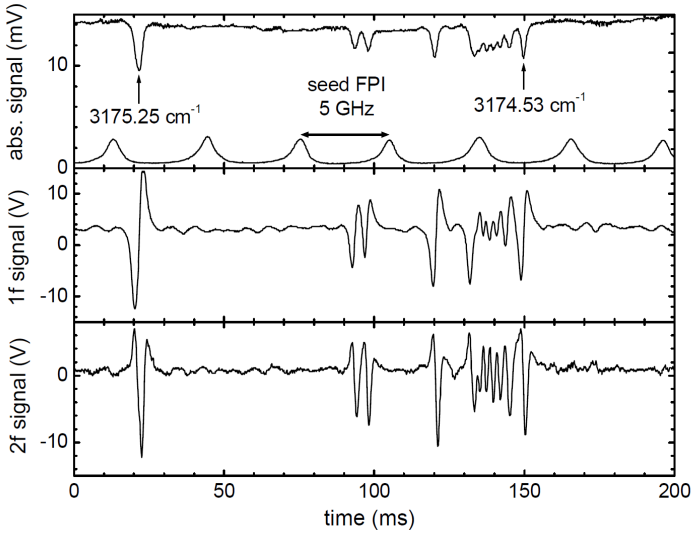

Figure 3.18: *WMS spectra demodulated at the 50 kHz modulation frequency (1f) and its second harmonic (2f). Also shown is the simultaneously recorded direct absorption spectrum (upper plot, top trace) and DBR seed laser transmission through a reference Fabry–Perot interferometer (upper plot, lower trace). Line assignments indicated on the direct absorption spectrum were made from the HITRAN database [14].*

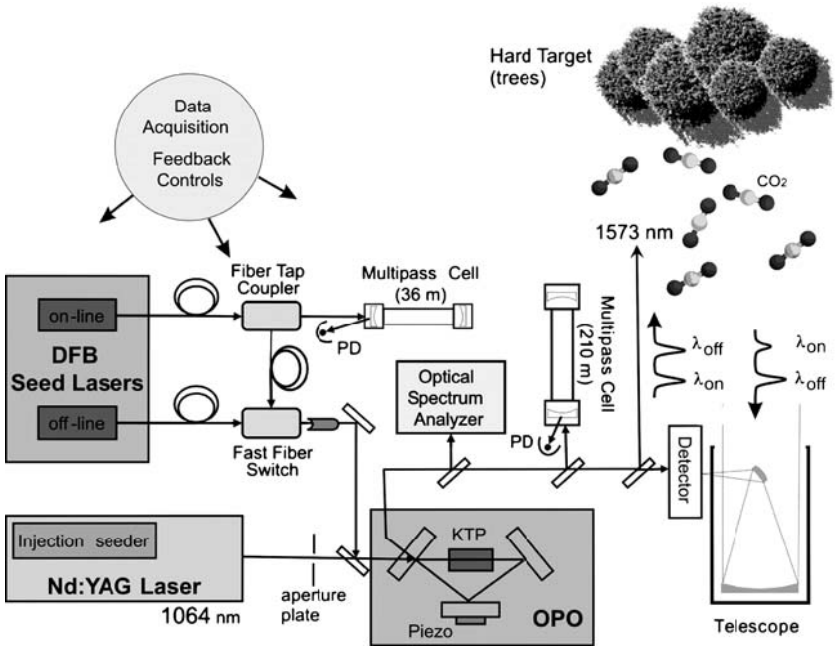

Figure 3.19: *Schematic diagram of an OPO-based DIAL system, in this case for atmospheric CO_2 concentrations measurements [82].*

can be used to implement WMS and FMS detection.

Having a similar fiber amplified SRO setup, Arslanov and coworkers [15] demonstrated trace gas OPO-based WMS for trace-gas detection reaching a sensitivity of 0.8 ppbv in ethane (2996.9 cm^{-1}, recorded in 1.3 s), corresponding to a noise equivalent absorption sensitivity of $1.2 \times 10^{-9} cm^{-1}/Hz^{1/2}$. The authors also showed a broad continuous tunability, covering 35 $^{-1}$, while recording absorption features of ethane, methane and water. The latter demonstrates the multicomponent capabilities, necessary for life-science applications.

3.4.7 Remote sensing

Optical remote sensing came quickly under development after the invention of the laser. LIDAR (light detection and ranging) is able to remotely measure the concentration and the spatial distribution of gas clouds. Pulsed laser light travels through the atmosphere, scatters on atmospheric particles, molecules or objects, and backscattered light travels to an optical receiver (Fig. 3.19). The spatial distribution is determined on the arrival time of the pulses. The intensity of the reflected pulse as a function of the wavelength gives in-

formation about the type and quantity of the present gases. Various tunable laser sources have been used for LIDAR systems, but the limited tuning range and laser linewidth of most coherent sources created a problem on finding coincidences between interesting gaseous absorption lines and laser frequencies.

As early as 1978 an infrared OPO-based LIDAR system was built with a wavelength coverage from 1.4 to 4 μm and pulse energies up to 0.6 mJ (10 Hz repetition rate) [83, 84]. The system achieved a sensitivity at 4 μm of 0.9×10^{-6} parts of SO_2 per km and later, for CH_4 at 1.66 μm, they measured a methane concentration of 3.9 ppmv (standard deviation 19%) assuming a uniform distribution over the 5.4-km long path length.

Later, more refined LIDAR methods were developed using differential absorption lidar (DIAL). With DIAL a direct comparison is made between two closely spaced wavelengths; one absorbed strongly by the target gas (λ_{online}) and the other at a not absorbing wavelength ($\lambda_{offline}$). The differential absorption between the two wavelengths is a measure of the concentration of the gas as a function of range.

A diode-laser-seeded OPO DIAL system was used for the determination of airborne water in the upper troposphere and lower stratosphere at 942 nm. By injection seeding with a 4.5-mW external cavity diode laser system, the spectral width of the pulsed OPO was line-narrowed down to 190 MHz, generating 40 mJ/pulse [85]. The line-narrowed OPO fulfils the spectral and energy requirements for airborne water vapor measurements. In 2002 a modified system was used in an intercomparison study for atmospheric water vapor measurements (925-940 nm) between three airborne DIAL systems to draw conclusions for future field campaigns. Data were collected during flight on vertical water vapor profiles in the atmosphere with a 10-s temporal average (Fig. 3.20) [86]. OPO-based DIAL systems were also developed for atmospheric methane measurement [88]. With a pulsed injection-seeded OPO, capable of tuning over a range of 90 nm (1490-1580 nm), atmospheric methane was measured at a concentration of 1.78 ppmv, which correspond closely to the established value of methane in atmosphere. The OPO had an output energy of 5 mJ/pulse and a linewidth of 140 MHz. Methane was also measured at 3.3 μm with an OPO-based LIDAR system for urban atmosphere pollution studies [89]. The overall tunability of the system (1.41-4.24 μm) and short acquisition time of 1 s makes the described LIDAR system capable of infrared remote sensing of multiple molecules in the atmosphere.

For atmospheric carbon dioxide measurements a DIAL-OPO system was used at 1.57 μm for horizontal mapping using a topographic target [82]. For the first time, measurements were performed on the diurnal variations of CO_2 at 1.57 μm, using a direct detection receiving system. Sakaizawa et al. [90] extended the described approach to measure vertical CO_2 profiles at 1.6 μm. The described LIDAR could be used to observe CO_2 with 2% statistical error in the troposphere from a few hundred meters to 5.2 km.

A femtosecond infrared LIDAR system based on a superbroadband OPO at 3 μm (pulse duration 100 fs, pulse energy 50 μJ, 1 kHz repetition rate) and its capability for

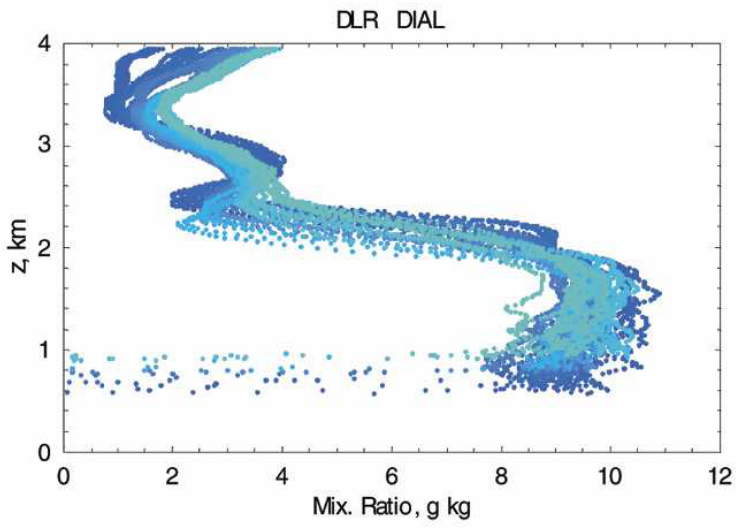

Figure 3.20: *Water-vapor profiles (mixing ratio against height) of the atmosphere measured with the DLR-DIAL (Deutsche Luft und Raumfahrt) platform during the formation flight on 7-8 June 2002. Data are with a temporal resolution of 10 s and an effective vertical resolution of 195m [87].*

remote sensing have been studied for multicomponent aerosols and atmospheric gases pollution [90]. The transmission spectrum of tributylamine ($(C_4H_9)_3N$) was recorded as an example of hydrocarbon atmospheric pollutant.

A versatile mobile laser LIDAR system for multiple remote-sensing tasks, ranging from air-pollutant mapping to aquatic and terrestrial monitoring, has been developed and described by Weibring et al. [91]. The OPO- based source was capable of generating a very wide wavelength range from 220 nm to 4 μm. The authors demonstrated atmospheric monitoring on several example ranging from atomic mercury emission from a chlorine-alkali plant to sulfur dioxide emission from the Italian volcano Mount Etna. The described LIDAR transmitter extended the measurements capabilities far beyond the standard DIAL methods and enabled simultaneous measurement of multiple species or resolving interference effects between compounds of interest and background gases such as CO_2 and water.

A portable gas imager employing a fiber-pumped OPO was demonstrated in 2002 [92]. The handheld device should meet the demand for gas imaging in the natural-gas industries. The target species is methane, the primary component of natural gas. This industry, but also the petroleum refining industry, needs remote surveillance for (indoor)

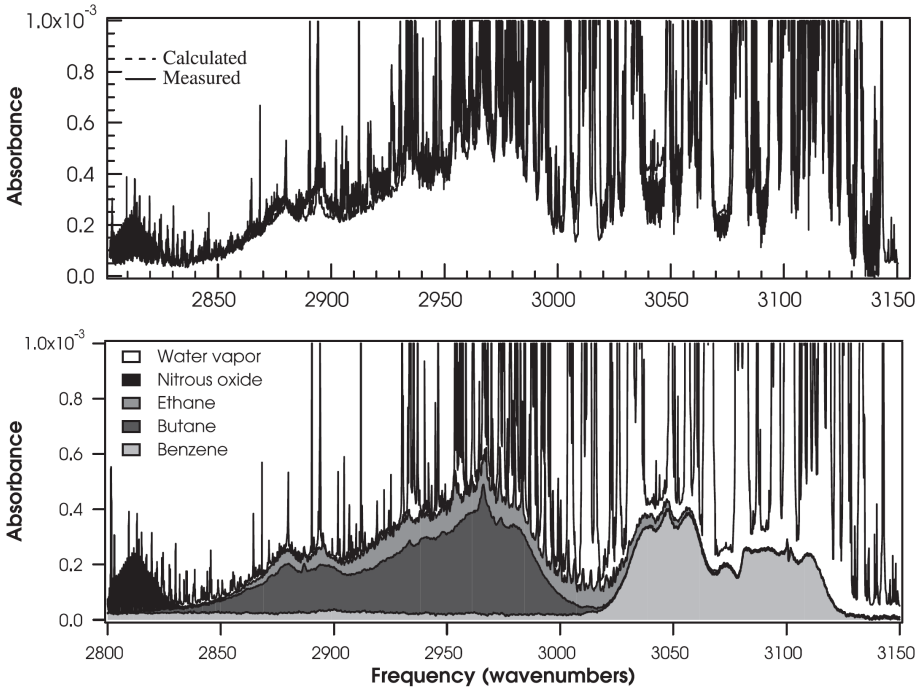

Figure 3.21: *A long-wavelength scan with cavity ring-down spectroscopy of a gas mixture consisting nitrous oxide (50 ppmv), butane (324 ppbv), benzene (1.69 ppmv), ethane (540 ppbv), and water vapor (40% RH at 23 °C). The scan was assembled from 27 individual scan segments. The lower panel shows the calculated total spectrum and the contribution from the individual chemical constituents. The upper panel shows the calculated spectrum overlaid with the measured spectrum [92].*

gas leaks, the latter for a blend of organic hydrocarbons. For these gasses the strongest infrared absorptions are those attributable to the CH-stretch vibrations with maxima near 3.3 μm wavelength. The nature of the absorption spectra of these molecules varies with the size of the molecule. Methane exhibits a typical 'small- molecule' spectrum with resolved rotational lines having a pressure-broadened line width of $\sim$0.1 cm^{-1}. While refinery hydrocarbons such as butane exhibit a 'large-molecule' spectrum in which individual rotational lines cannot be resolved and the rovibrational band has a broad (20-40 cm^{-1}) smooth structure (Fig. 3.21).

The portable imager consisted of a miniature, singlefrequency diode-pumped Nd:YAG seed laser whose output is directed into the core of a double-clad Yb-doped fiber amplifier resulting in 4.2W single-frequency output power directed to a SRO generating 250-300mW of idler power. At full OPO power, the portable system is capable of imaging at

ranges up to 9m. The OPO was coupled to a raster-scanned camera and laser-illuminated gas images were created using laser radiation backscattered from solid objects in the field-of-view of the camera.

3.5 Conclusions

OPOs can fulfil a wide variety of criteria for sensitive molecular gas sensing in a range of applications. One of the main advantages of the OPO is that it can access the infrared wavelength region where many molecules have their fundamental rovibrational transitions. Other laser sources either do not exist at this wavelength region, or have a very low power. As shown in this review, combinations of the OPO with all kind of conventional laser-based spectroscopic methods, such as WMS, FMS, CRDS, CEAS (ICOS), PA, QEPAS or LIDAR are possible. Due to its high output power and narrow linewidth the OPO can be an excellent source for sensitive high-resolution spectroscopy. In addition, owing to quasiphase matching in nonlinear crystals cw OPOs offer much wider wavelength tuning ranges as compared with other laser sources.

For a particular problem, one has to consider which spectroscopic method should be combined with the OPO. High-sensitivity experiments require a high-power laser and sensitive methods; robust methods such as PA and ICOS are more suitable for 'field' measurements; detection of large volatile molecules requires a widely tunable or broadband sources; remote sensing applications uses pulsed OPO-based LIDAR systems; high temporal resolution is on demand in life sciences where rapid detection of trace gases is required. All these approaches are accessible using OPOs. The incorporation of highly engineered products from the telecom industry will advance the goals for sensing at lower costs. For the future, the extension of the spectral infrared coverage up to 20 μm is of interest, through the use of patterned semiconductor materials, such as GaAs.

Acknowledgements. This research was financially supported by the Dutch Technology Foundation (STW); the Dutch Ministry of Economic Affairs, Agriculture & Innovation; the European Commission under the programmes: FP6-NESTA-0025042 'the Optical Nose'; FP6-Infrastructures-026183 'Life Science Trace Gas Facility' and FP7-ERA-NET+, under the iMERA+ project, contract number 217257.

References

[1] J. A. Giordmaine and R. C. Miller, "Tunable coherent parametric oscillation in linbo3 at optical frequencies," *Phys. Rev. Lett.*, vol. 14, pp. 973–976, 1965.

[2] E. L. Kerr and J. G. Atwood, "The laser illuminated absorptivity spectrophone, a method for measurement of weak absorptivity in gases at laser wavelengths," *Appl. Opt.*, vol. 7, pp. 915–921, 1968.

[3] J. A. Hodgeson, W. A. McClenny, and P. L. Hanst, "Air pollution monitoring by advanced spectroscopic techniques," *Science*, vol. 182, pp. 248–258, 1973.

[4] J. J. Scherer, D. Voelkel, D. J. Rakestraw, J. B. Paul, C. P. Collier, R. J. Saykally, and A. Oi??Keefe, "Infrared cavity ring down laser absorption spectroscopy," *Chem. Phys. Lett.*, vol. 245, pp. 273–280, 1995.

[5] M. H. Dunn and M. Ebrahimzadeh, "Generation of tunable light from continuous-wave to femtosecond pulses," *Science*, vol. 286, pp. 1513–1517, 1999.

[6] F. Huisken, M. Kaloudis, and A. Kulcke, "Infrared spectroscopy of small size-selected water clusters," *J. Chem. Phys.*, vol. 104, pp. 17–25, 1996.

[7] E. V. Kovalchuk, D. Dekorsy, A. I. Lvovsky, C. Braxmaier, J. Mlynek, A. Peters, and S. Schiller, "High-resolution doppler-free molecular spectroscopy with a continuous-wave optical parametric oscillator," *Opt. Lett.*, vol. 26, pp. 1430–1432, 2001.

[8] M. Vainio, M. Siltanen, J. Peltola, and L. Halonen, "Grating-cavity continuous-wave optical parametric oscillators for high-resolution mid-infrared spectroscopy," *Appl. Opt.*, vol. 50, pp. A1–A10, 2010.

[9] M. M. J. W. van Herpen, S. C. Li, S. E. Bisson, and F. J. M. Harren, "Photoacoustic trace gas detection of ethane using a continuously tunable, continuous-wave optical parametric oscillator based on periodically poled lithium niobate," *Appl. Phys. Lett*, vol. 81, pp. 1157–1159, 2002.

[10] G. W. Baxter, H. D. Barth, and B. J. Orr, "Laser spectroscopy with a pulsed, narrowband infrared optical parametric oscillator system: a practical, modular approach," *Appl. Phys. B*, vol. 66, pp. 653–657, 1998.

[11] A. Berrou, M. Raybaut, A. Godard, and M. Lefebvre, "High-resolution photoacoustic and direct absorption spectroscopy of main greenhouse gases by use of a pulsed entangled cavity doubly resonant opo," *Appl. Phys. B*, vol. 98, pp. 217–230, 2010.

[12] G. von Basum, D. Halmer, P. Hering, M. Murtz, S. Schiller, F. Muller, A. Popp, and A. Kuhnemann, "Parts per trillion sensitivity for ethane in air with an optical parametric oscillator cavity leak-out spectrometer," *Appl. Phys. B*, vol. 29, pp. 797–799, 2004.

[13] A. K. Y. Ngai, S. T. Persijn, G. von Basum, and F. J. M. Harren, "Automatically tunable continuous-wave optical parametric oscillator for high-resolution spectroscopy and sensitive trace-gas detection," *Appl. Phys. B*, vol. 85, pp. 173–180, 2006.

[14] I. D. Lindsay, P. Gross, C. J. Lee, B. Adhimoolam, and K.-J. Boller, "Mid-infrared wavelength- and frequency modulation spectroscopy with a pump-modulated singly-resonant optical parametric oscillator," *Opt. Express*, vol. 14, pp. 12341–12346, 2006.

[15] D. D. Arslanov, M. Spunei, A. K. Y. Ngai, S. M. Cristescu, I. D. Lindsay, S. T. Persijn, K. J. Boller, and F. J. M. Harren, "Rapid and sensitive trace gas detection with continuous wave optical parametric oscillator-based wavelength modulation spectroscopy," *Appl. Phys. B*, vol. 103, pp. 223–228, 2011.

[16] J. A. Armstrong, N. Bloembergen, J. Ducuing, and P. S. Pershan, "Interactions between light waves in a nonlinear dielectric," *Phys. Rev.*, vol. 127, pp. 1918–1939, 1962.

[17] P. A. Franken and J. F. Ward, "Optical harmonic and nonlinear phenomena," *Rev. Mod. Phys.*, vol. 35, pp. 23–39, 1963.

[18] L. E. Myers, R. C. Eckardt, M. M. Fejer, R. L. Byer, W. R. Bosenberg, and J. W. Pierce, "Quasi-phase-matched optical parametricoscillators in bulk periodically poled linbo3," *J. Opt. Soc. Am. B*, vol. 12, pp. 2102–2116, 1995.

[19] W. R. Bosenberg, A. Drobshoff, J. I. Alexander, L. E. Myers, and R. L. Byer, "Continuous-wave singly resonant optical parametric oscillator based on periodically poled linbo3," *Opt. Lett.*, vol. 21, pp. 713–715, 1996.

[20] Y. Furukawa, K. Kitamura, S. Takekawa, K. Niwa, and H. Hatano, "Stoichiometric mg:linbo3 as an

effective material for nonlinear optics," *Opt. Lett.*, vol. 23, pp. 1892–1894, 1998.

[21] K. L. Vodopyanov, O. Levi, P. S. Kuo, T. J. Pinguet, J. S. Harris, M. M. Fejer, B. Gerard, L. Becouarn, and E. Lallier, "Optical parametric oscillation in quasi-phase-matched gaas," *Opt. Lett.*, pp. 1912–1914, 2004.

[22] M. E. Klein, D. H. Lee, J. P. Meyn, K. J. Boller, and R. Wallenstein, "Singly resonant continuous-wave optical parametric oscillator pumped by a diode laser," *Opt. Lett.*, vol. 24, pp. 1142–1144, 1999.

[23] M. M. J. W. van Herpen, S. E. Bisson, A. K. Y. Ngai, and F. J. M. Harren, "Combined wide pump tuning and high power of a continuous-wave, singly resonant optical parametric oscillator," *Appl. Phys. B*, vol. 78, pp. 281–286, 2004.

[24] I. D. Lindsay, B. Adhimoolam, P. Gross, M. E. Klein, and K. J. Boller, "110ghz rapid, continuous tuning from an optical parametric oscillator pumped by a fiber-amplified dbr diode laser," *Optics Express*, vol. 13, pp. 1234–1239, 2005.

[25] A. Henderson and R. Stafford, "Low threshold, singly-resonant cwopo pumped by an all-fiber pump source," *Opt. Express*, vol. 14, pp. 767–772, 2006.

[26] M. van Herpen, S. E. Bisson, and F. J. M. Harren, "Continuous-wave operation of single frequency optical parametric oscillator at 4-5 um based on periodically poled linbo3," *Opt. Lett.*, vol. 28, pp. 2497–2499, 2003.

[27] J. Kiessling, R. Sowade, I. Breunig, K. Buse, and V. Dierolf, "Cascaded optical parametric oscillations generating tunable terahertz waves in periodically poled lithium niobate crystals," *Opt. Express*, vol. 17, pp. 87–91, 2009.

[28] E. Andrieux, T. Zanon, M. Cadoret, A. Rihan, and J.-J. Zondy, "500 ghz mode-hop-free idler tuning range with a frequency-stabilized singly resonant optical parametric oscillator," *Opt. Lett.*, vol. 36, pp. 1212–1214, 2011.

[29] I. Breunig, J. Kiessling, B. Knabe, R. Sowade, and K. Buse, "Hybridly-pumped continuous-wave optical parametric oscillator," *Opt. Express*, vol. 16, pp. 5662–5666, 2008.

[30] T. Beckmann, H. Linnenbank, H. Steigerwald, B. Sturman, D. Haertle, K. Buse, and I. Breunig, "Highly tunable low-threshold optical parametric oscillation in radially poled whispering gallery resonators," *Phys. Rev. Lett.*, vol. 106, no. 143903-1–4, 2011.

[31] F. Adler, K. C. Cossel, M. J. Thorpe, I. Hartl, M. E. Fermann, and J. Ye, "Phase-stabilized, 1.5 w frequency comb at 2.8-4.8 um," *Opt. Lett.*, vol. 34, pp. 1330–1332, 2009.

[32] F. Adler, P. Maslowski, A. Foltynowicz, K. C. Cossel, T. C. Briles, I. Hartl, and J. Ye, "Mid-infrared fourier transform spectroscopy with a broadband frequency comb," *Opt. Express*, vol. 18, pp. 21861–21872, 2010.

[33] A. G. Bell, "On the production and reproduction of sound by light, american journal of science," *Am. J. Sciences*, vol. XX, pp. 305–324, 1880.

[34] L. B. Kreuzer, "Ultralow gas concentration infrared absorption," *J. Appl. Phys.*, vol. 42, pp. 2934–2943, 1971.

[35] J. de Gouw, S. te Lintel Hekkert, J. Mellqvist, C. Warneke, E. L. Atlas, F. C. Fehsenfeld, A. Fried, G. J. Frost, F. J. M. Harren, J. S. Holloway, B. Lefer, R. Lueb, J. F. Meagher, D. D. Parrish, M. Patel, L. Pope, D. Richter, C. Rivera, T. B. Ryerson, and J. Samuel, "Airborne measurements of ethene from industrial sources using laser photoacoustic spectroscopy," *Environ. Sci. Technol.*, pp. 2437–2442, 2009.

[36] F. Muller, A. Popp, F. Kuhnemann, and S. Schiller, "Transportable, highly sensitive photoacoustic spectrometer based on a continuous-wave dual-cavity optical parametric oscillator," *Opt. Express*, vol. 11, pp. 2820–2825, 2003.

[37] S. C. F.J.M. Harren, S.T. Persijn, "Photoacoustic spectroscopy," in *Handbook of Metrology* (M.Glaser

and M. Kochsiek, eds.), pp. 581–622, Weinheim: Wiley-VCH, 2009.

[38] J. G. Haub, M. J. Johnson, and B. J. Orr, "Continuously tunable, injection seeded ?-barium borate optical parametric oscillator- spectroscopic applications," *Appl. Phys. Lett.*, vol. 58, pp. 1718–1720, 1991.

[39] A. Bohren and M. W. Sigrist, "Optical parametric oscillator based difference frequency laser source for photoacoustic trace gas spectroscopy in the 3 ?m mid-ir range," *Infrared Phys. Technol.*, vol. 38, pp. 423–435, 1997.

[40] D. Costopoulos, A. Miklos, and P. Hess, "Detection of n2o by photoacoustic spectroscopy with a compact, pulsed optical parametric oscillator," *Appl. Phys. B*, vol. 75, pp. 385–389, 2002.

[41] A. Miklos, C. H. Lim, W. W. Hsiang, G. C. Liang, A. H. Kung, A. Schmohl, and P. Hess, "Photoacoustic measurement of methane concentrations with a compact pulsed optical parametric oscillator," *Appl. Opt.*, vol. 41, pp. 2986–2993, 2002.

[42] F. Kuhnemann, K. Schneider, A. Hecker, A. A. E. Martis, W. Urban, S. Schiller, and J. Mlynek, "Photoacoustic trace-gas detection using a cw single-frequency parametric oscillator," *Appl. Phys. B*, vol. 66, pp. 741–745, 1998.

[43] M. M. J. W. van Herpen, A. K. Y. Ngai, S. E. Bisson, J. H. P. Hackstein, E. J. Woltering, and F. J. M. Harren, "Optical parametric oscillator-based photoacoustic detection of co2 at 4.23 i??m allows real-time monitoring of the respiration of small insects," *Appl. Phys. B*, vol. 82, pp. 665–669, 2006.

[44] F. Keppler, J. T. G. Hamilton, M. Brass, and T. Rockmann, "Methane emissions from terrestrial plants under aerobic conditions," *Nature*, vol. 439, pp. 187–191, 2006.

[45] T. A. Dueck, R. de Visser, H. Poorter, S. Persijn, A. Gorissen, W. de Visser, A. Schapendonk, J. Verhagen, J. Snel, F. J. M. Harren, A. K. Y. Ngai, F. Verstappen, H. Bouwmeester, L. A. C. J. Voesenek, and A. van der Werf, "No evidence for substantial aerobic methane emission by terrestrial plants: a 13c labelling approach," *New Phytol.*, vol. 175, pp. 29–35, 2007.

[46] A. A. Kosterev, A. Y. Bakhirkin, R. F. Curl, and F. K. Tittel, "Quartz-enhanced photoacoustic spectroscopy," *Opt. Lett.*, vol. 27, pp. 1902–1904, 2002.

[47] A. K. Y. Ngai, S. T. Persijn, I. D. Lindsay, A. A. Kosterev, P. Gro?, C. J. Lee, S. M. Cristescu, F. K. Tittel, K.-J. Boller, and F. J. M. Harren, "Continuous wave optical parametric oscillator for quartz-enhanced photoacoustic trace gas sensing," *Appl. Phys. B*, vol. 89, pp. 123–128, 2007.

[48] V. Koskinen, J. Fonsen, K. Roth, and J. Kauppinen, "Cantilever enhanced photoacoustic detection of carbon dioxide using a tunable diode laser source," *Appl. Phys. B*, vol. 86, pp. 451–454, 2007.

[49] S. E. Bisson, K. M. Armstrong, T. J. Kulp, and M. Hartings, "Broadly tunable, mode-hop-tuned cw optical parametric oscillator based on periodically poled lithium niobate," *Appl. Opt.*, vol. 40, pp. 6049–6055, 2001.

[50] A. O'Keefe and D. A. G. Deacon, "Cavity ring-down optical spectrometer for absorption measurements using pulsed laser sources," *Rev. Sci. Instrum.*, vol. 59, pp. 2544–2551, 1988.

[51] G. Berden, R. Peeters, and G. Meijer, "Cavity ring-down spectroscopy: Experimental schemes and applications," *Int. Rev. Phys. Chem.*, vol. 19, pp. 565–607, 2000.

[52] G. Berden and R. Engeln in *Cavity ring-down spectroscopy: Techniques and applications* (M.Glaser and M. Kochsiek, eds.), pp. 581–622, Weinheim: Wiley and Sons, 2009.

[53] R. D. van Zee, J. T. Hodges, and J. P. Looney, "Pulsed, single-mode cavity ring down spectroscopy," *Appl. Opt.*, vol. 38, pp. 3951–3960, 1999.

[54] J. Morville, D. Romanini, A. Campargue, and R. Bacis, "Opo-pulsed crds of the visible collision induced absorption bands of oxygen at low temperature," *Chem. Phys. Lett.*, vol. 363, pp. 498–504, 2002.

[55] A. Popp, F. Muller, F. Kuhnemann, S. Schiller, G. von Basum, H. Dahnke, P. Hering, and M. Murtz,

"Ultra-sensitive mid-infrared cavity leak-out spectroscopy using a cw optical parametric oscillator," *Appl. Phys. B*, vol. 75, pp. 751–754, 2002.

[56] G. von Basum, D. Halmer, P. Hering, M. Murtz, S. Schiller, F. Muller, A. Popp, and F. Kuhnemann, "Parts per trillion sensitivity for ethane in air with an optical parametric oscillator cavity leak-out spectrometer," *Opt. Lett.*, vol. 29, pp. 797–799, 2004.

[57] S. Persijn, F. Harren, and A. van der Veen, "Quantitative gas measurements using a versatile opo-based cavity ringdown spectrometer and the comparison with spectroscopic databases," *Appl. Phys. B*, vol. 100, pp. 383–390, 2010.

[58] L. S. Rothman, I. E. Gordon, A. Barbe, D. C. Benner, P. F. Bernath, M. Birk, V. Boudon, L. R. Brown, A. Campargue, J.-P. Champion, K. Chance, L. H. Coudert, V. Dana, V. M. Devi, S. Fally, J.-M. Flaud, R. R. Gamache, A. Goldman, D. Jacquemart, I. Kleiner, N. Lacome, W. J. Lafferty, J.-Y. Mandin, S. T. Massie, S. N. Mikhailenko, C. E. Miller, N. Moazzen-Ahmadi, O. V. Naumenko, A. V. Nikitin, J. Orphal, V. I. Perevalov, A. Perrin, A. Predoi-Cross, C. P. Rinsland, M. Rotger, M. Simeckova, M. A. H. Smith, K. Sung, S. A. Tashkun, J. Tennyson, R. A. Toth, A. C. Vandaele, and J. V. Auwera, "The hitran 2008 molecular spectroscopic database," *J. Quantum Spectrosc. Radiat. Transf.*, vol. 110, pp. 533–572, 2009.

[59] P. M. Chu, F. R. Guenther, G. C. Rhoderick, and W. J. Lafferty, "The nist quantitative infrared database," *J. Res. Natl. Inst. Stand. Technol.*, vol. 104, pp. 59–81, 1999.

[60] S. W. Sharpe, T. J. Johnson, R. L. Sams, P. M. Chu, G. C. Rhoderick, and P. A. Johnson, "Gas-phase databases for quantitative infrared spectroscopy," *Appl. Spectrosc.*, vol. 58, pp. 1452–1461, 2004.

[61] A. K. Y. Ngai, S. T. Persijn, and F. J. M. Harren, "Selective trace gas detection of complex molecules with a continuous wave optical parametric oscillator using a planar jet expansion," *Appl. Phys. Lett.*, vol. 90, pp. 081109–1–3, 2007.

[62] H. Verbraak, A. K. Y. Ngai, S. T. Persijn, F. J. M. Harren, and H. Linnartz, "Mid-infrared continuous wave cavity ring down spectroscopy of molecular ions using an optical parametric oscillator," *Chem. Phys. Lett.*, vol. 442, pp. 145–149, 2007.

[63] C. S. Gudeman, M. H. Begemann, J. Pfaff, and R. J. Saykally, "Velocity modulated infrared laser spectroscopy of molecular ions: the ?1 band of hco+," *Phys. Rev. Lett.*, vol. 50, pp. 727–731, 1983.

[64] A. O'Keefe, "Integrated cavity output analysis of ultra weak absorption," *Chem. Phys. Lett.*, vol. 293, pp. 331–336, 1998.

[65] R. Engeln, G. Berden, R. Peeters, and G. Meijer, "Cavity enhanced absorption and cavity enhanced magnetic rotation spectroscopy," *Rev. Sci. Instrum.*, vol. 69, pp. 3763–3769, 1998.

[66] A. O'Keefe, J. J. Scherer, and J. B. Paul, "cw integrated cavity output spectroscopy," *Chem. Phys. Lett.*, vol. 307, pp. 343–349, 1999.

[67] J. B. Paul, L. Lapson, and J. G. Anderson, "Ultrasensitive absorption spectroscopy with a high-finesse optical cavity and off-axis alignment," *Appl. Opt.*, vol. 40, pp. 4904–4910, 2001.

[68] in *Lasers and Electro-optic* (C. C. Davis, ed.), p. 88, Cambridge, United Kingdom: Cambridge University Press, 2002.

[69] D. Herriott, H. Kogelnik, and R. Kompfner, "Off-axis paths in spherical mirror interferometers," *Appl. Opt.*, vol. 3, pp. 523–526, 1964.

[70] D. R. Herriott and H. J. Schulte, "Folded optical delay lines," *Appl. Opt.*, vol. 4, pp. 883–889, 1965.

[71] G. S. Engel, W. S. Drisdell, F. N. Keutsch, E. J. Moyer, and J. G. Anderson, "Ultrasensitive near-infrared integrated cavity output spectroscopy technique for detection of co at 1.57 ?m: new sensitivity limits for absorption measurements in passive optical cavities," *Appl. Opt.*, vol. 45, pp. 9221–9229, 2006.

[72] A. F. Nieuwenhuis, C. J. Lee, B. Sumpf, P. J. M. van der Slot, G. Erbert, and K. J. Boller, "One-watt level mid-ir output, singly resonant, continuous-wave optical parametric oscillator pumped by a monolithic

diode laser," *Opt. Express*, vol. 18, pp. 11123–11131, 2010.

[73] A. Henderson, "Mid-ir tunable lasers probe hydrocarbon molecules," *Photonics Spectra*, pp. 72–77, 2009.

[74] G. K. Samanta and M. Ebrahim-Zadeh, "High-power, continuous-wave, optical parametric oscillator pumped by an optically pumped semiconductor laser at 532 nm," *Opt. Lett.*, vol. 35, pp. 1986–1988, 2010.

[75] D. D. Arslanov, S. M. Cristescu, and F. J. M. Harren, "Optical parametric oscillator based off-axis integrated cavity output spectroscopy for rapid chemical sensing," *Opt. Lett.*, vol. 35, pp. 3300–3302, 2010.

[76] J. U. White, "Very long optical paths in air," *J. Opt. Soc. Am.*, vol. 66, pp. 411–416, 1976.

[77] P. Werle and F. Slemr, "Signal-to-noise ratio analysis in laser absorption spectrometers using optical multipass cells," *Appl. Opt.*, vol. 30, pp. 430–434, 1991.

[78] P. Werle, "A review of recent advances in semiconductor laser based gas monitors," *Spectrochim. Acta A*, vol. 54, pp. 197–236, 1998.

[79] D. S. Bomse, A. C. Stanton, and J. A. Silver, "Frequency modulation and wavelength modulation spectroscopies: comparison of experimental methods using a lead-salt diode laser," *Appl. Opt.*, vol. 31, pp. 718–731, 1992.

[80] F. S. Pavone and M. Inguscio, "Frequency- and wavelength-modulation spectroscopies: Comparison of experimental methods using an algaas diode laser," *Appl. Phys. B*, vol. 56, pp. 118–122, 1993.

[81] J. Ng, A. H. Kung, A. Miklos, and P. Hess, "Sensitive wavelength-modulated photoacoustic spectroscopy with a pulsed optical parametric oscillator," *Opt. Lett.*, vol. 29, pp. 1206–1208, 2004.

[82] A. Amediek, A. Fix, M. Wirth, and G. Ehret, "Development of an opo system at 1.57 mu m for integrated path dial measurement of atmospheric carbon dioxide," *Appl. Phys. B*, vol. 92, pp. 295–302, 2008.

[83] R. A. Baumgartner and R. L. Byer, "Continuously tunable ir lidar with applications to remote measurements of so2 and ch4," *Appl. Opt.*, vol. 17, pp. 3555–3561, 1978.

[84] M. Endemann and R. L. Byer, "Remote single-ended measurements of atmospheric temperature and humidity at 1.77 i??m using a continuously tunable source," *Opt. Lett.*, vol. 5, pp. 452–454, 1980.

[85] G. Ehret, A. Fix, V. Wei?, G. Poberaj, and T. Baumert, "Diode-laser-seeded optical parametric oscillator for airborne water vapor dial application in the upper troposphere and lower stratosphere," *Applied Physics B*, vol. 67, pp. 427–431, 1998.

[86] A. Behrendt, V. Wulfmeyer, P. D. Girolamo, C. Kiemle, H. S. Bauer, T. Schaberl, D. Summa, D. N. Whiteman, B. B. Demoz, E. V. Browell, S. Ismail, R. Ferrare, S. Kooi, G. Ehret, and J. H. Wang, "Intercomparison of water vapor data measured with lidar during ihop 2002," *J. Atmos. Ocean. Tech.*, vol. 24, pp. 3–21, 2007.

[87] A. Behrendt, V. Wulfmeyer, C. Kiemle, G. Ehret, C. Flamant, T. Schaberl, H. S. Bauer, S. Kooi, S. Ismael, R. Ferrare, E. V. Browell, and D. N. Whitemann, "Intercomparison of water vapor data measured with lidar during ihop 2002," *J. Atmos. Ocean. Tech.*, vol. 24, pp. 22–39, 2007.

[88] M. J. T. Milton, T. D. Gardiner, F. Molero, and J. Galech, "Injection-seeded optical parametric oscillator for range-resolved dial measurements of atmospheric methane," *Opt. Commun.*, vol. 142, pp. 153–160, 1997.

[89] V. S. Airapetyan, "Measurement of absorption spectra for atmospheric methane by a lidar system with tunable emission wavelength in the range 1.41-4.24 ?m," *J. Appl. Spectrosc.*, vol. 76, pp. 268–272, 2009.

[90] D. Sakaizawa, C. Nagasawa, T. Nagai, M. Abo, Y. Shibata, M. Nakazato, and T. Sakai, "Development of a 1.6 um differential absorption lidar with a quasi-phase-matching optical parametric oscillator and photon-counting detector for the vertical co2 profile," *Appl. Opt.*, vol. 48, pp. 748–757, 2009.

[91] P. Weibring, H. Edner, and S. Svanberg, "Versatile mobile lidar system for environmental monitoring,"

Appl. Opt., vol. 42, pp. 3583–3594, 2003.

[92] T. J. Kulp, S. E. Bisson, R. P. Bambha, T. A. Reichardt, U. B. Goers, K. W. Aniolek, D. A. V. Kliner, B. A. Richman, K. M. Armstrong, R. Sommers, R. Schmitt, P. E. Powers, O. Levi, T. Pinguet, M. Fejer, J. P. Koplow, L. Goldberg, and T. G. Mcrae, "The application of quasi-phase-matched parametric light sources to practical infrared chemical sensing systems," *Appl. Phys. B*, vol. 75, pp. 317–325, 2002.

Chapter 4

Rapid and sensitive trace gas detection with continuous wave Optical Parametric Oscillator-based Wavelength Modulation Spectroscopy

Abstract

A fiber-amplified Distributed Bragg Reflector diode laser is used to pump a continuous wave, singly resonant Optical Parametric Oscillator (OPO). The output radiation covers the 3–4 μm with ability of rapid (100 THz/s) and broad modehop-free tuning (5 cm^{-1}). Wavelength Modulation Spectroscopy is combined with the OPO to take optimal advantage of the spectral scan speed. The sensitivity of the system was determined as 0.8 ppbv (parts-perbillion by volume) for ethane (C_2H_6) for the absorption peak at 2996.9 cm^{-1} recorded in 1.3 seconds, corresponding to a noise equivalent absorption sensitivity (NEAS) of 1.2×10^{-9} $cm^{-1}/Hz^{1/2}$. A comparison between results using the 1st, 2nd and 4th harmonic derivative signal from wavelength modulation was performed. The broad continuous tunability was demonstrated by covering 35 cm^{-1} while recording absorption

This work has been published in:
D. D. Arslanov, M. Spunei, A. K. Y. Ngai, S. M. Cristescu, I. D. Lindsay, S. T. Persijn, K. J. Boller, and F. J. M. Harren, "Rapid and sensitive trace gas detection with continuous wave Optical Parametric Oscillator-based Wavelength Modulation Spectroscopy" Appl. Phys. B, **103** 223–228 (2011).

features of ethane, methane and water.

4.1 Introduction

To unravel highly dynamic processes in the life sciences there is an increasing need for time-resolved measurements of trace gas emissions. Examples of such processes include the release of aldehydes, alcohols, and acetates by plants subject to attack by herbivores [1, 2]; CO_2, H_2O and CH_4 release in insect respiration [3]; or in humans, the kinetics of the gas composition of a single breath exhalation [4]. Capturing all details of the emission pattern requires an instrument which combines a high sensitivity at the ppbv level within a second time scale resolution or beyond. This goal has been partially achieved by several research groups using quantum cascade lasers in combination with spectroscopic techniques, such as cavity ring-down [5], frequency modulation, and wavelength modulation spectroscopy [6, 7]. However, most of these instruments only allow monitoring of a single gas due to the limited scanning range of the quantum cascade laser. Moreover, the time resolution is still an issue when second or sub-second time of measurement is required.

As many gases have strong absorptions in the midinfrared region, we chose to tackle this problem by using the well-developed tuning and modulation abilities of diode lasers in the near-infrared region and transfer these to the 3–4 μm range, by using a continuous wave Singly-Resonant Optical Parametric Oscillator (SR-OPO) [7–11]. Such a combination is an ideal basis for trace gas detection by means of laser spectroscopy. Here, rapid and wide spectral tuning over 16.5 cm^{-1}, rapid mode-hop-free tuning over 5 cm^{-1} (scan rate: 100 THz/s), and broad continuous coverage over the complete 3–4 μm range could be performed [9]. Additionally, these characteristics are combined with a high average power of 1Watt, 100 MHz Optical Parametric Oscillator (OPO) linewidth, a long-term stability of 1.7×10^{-3} cm^{-1} over 30 minutes and the ability to simply set and lock any wavelength within a pump tuning range. This SR-OPO could be combined with Direct Absorption Spectroscopy (DAS), which offers a simple mechanism to record trace gases. However it does not provide a high sensitivity [12] due to is short effective path length. Even by using of multiple pass cells optical path lengths cannot exceed a few hundreds of meters. To improve the sensitivity one can modulate the input signal with kHz-MHz frequency and demodulate absorption signal by using a lock-in amplifier. With this method at least an order of magnitude is gained in sensitivity. In [7] Wavelength Modulation Spectroscopy (WMS) and Frequency Modulation Spectroscopy (FMS) techniques were demonstrated using a mid-IR OPO pumped by a fiber-amplified diode laser. In this paper, we extend this approach and present rapid and sensitive trace gas measurements by using a multi-pass cell in combination with WMS. This method provides rapid recordings at the ppbv level sensitivity for gases such as ethane, methane, hydrogen cyanide, etc. and

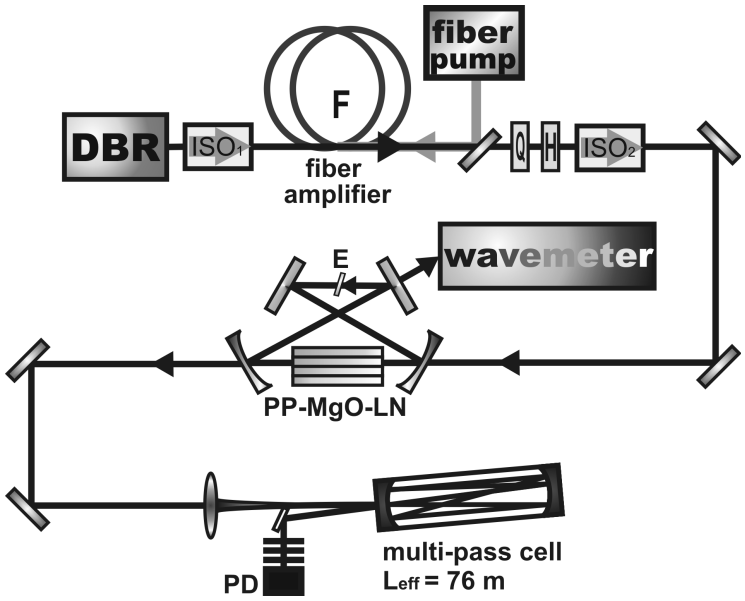

Figure 4.1: *Experimental setup. DBR Distributed Bragg Reflector diode laser, ISO*1 *and* 2 *isolators (to reduce feedback into the DBR laser), F double-clad Yb-doped fiber, Q quarter-wave-plate, H half-wave-plate, PP − MgO − LN MgO-doped periodically poled lithium niobate crystal, E intra-cavity etalon, multi − passcell, PD photodetector.*

opens up new applications in medical and life sciences [13].

4.2 Experimental setup

The experimental setup of the SR-OPO is shown in Fig. 4.1 and is described earlier [9], here only a short description is given. An 80 mW multi-section Distributed Bragg Reflector (DBR) diode laser (Eagleyard Photonics, linewidth 40 MHz [9]) with an output wavelength of 1082 nm is used to seed a 30 m long double-clad Yb-doped fiber amplifier pumped by a 25 W fiber-coupled 976 nm cw diode laser bar. The output of the fiber amplifier (7.5 W) is used to pump the OPO. To suppress stimulated Brillouin scattering inside the fiber amplifier, a fast modulation ($\geq$2 MHz) was applied to the gain section of the DBR laser, which resulted in a broadening of the output linewidth of this pump system to 100 MHz [8, 9].

The SR-OPO cavity [9, 11] consists of a four-mirror bowtie ring design with two concave mirrors (R = 10 cm) and two flat mirrors, all being highly transparent for pump and idler, and highly reflective for the signal wavelength. The pump beam was focused

using a 75 mm CaF_2 lens in a 5% MgO-doped PPLN crystal (HC Photonics) with a length of 5 cm and with seven poling periods ranging from 28.5 to 31.5 μm. To suppress etalon effects one of the two edges had a slight wedge of 1 degree and both sides were antireflective coated for the pump, signal and idler wavelengths. The crystal was placed in an oven capable of maintaining temperatures from 20 to 200 °C with a stability of 0.02 °C. In some of the experiments an uncoated 400-μm-thick solid YAG etalon (free spectral range 207 GHz) was inserted in the OPO cavity to enhance long-term frequency stability. Up to 1 W of idler output was produced at a pump power of 7.5 W with a power stability better than 3%.

Tuning of the OPO was performed in three steps. The first step was selecting an appropriate poling period of the PPLN crystal to roughly adjust the idler frequency at a wavelength between 3 and 4 μm. Then, by changing the crystal temperature the output wavelength can be changed within a 200 cm^{-1} range [10]; thirdly a fast, 5 cm^{-1}-range, mode-hop-free tuning can be achieved with the diode DBR pump laser. The latter is achieved by synchronously sweeping the current through resistive heaters of the DBR and the phase sections of the multi-section diode laser. Mode-hop-free tuning or the absence of multimode operation of the idler is confirmed by the absence of discontinuities or broadened absorption lines, respectively, in the measured gas absorption spectra. By choosing the appropriate amplitudes and DC offsets the mode-hop-free range can be shifted within a total range of 16.5 cm^{-1} [7, 8]. For fast scans the relative idler frequency was monitored using a 5- cm-thick germanium (Ge) etalon (see Fig. 4.2a) (FSR = 1.1 GHz). For 'slow' experiments a wavelength meter was used (Bristol Instruments 621A) with a repetition rate of 2 Hz.

To benefit from the fast scanning capabilities, the OPO was combined with wavelength modulation spectroscopy in a multi-pass absorption cell [14]. Using an anti-reflective coated (<0.5%) f = 50 cm ZnSe lens, the idler beam was focused into the multi-pass cell (Aerodyne, AMAC-76) with an absorption path length of 76 m and a volume of 300 ml. The original entrance window of the cell was replaced with an anti-reflective coated window to suppress etalon effects. The gas flow mixture was continuously flushed through this absorption cell. To maintain a $\sim$100 mbar pressure inside the cell a pressure controller and a needle valve are used, respectively in the entrance flow to the cell (Brooks Instrument 0154 and 5850) and in the exit flow towards the vacuum pump (Pfeiffer Vacuum MVP 015-4).

After the cell, the idler beam was detected with a fast HgCdZnTe thermo-electrically cooled photodetector (1 MHz bandwidth, VIGO System PDI-2TE-4). To prevent saturation of the detector, the idler beam power of the OPO was reduced by using a pair of diaphragms. For the wavelength modulation experiments we used a 25 kHz modulation frequency on top of the 2 MHz applied to the DBR diode laser. The detected signal was demodulated with a lock-in amplifier (Stanford Research Systems SR830 DSP) at the first, second and fourth harmonic, and recorded with an oscilloscope (Tektronix

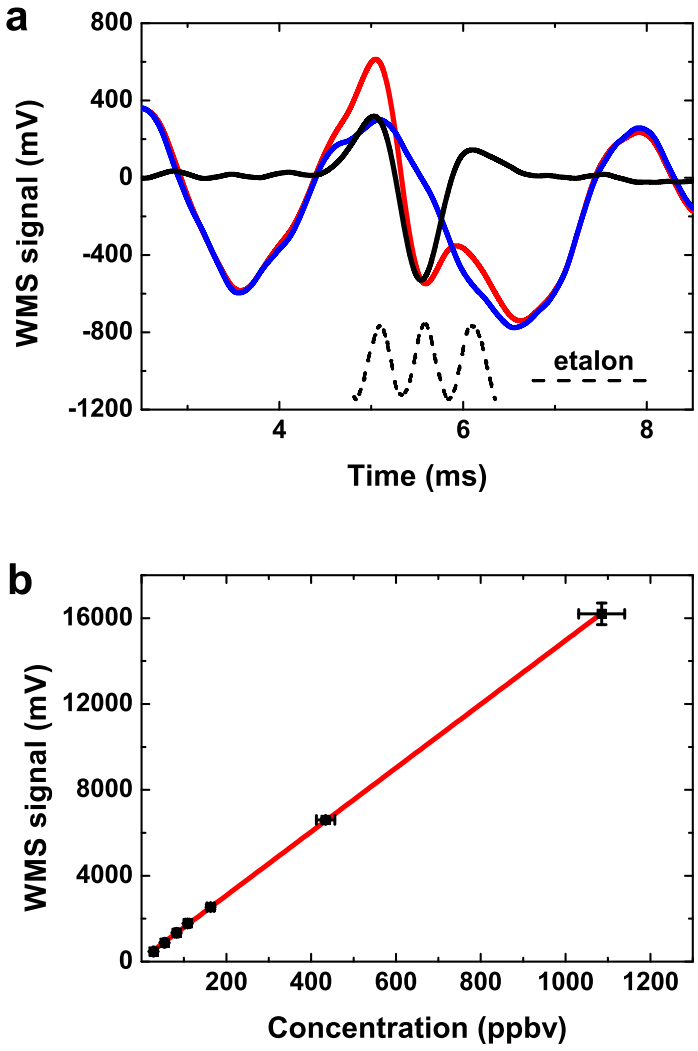

Figure 4.2: *Example of the 2nd harmonic wavelength modulation signal while scanning across a 50 ppbv ethane absorption peak at 2996.9 cm^{-1}. The red line represents the raw data, the blue line shows the background signal and the black solid line is the data with the background subtracted. The dashed line is the fringes pattern from the 5-cm-thick Ge etalon with FSR ∼1.1 GHz and FWHM ∼500 MHz. (b) Second derivative WMS signal due to ethane peak at 2996.9 cm^{-1} measured at different concentrations between 28 and 1085 ppbv. A linear dependence on the concentration is shown with the fitted red line. Each concentration was measured three times. The detection limit determined from the data is 0.8 ppbv over 1.3 second, corresponding to a NEAS of 1.2 × 10^{-9} $cm^{-1}/Hz^{1/2}$.*

TDS3032B) connected to the PC and data acquisition card (National Instruments PCI-6229).

4.3 Results and discussion

Scans were made over an ethane (C_2H_6) absorption feature at 2996.9 cm^{-1} to determine the sensitivity of the wavelength modulation system and to demonstrate the linear response at different concentrations. For this we used a calibrated mixture of 21.7 ppmv $\pm$ 5% (parts-per-million by volume) C_2H_6 in nitrogen (Air Liquide). To fill the multiple pass with calibrated concentrations down to the low part-sper-billion level (ppbv) two mass flow controllers (Brooks Instrument, model 5850, 5 l/h) were used to dynamically dilute the calibrated ethane mixture with pure nitrogen (Air Liquide), varying the flow rates through the mass flow controllers. To even dilute the mixture further a second stage of two mass flow controllers was used at the exit of the first pair. In such a way the applied ethane concentration could be diluted in a controlled way by a factor 103, meanwhile keeping a constant pressure inside the detection cell which was usually set in the range of 100–300 mbar during different experiments. With a cell volume of 300 ml and an operating pressure of 250 mbar this results in an effective gas volume of 75 ml. For a flow rate of 5 l/h this corresponds to a ventilation time of 54 s.

Figure 4.2a shows the second derivative signal for the absorption line of 50 ppbv ethane with and without background signal subtraction. For this, the phase and DBR sections of the diode laser were synchronously scanned by applying a 100 Hz saw tooth signal to each of the sections with the appropriate amplitude and DC offsets. Signals represent a 128 sweep average containing 10 000 points collected on the oscilloscope in 1.3 s. The strong interference fringes in the background signal are caused by overlap of the beam spots within the multi-pass cell. Even utilizing antireflection coated optical components such as windows and lenses, a time-dependent variation was observed in the background signal during frequency scans. The background was, therefore, measured with a pure nitrogen fill in the multipass cell before each new concentration point was recorded and then subsequently subtracted.

The ethane absorption was determined by the peak-peak value of the second derivative at different concentrations ranging from 28 to 1085 ppbv (Fig. 4.2b). WMS does not provide a real absorption signal; the harmonic component is directly proportional to the species concentration [15]. For each concentration, three measurement points were taken representing an average of 128 sweeps over the absorption feature. The linear fit with an R-square value of 0.9998 can be observed over a large dynamic range of concentrations. The detection limit (1σ) of the WMS recordings was determined as 0.8 ppbv in 1.3 second for the 76 meter absorption path length, which corresponds to a NEAS of 1.2×10^{-9} $cm^{-1}/Hz^{1/2}$ [16]. This proves that the OPO based WMS is a powerful tool

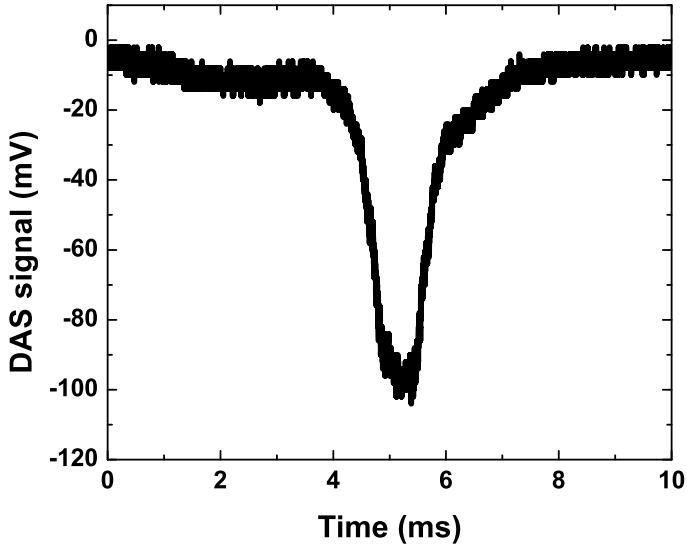

Figure 4.3: *DAS signal of 2 ppmv of ethane at 2996.9 cm^{-1} measured by using a 76-meter multiple pass cell. The signal is collected from 1000 averages recorded in 1 s.*

for a trace gas detection, providing simultaneously with a ppbv level of sensitivity and a second time resolution.

Using only direct absorption spectroscopy (DAS) with the 76-meter multi-pass cell we achieved a detection limit of ∼100 ppbv (∼1000 scans, acquisition time 1 s). As an example of DAS measurements 2 ppmv absorption signal of C_2H_6 is shown on the Fig 4.3. This particular absorption feature consists of dozens of individual lines which are not resolved under the conditions used in the experiments here. This also has an effect on the WM measurements which do not show the nice pictures that you normally have when measuring individual lines. In spite of the 125 times worse sensitivity DAS has some advantages over WMS: the lack of a lock-in amplifier and the possibility of having of a laser scanning rate, limited only by the laser. In WMS, the laser scanning rate is limited, because the modulation frequency has to be orders of magnitude higher than the scanning frequency for best performance. In our experiments with WMS we have used a 100 Hz laser scanning rate instead of the potentially available few kHz. As such, for a high gas concentration and the necessity of a fast time response DAS could be advantageous.

For comparison, we performed next to the 2nd harmonic detection in WMS addi-

tional experiments using the 1st and 4th harmonic absorption derivatives. Figure 4.4a and Fig 4.5a show examples of 50 ppbv for the first and fourth derivatives signal of ethane at the same wavelength (2996.9 cm^{-1}). Figure 4.4b and Fig 4.5b show the linear response (with their linear fits) of the signal for the range of concentrations from 28 to 160 ppbv for the first and fourth harmonics, respectively. These measurements were done at 160 mbar pressure inside the absorption cell and the scanning rate of the laser of 100 Hz. This allows determining the detection limit as 0.9 ppbv of ethane in 1.3 second for both cases, giving comparable results with the second derivative experiment of a noise equivalent absorption sensitivity of 1.3×10^{-9} $cm^{-1}/Hz^{1/2}$.

Although we used various parameters (time constant, pressures) in order to measure the 1st, 2nd and 4th harmonics with the lock-in amplifier we get similar results in NEAS values, the signals are higher at the 1st harmonic, the noise values increase proportionally, resulting in comparable signal-to-noise values. Besides this, depending on the background fringe pattern periodicity (caused by the etalon effect between the mirrors in the detection cell) it is in our case more advantageous to measure at the 2nd and 4th harmonic due to the higher contrast factor. This can be easily seen comparing Figs. 4.2a, 4.4a and 4.5a. A concentration of 50 ppbv ethane was measured in all cases, but the raw signal of the 4th harmonic (red line Fig. 4.5a) intuitively gives more information about the real absorption signal than the raw 2nd harmonic signal (red line Fig. 4.2a) and even more than the 1st (red line Fig. 4.4a). It can be useful to work with the 4th harmonic because of the presence of many time-dependent variables in the experiment, such as pressure and temperature of the cell, gas flow mixture into the cell, wavelength stability of the laser, etc. To be more precise and to be able to compare various results we have measured regularly the background signal between each concentration point to correct the data.

The above experiments are devoted to single gas detection, while in life sciences the study of physiological processes frequently requires monitoring of a number of gases, simultaneously. The advantage of using this OPO in comparison to other laser sources is its wide tunability from 3 to 4 μm, giving an opportunity to detect several gaseous compounds in one laser scan. The whole OPO tuning range can be used as the multipass cell is equipped with metallic mirrors with broadband reflection spectra from the visible to mid infrared. To extend the scanning range the crystal temperature is changed. To record a range of 35.4 cm^{-1} three pump laser scans (6.5 seconds per scan) were made at different PP-MgO-LN crystal temperatures. Figure 4.6a depicts the 2nd harmonic signal of a 100 mbar mixture of lab air and ethane. In the spectrum absorption peaks are visible of ethane (5.9 ppmv), methane (1.2 ppmv) and water (0.9%, calibrated with a hygrometer). The spectra for these gases were also calculated based on HITRAN data [17] using a pseudo-Voigt profile [18], which are presented on the Fig. 4.6b.

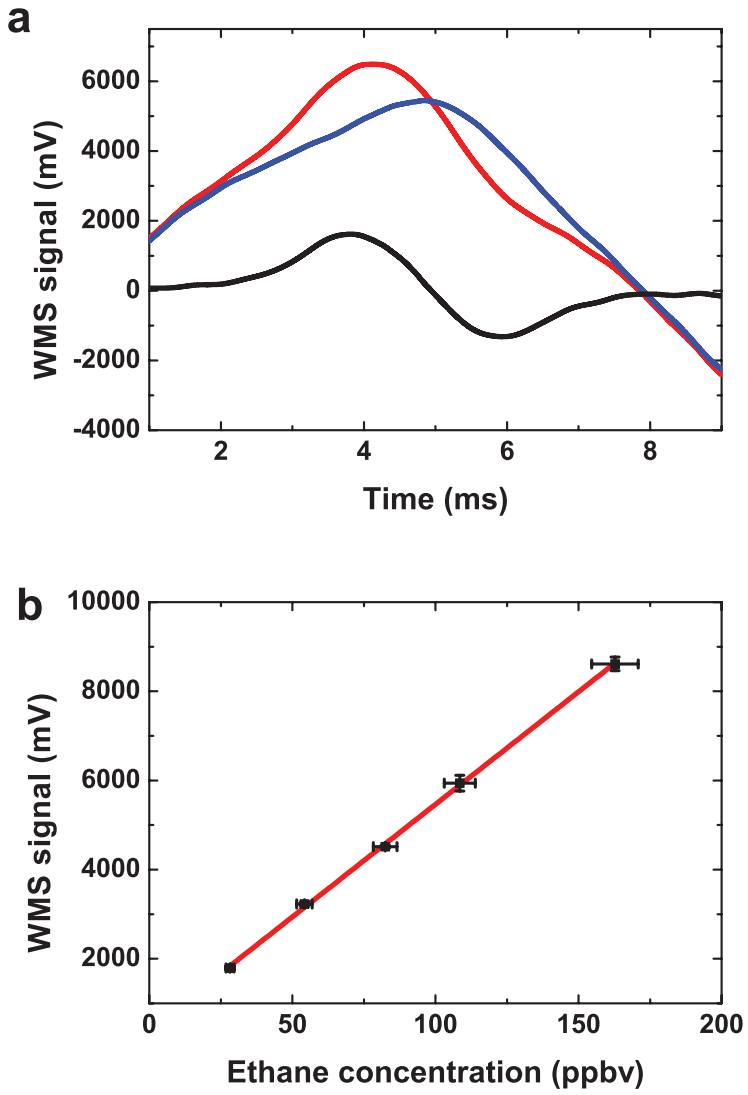

Figure 4.4: *(a) Example of the 1st harmonic WMS signal while scanning across a 50 ppbv ethane absorption peak at 2996.9 cm^{-1}. The red line represents the raw data, the blue line shows the background signal and the black line is the data with the background subtracted. (b) First derivative WMS signal due to the ethane peak at 2996.9 cm^{-1} measured at different concentrations between 28 and 160 ppbv. A linear dependence on the concentration is shown with the fitted red line. Each concentration was measured three times. The detection limit determined from the data is 0.9 ppbv over 1.3 second, corresponding to a NEAS of 1.3×10^{-9} $cm^{-1}/Hz^{1/2}$.*

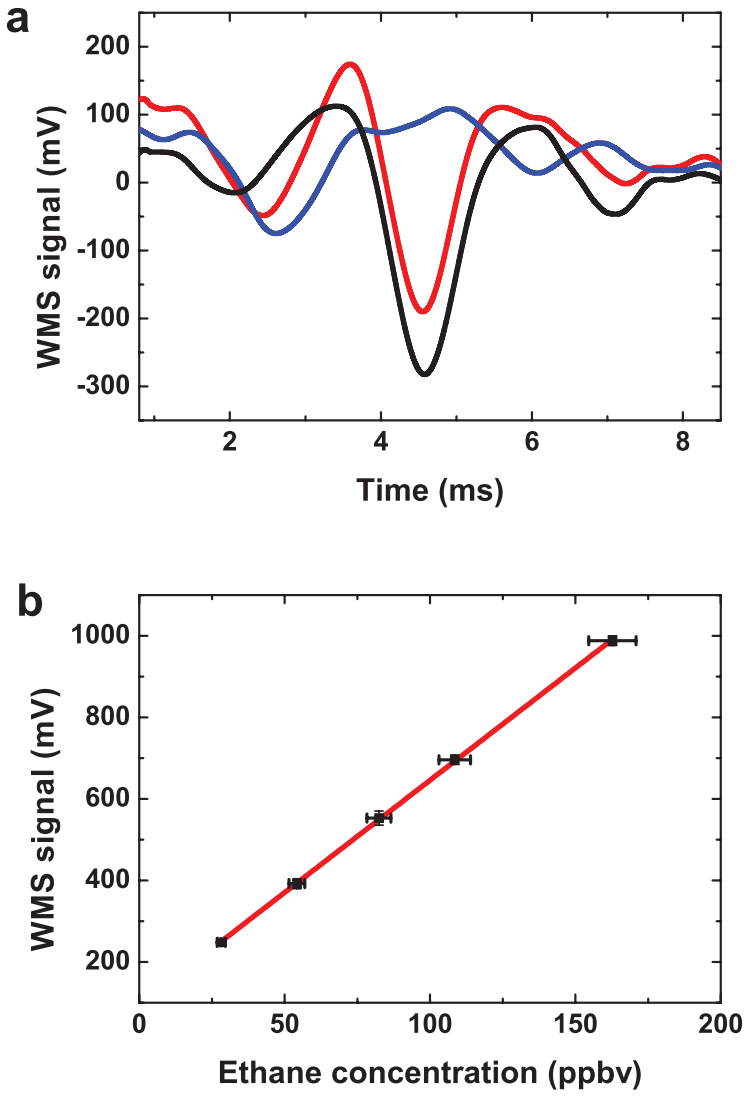

Figure 4.5: *(a) Example of the 4th harmonic WMS signal while scanning across a 50 ppbv ethane absorption peak at 2996.9 cm^{-1}. The red line represents the raw data, the blue line shows the background signal and the black line is the data with the background subtracted. (b) Fourth derivative WMS signal due to ethane peak at 2996.9 cm^{-1} measured at different concentrations between 28 and 160 ppbv. A linear dependence on the concentration is shown with the fitted red line. Each concentration was measured three times. The detection limit determined from the data is 0.9 ppbv over 1.3 second, corresponding to a NEAS of 1.3×10^{-9} $cm^{-1}/Hz^{1/2}$.*

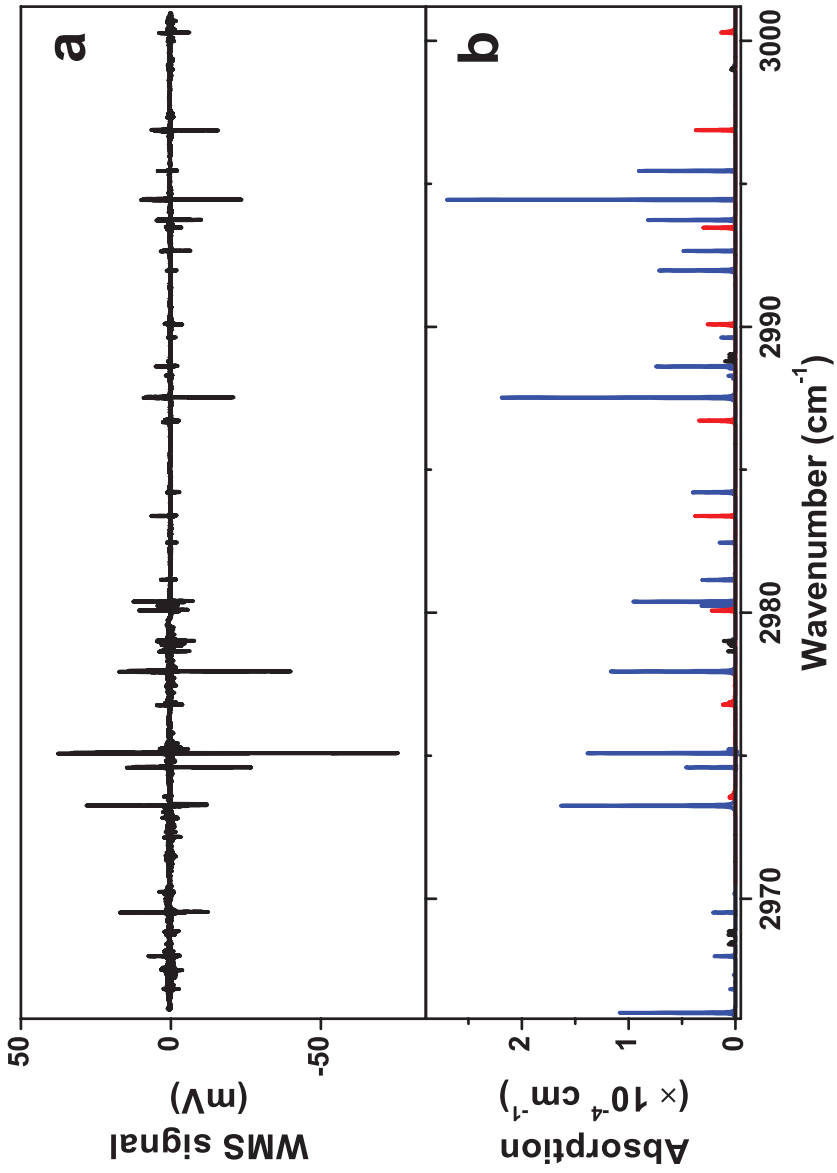

Figure 4.6: *(a) Wide-range WMS recorded using 2nd harmonic detection. The 100 mbar gas in the multi-pass cell consisted of 5.9 ppmv ethane, 1.2 ppmv methane and 0.9% water. The 35.4 cm^{-1} range was covered by making three pump laser scans at different PP-MgO-LN crystal temperatures to shift the idler wavelength to another spectral window. (b) Calculated spectrum based on HITRAN data for 5.9 ppmv ethane (red line), 1.2 ppmv methane (black line) and 0.9% water (blue line).*

4.4 Conclusions

The detection limit of 0.8 ppbv, measured in 1.3 seconds (NEAS of 1.2×10^{-9} cm^{-1}/Hz$^{1/2}$) for ethane clearly demonstrates that a SR-OPO, pumped by a fiber-amplified diode laser, in combination with WMS using a multiple pass cell, can be a powerful tool for rapid and sensitive trace gas detection in the wavelength tuning range of the OPO between 3–4μm. Moreover, the approach allows recording over a wide spectral range (see Fig. 4.6), which offers attractive possibilities for capturing multi-component gas mixtures. Such utilities are necessary for applications within Life Science, which require a fast, sensitive detector with multi-component capabilities. The OPO enables recording of several individual absorption lines, spread over a wider spectroscopic range ignoring other spectroscopic features in between. In general the sensitivity of wavelength modulation spectroscopy is limited, due to the fringe patterns on the background signal that are induced by etalon effects between optic elements. This can be improved by recording the background signal and the total gas absorption signal, simultaneously. As such, most fringes and time-dependent fluctuations can be canceled out, thereby improving the sensitivity.

Acknowledgements This research was financially supported by the Dutch Technology Foundation STW and the European Commission under the program New and Emerging Science and Technologies, contract number FP6-NESTA-0025043 'Optical Nose'. I.D. Lindsay acknowledges support of the European Commission in the form of a Marie Curie Intra-European Fellowship.

References

[1] T. C. J. Turlings, U. B. Lengwiler, M. L. Bernasconi, and D. Wechsler, "Timing of induced volatile emissions in maize seedlings," vol. 207, pp. 146–152, 1998.

[2] A. Kessler and I. T. Baldwin, "Defensive function of herbivore-induced plant volatile emissions in nature," vol. 291, pp. 2141–2144, 2001.

[3] S. K. Hetz and T. J. Bradley, "Insects breathe discontinuously to avoid oxygen toxicity," vol. 433, pp. 516–519, 2005.

[4] B. W. M. Moeskops, H. Naus, S. M. Cristescu, and F. J. M. Harren, "Quantum cascade laser-based carbon monoxide detection on a second time scale from human breath," *Appl. Phys. B*, vol. 82, pp. 649–654, 2006.

[5] G. Berden and R. P. G. Meijer, "Cavity ring-down spectroscopy: Experimental schemes and applications," *Int. Rev. Phys. Chem.*, vol. 19, pp. 565–607, 2000.

[6] P. Werle, K. Maurer, and F. D. T. L. A. P. R. Kormann, R. Mucke, "Spectroscopic gas analyzers based on

indium-phosphide, antimonide and lead-salt diode-lasers," *Spectrochim. Acta A*, vol. 58, pp. 2361–2372, 2002.

[7] I. D. Lindsay, P. Gros, J. Lee, B. Adhimoolam, and K. J. Boller, "Mid-infrared wavelength- and frequencymodulation spectroscopy with a pump-modulated singly-resonant optical parametric oscillator," *Opt. Express*, vol. 14, pp. 12341–12346, 2006.

[8] A. K. Y. Ngai, S. T. Persijn, I. D. Lindsay, A. A. Kosterev, P. Gross, C. J. Lee, S. M. Cristescu, F. K. Tittel, K. J. Boller, and F. J. M. Harren, "Continuous wave optical parametric oscillator for quartz-enhanced photoacoustic trace gas sensing," *Appl. Phys. B*, vol. 89, pp. 123–128, 2007.

[9] I. D. Lindsay, B. Adhimoolam, P. Gross, M. E. Klein, and K. J. Boller *Opt. Express*, vol. 13, pp. 1234–1239, 2005.

[10] A. K. Y. Ngai, S. T. Persijn, G. von Basum, and F. J. M. Harren, "Automatically tunable continuous-wave optical parametric oscillator for high-resolution spectroscopy and sensitive trace-gas detection," *Appl. Phys. B*, vol. 85, pp. 173–180, 2006.

[11] M. M. J. W. van Herpen, S. E. Bisson, A. K. Y. Ngai, and F. J. M. Harren, "Combined wide pump tuning and high power of a continuous-wave, singly resonant optical parametric oscillator," *Appl. Phys. B*, vol. 78, pp. 281–286, 2004.

[12] P. Werle, R. Mucke, and F. Slemr *Appl. Phys. B*, vol. 57, pp. 131–139, 1993.

[13] S. M. Cristescu, S. T. Persijn, S. te Lintel Hekkert, and F. J. M. Harren, "Laser-based systems for trace gas detection in life sciences," *Appl. Phys. B*, vol. 92, pp. 343–349, 2008.

[14] B. W. M. Moeskops, S. M. Cristescu, and F. J. M. Harren, "Sub-part-per-billion monitoring of nitric oxide by use of wavelength modulation spectroscopy in combination with a thermoelectrically cooled, continuous-wave quantum cascade laser," *Opt. Lett.*, vol. 31, pp. 823–825, 2006.

[15] P. Werle, "A review of recent advances in semiconductor laser based gas monitors," *Spectrochim. Acta A*, vol. 54, pp. 197–236, 1998.

[16] E. J. Moyer, D. S. Sayres, G. S. Engel, J. M. S. Clair, F. N. Keutsch, N. T. Allen, J. H. Krol, and J. G. Anderson, "Design considerations in high-sensitivity off-axis integrated cavity output spectroscopy," *Appl. Phys. B*, vol. 92, pp. 467–474, 2008.

[17] L. S. Rothman, I. E. Gordon, A. Barbe, D. C. Benner, P. F. Bernath, M. Birk, V. Boudon, L. R. Brown, A. Campargue, J.-P. Champion, K. Chance, L. H. Coudert, V. Dana, V. M. Devi, S. Fally, J.-M. Flaud, R. R. Gamache, A. Goldman, D. Jacquemart, I. Kleiner, N. Lacome, W. J. Lafferty, J.-Y. Mandin, S. T. Massie, S. N. Mikhailenko, C. E. Miller, N. Moazzen-Ahmadi, O. V. Naumenko, A. V. Nikitin, J. Orphal, V. I. Perevalov, A. Perrin, A. Predoi-Cross, C. P. Rinsland, M. Rotger, M. Simeckova, M. A. H. Smith, K. Sung, S. A. Tashkun, J. Tennyson, R. A. Toth, A. C. Vandaele, and J. V. Auwera, "The hitran 2008 molecular spectroscopic database," *J. Quantum Spectrosc. Radiat. Transf.*, vol. 110, pp. 533–572, 2009.

[18] Y. Y. Liu, J. L. Lin, G. M. Huang, Y. Q. Guo, and C. X. Duan *J. Opt. Soc. Am. B*, vol. 18, pp. 666–, 2001.

Chapter 5

Optical Parametric Oscillator based Off-Axis Integrated Cavity Output Spectroscopy for rapid chemical sensing

Abstract

An optical parametric oscillator (OPO), pumped by a fiber-amplified diode laser, is combined with off-axis integrated cavity output spectroscopy (OA-ICOS). The cw OPO (power 1.2 W, tunability 3–4 μm, 5 cm^{-1} mode-hop-free tuning) has a tuning speed of 100 THz/s, which is ideal for rapid and sensitive trace gas detection. Combined with OA-ICOS, a detection limit of 50 parts per trillion by volume (1×10^{12}) of ethane (C_2H_6) in nitrogen was obtained in 0.25 s at 2997 cm^{-1}, corresponding to a noise equivalent absorption sensitivity of 4.8×10^{-11} $cm^{-1}Hz^{-1/2}$. The system demonstrates real-time measurements of methane and water in exhaled human breath.

This work has been published in:
D. D. Arslanov, S. M. Cristescu, and F. J. M. Harren, "Optical parametric oscillator based off-axis integrated cavity output spectroscopy for rapid chemical sensing" Opt. Lett. **35**, 3300-3302 (2010).

5.1 Introduction

Trace gases are distinctive markers of biological processes occurring in plants, animals, and humans [1–3]. An excellent method for highly sensitive and selective detection of these volatile organic compounds is laser spectroscopy in the mid-IR wavelength region; at that wavelength, many molecules have strong distinctive absorption patterns [2]. It is of most interest to capture gas-mixing concentrations at a subsecond time scale, e.g., to investigate the reaction of an insect or plant on an environmental change, but also to monitor during the single breath of a human subject. Next to blood, urine, or tissue sampling, the breath test can be important in yielding clinical information for diagnosis of diseased states or to monitor therapy [4]. The major advantage of analyzing on-line exhaled breath is that it is noninvasive, represents minimal risk, and can be sampled repetitively, thereby avoiding the risks taken during off-line gas analysis, in which systematic errors can be introduced during collection, concentration, and transport of the sample. Here, on-line analysis means that the sample is taken during the last part of the exhalation. Since this period is only a few seconds,wedeveloped a fast-scanning cw OPO, pumped by a fiber-amplified diode laser [5, 6] in combination with a fast spectroscopic trace-gas detection scheme.

There are several basic laser-based spectroscopic techniques, such as photoacoustic spectroscopy (PAS), wavelength modulation spectroscopy, cavity ring-down spectroscopy (CRDS), and integrated cavity output spectroscopy (ICOS), also called cavity-enhanced absorption spectroscop. PAS can be very sensitive and efficient owing to its easy alignment and simple use; however, it cannot be used at a subsecond time scale [2, 7]. Wavelength modulation [8] is in general less sensitive than the cavity enhanced methods CRDS and ICOS.Within ICOS [9, 10], a gas-detection cell is used with two highly reflective end mirrors (>99.9%), resulting in a very high finesse cavity [ratio between the free spectral range (FSR) and FWHM of the cavity mode: $F > 8000$]. In contrast to cw CRDS [11], the laser light is not locked on each cavity mode but swept over the gas absorption line. Moreover, opposite to on-axis alignment at the center of the optical cavity, off-axis injection of the laser light (OA-ICOS) into the cavity will generate spatially separated, multiple reflections within the cavity before the reentrant condition of the optical beam is fulfilled. Therefore, OA-ICOS is effectively lowering the FSR of the cavity, producing a dense mode structure [12, 13]. In a successful off-axis alignment, many cavity modes exist underneath every molecular transition and the laser linewidth should be broad with regard to the FSR of the cavity, but narrow with regard to the molecular line. Even narrowband lasers couple to many cavity modes simultaneously, which gives alignment robustness at the cost of cavity throughput power. One big advantage of OA-ICOS as compared with CRDS is that it can be used without limitations concerning ring-down time or mode matching between the laser frequency and the FSR.

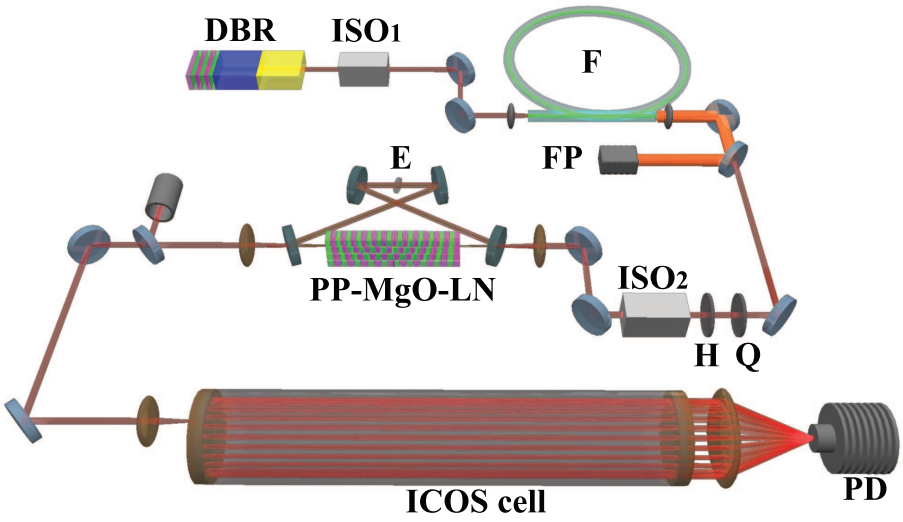

Figure 5.1: *Experimental setup. DBR, distributed Bragg reflector diode laser; ISO*1 *and* 2*, isolators; F, double-clad Yb-doped fiber; FP, fiber pump diode-laser bar; Q, quarter-wave plate; H, half-wave plate; PP − MgO − LN, MgO-doped periodically poled lithium niobate crystal; E, intracavity etalon; ICOScell, integrated cavity output spectroscopy cell; PD, photodetector.*

5.2 Experimental

Our experimental setup is shown on the Fig. 5.1 and is described elsewhere [5]. An 80 mW multisection distributed Bragg reflector (DBR) diode laser (Eagleyard Photonics) with an output wavelength at 1082 nm is used to seed a 30-m-long double-clad Yb-doped fiber amplifier (F), which is pumped by a 25 W fiber-coupled 976 nm cw diode-laser bar (FP). Two isolators (ISO 1 and 2) are used to prevent any feedback, while a quarter-wave plate (Q) and half-wave plates (H) are for polarization control. An output power of 7.5 W is then available. By synchronized tuning of the phase section of the DBR laser, 3 cm^{-1} wide mode-hop-free tuning ranges can be achieved at scanning rates of 1 kHz. Slower scanning rates will cover a wider wavelength range (e.g., 5 cm^{-1} at 100 Hz). The effective output linewidth of the DBR laser is 100 MHz. The singly resonant cw OPO cavity consists of a four-mirror bow-tie ring design. The pump beam was focused in a 5% MgO-doped periodically poled lithium niobate crystal with seven poling periods ranging from 28.5 to 31.5 μm. The crystal was placed in an oven capable of maintaining temperatures from 20 °C to 200 °C with a stability of 0.02 °C. Up to 1.2 W of idler output was produced at a pump power of 7.5 W.

ForOA-ICOS, the high-finesse optical cavitywasformed by a pair of highly reflective

(R $\sim$ 99.98 % at 3.3 μm, Nova- Wave Technology) 2 in. diameter (1 in. = 2.54 cm) concave (R = 1 m) mirrors and a 60-cm-long stainless steel tube with an inner diameter of 40 mm with two inlets/outlets for gas exchange. The transmitted laser intensity was focused by an off-axis parabolic mirror (not shown) and a secondary lens (f = 5 cm) to the fast (HgCdZnTe) thermoelectrically cooled photodetector (VIGO Systems PDI-2TE-4), which has a time response of 20 ns.

5.3 Results and discussion

The absorption is measured as an integrated signal from all the light transmitted through the cavity (see Fig. 5.1). We investigated if the signal-to-noise ratio (SNR) can be increased by aligning the cell more off-axis [12–14]. For that, each end of the cell was attached to an independent twodimensional translation stage. After proper on-axis alignment, both ends were translated orthogonally to the cavity axis in ahorizontal direction-collinear over the samelength. As such, the laser beam draws a horizontal line on the mirror surfaces. Then the mirrorswere translated vertically for the double length, but in opposite directions. In this case, the beamforms a circular pattern on each mirror with a diameter depending on the translation length. To study the offaxis alignment,we used a mixture of 20 parts per billion by volume (ppbv, 1×10^{-9}) of ethane(C_2H_6) in nitrogen,which was continuously flushed throughthe cell with a flowspeed of 5 l/h, creating a homogenous distributed gasmixture at a constant pressure of 250 mbar. The pressure was kept at this constant value by using a pump, mass flow controllers, and a needle valve. The laser scans were made over an ethane absorption feature at 2996.9 cm^{-1}. Various off-axis alignment distanceswereappliedandthe results are shown in Figs. 2 and 3(a). Each data point was recorded at a laser scanning rate of 1 kHz and an integration time of 0.25 s. Fig. 5.2 shows clearly the difference between on-axis and off-axis alignment at 7, 21, and 35 mm diameter of the circular pattern. Fig. 5.3(a) shows the increase of SNR, due to the fact that the signal stays at almost the same level for the different off-axis parameters,while the noise is decreased considerably.

The SNR can be also increased by increasing the scan speed of the laser. Fig. 5.3(b) shows, at a fixed off-axis diameter (35 mm), the results of various scanning rates between 32 Hz and 2 kHz. The noise decreases when the signal is integrated over more scans in the fixed time frame of 0.25 s. To determine the overall sensitivity of the OPO-based OA-ICOS setup, several ethane concentrations were recorded at 2996.9 cm^{-1}. A linear response (not shown) allows determining a detection limit of 50 parts per trillion by volume (pptv, 1×10^{-12}) of C_2H_6 measured in 0.25 s. This corresponds to a noise equivalent absorption sensitivity [10] of 4.8×10^{-11} $cm^{-1}Hz^{-1/2}$, the lowest value achieved in the mid-IR region at around 3.3 μm up to now.

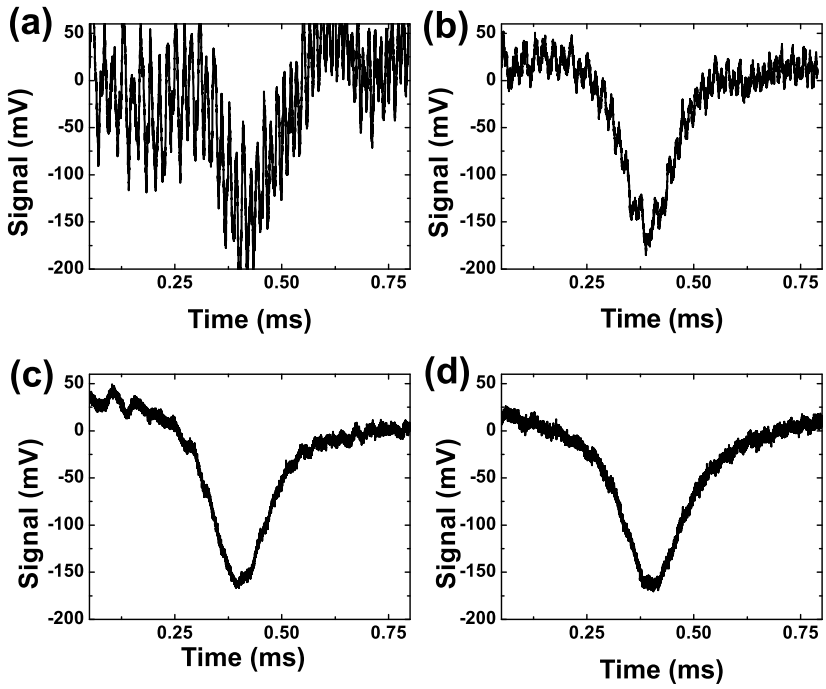

Figure 5.2: *20 ppbv of ethane (C_2H_6) mixture in nitrogen recorded in 0.25 s at a scanning rate of 1 kHz and a wavelength of 2996.9 cm^{-1} for the cases (a) almost on-axis alignment, (b) 7 mm diameter off-axis alignment, (c) 21 mm, and (d) 35 mm.*

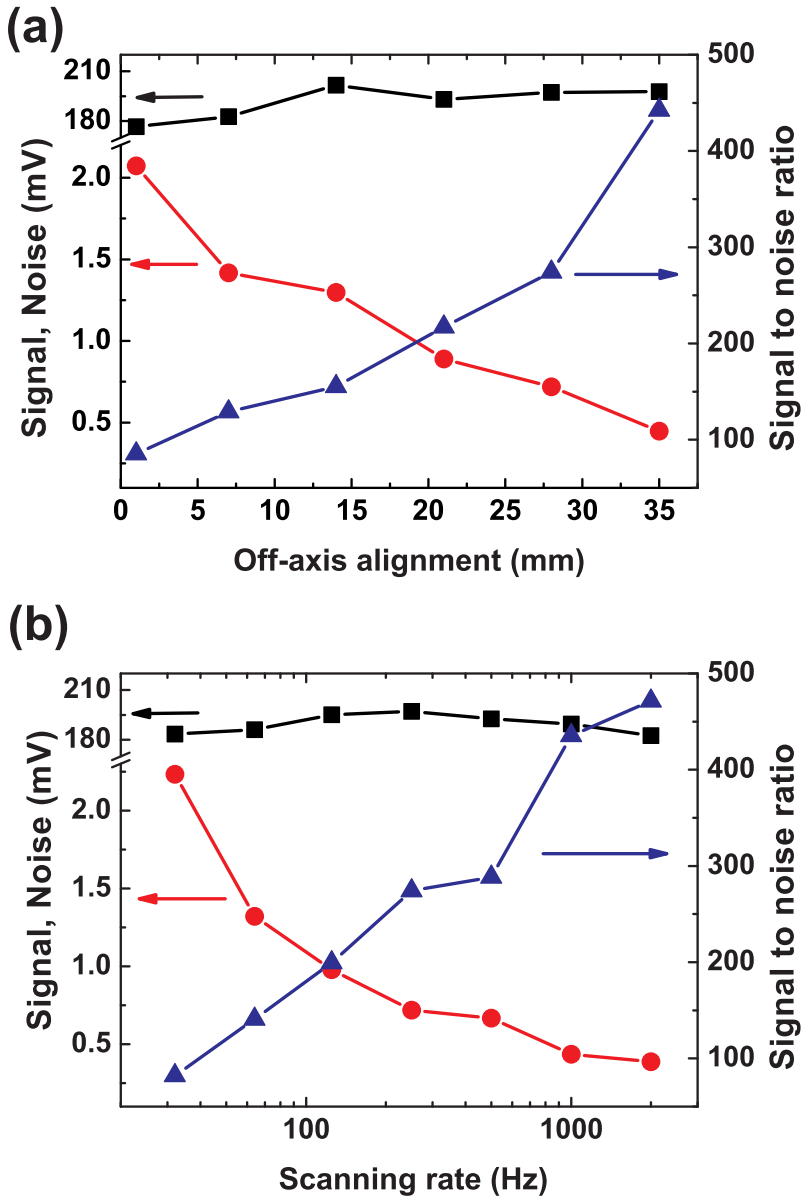

Figure 5.3: *Signal (squares, left vertical scale), noise (circles, left scale), and SNR (triangles, right vertical scale) depending on (a) off-axis alignment parameter at a scanning rate of 1 kHz, and on (b) scanning rate at a fixed off-axis diameter of 35 mm.*

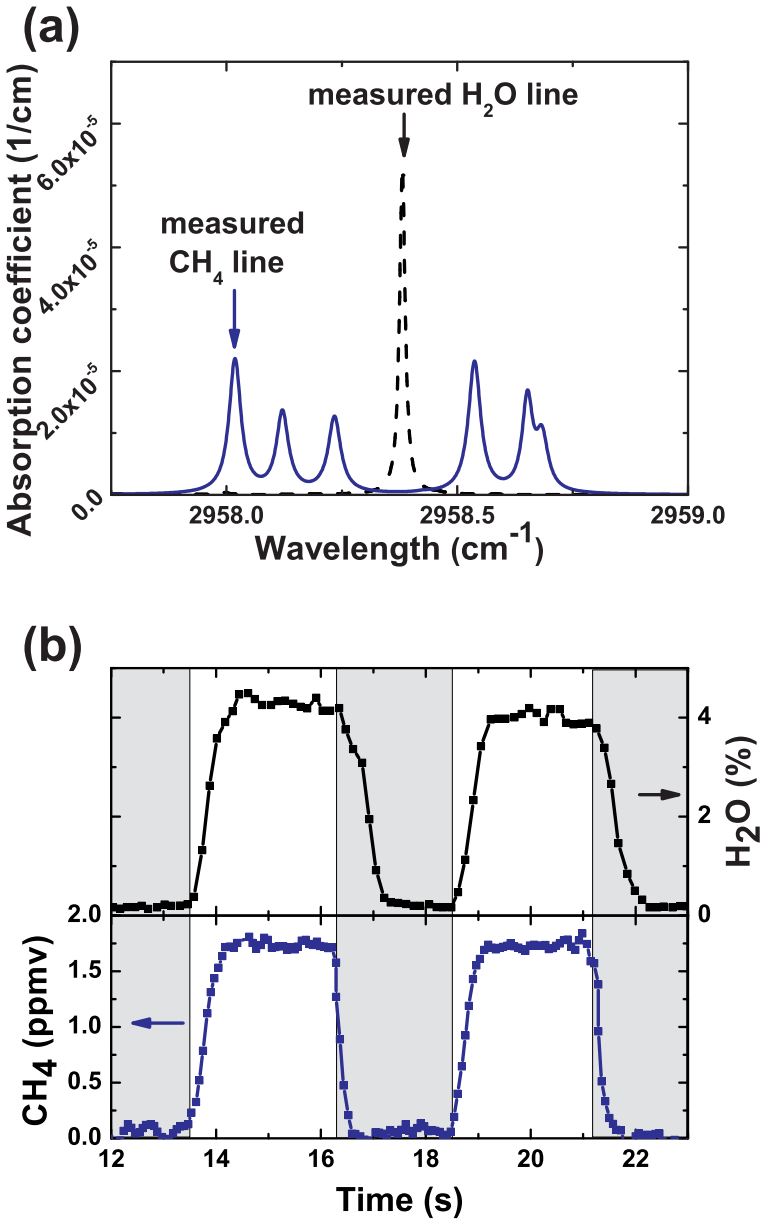

Figure 5.4: *(a) Simulated spectra for 1 cm path length and a pressure of 250 mbar of 1.7 ppmv of methane (solid curve) and 2% of water (dashed curve) based on HITRAN 2008 database. (b) Dynamics of water (upper graph, right scale) and methane (lower graph, left scale) concentration measured in exhaled human breath, in real time. White sections correspond to exhalation, gray to inhalation.*

The setup was used to measure methane (CH_4) and water concentrations in exhaled human breath, in real time. Even if the person does not havemethanogenic bacteria in his or her intestines that is emitting elevated CH_4 levels in the exhaled breath, the exhaled methane concentration will be equal to the inhaled atmospheric methane concentration, which has an average value of 1.7 parts per million by volume (ppmv, 1×10^{-6}) [15] The measurements were performed at the top of the methane line at 2958 cm^{-1} and the water line at 2958.4 cm^{-1} at a pressure of 250 mbar. The simulation spectra for the 1.7 ppmv of methane and 2% of water based on the HITRAN 2008 database [16] are shown on the Fig. 5.4(a). For this experiment, a high-capacity vacuum pump (15 l/ min) was used to keep up with the human exhalation speed. For exhalation, a two-way nonrebreathing T-shape valve (Hans Rudolph Inc.) [17] was used. During inhalation (via the nose), the cell was flushed with nitrogen [Fig. 5.4(b)]. During exhalation, the nitrogen flow was blocked and exhaled air went into the cell. Fig. 5.4(b) represents the methane and water concentration dynamics during breathing. It clearly shows a subsecond (0.1 s) time resolution for the measurements.

5.4 Conclusion

In summary, the results clearly show that an OPO, pumped by a fiber-amplified diode laser, in combination with OA-ICOS is a powerful tool for the rapid and sensitive detection of trace gases. This approach can be easily extended to multicomponent gas detection and real applications in life sciences. Here, we demonstrate on-line breath sampling that requires detection capability at the ppbv level for multiple gas compounds at a subsecond time resolution.

References

[1] A. Kessler and I. T. Baldwin, "Defensive function of herbivore-induced plant volatile emissions in nature," *Science*, vol. 291, pp. 2141–2144, 2001.

[2] S. M. Cristescu, S. T. Persijn, S. te Lintel Hekkert, and F. J. M. Harren, "Laser-based systems for trace gas detection in life sciences," *Appl. Phys. B*, vol. 92, pp. 343–349, 2008.

[3] S. K. Hetz and T. J. Bradley, "Insects breathe discontinuously to avoid oxygen toxicity," *Nature*, vol. 433, pp. 516–519, 2005.

[4] T. H. Rysby, "Volatile organic compounds as markers in normal and diseased states," in *Disease markers in exhaled breath: Basic mechanisms and clinical applications* (N. Marczin and M. H. Yacoub, eds.), pp. 113–122, NATO ASI Series, Baltimore, USA: IOS Press, 2002.

[5] I. D. Lindsay, B. Adhimoolam, P. Gross, M. E. Klein, and K. J. Boller, "110ghz rapid, continuous tuning from an optical parametric oscillator pumped by a fiber-amplified dbr diode laser," *Opt. Expr*, vol. 13, pp. 1234–1239, 2005.

[6] A. K. Y. Ngai, S. T. Persijn, I. D. Lindsay, A. A. Kosterev, P. Gross, C. J. Lee, S. M. Cristescu, F. K. Tittel,

K. J. Boller, and F. J. M. Harren, "Continuous wave optical parametric oscillator for quartz-enhanced photoacoustic trace gas sensing," *Appl. Phys. B*, vol. 89, pp. 123–128, 2007.

[7] J. A. de Gouw, S. T. L. Hekkert, J. Mellqvist, C. Warneke, E. L. Atlas, F. C. Fehsenfeld, A. Fried, G. J. Frost, F. J. M. Harren, J. S. Holloway, B. Lefer, R. Lueb, J. F. Meagher, D. D. Parrish, M. Patel, L. Pope, D. Richter, C. Rivera, T. B. Ryerson, J. Samuelsson, J. Walega, R. A. Washenfelder, P. Weibring, and X. Zhu, "Airborne measurements of ethene from industrial sources using laser photo-acoustic spectroscopy," *Environ. Sci. Technol.*, vol. 43, pp. 2437–2442, 2009.

[8] B. W. M. Moeskops, S. M. Cristescu, and F. J. M. Harren, "Sub-part-per-billion monitoring of nitric oxide by use of wavelength modulation spectroscopy in combination with a thermoelectrically cooled, continuous-wave quantum cascade laser," *Opt. Lett*, vol. 31, pp. 823–825, 2006.

[9] A. O'Keefe, J. J. Scherer, and J. B. Paul, "cw integrated cavity output spectroscopy," *Chem. Phys. Lett.*, vol. 307, pp. 343–349, 1999.

[10] E. J. Moyer, D. S. Sayres, G. S. Engel, J. M. S. Clair, F. N. Keutsch, N. T. Allen, J. H. Kroll, and J. G. Anderson, "Design considerations in high-sensitivity off-axis integrated cavity output spectroscopy," *Appl. Phys. B*, vol. 92, pp. 467–474, 2008.

[11] J. Morville, S. Kassi, M. CHenevier, and D. Romanini, "Fast, low-noise, mode-by-mode, cavity-enhanced absorption spectroscopy by diode-laser self-locking," *Appl. Phys. B*, vol. 80, pp. 1027–1038, 2005.

[12] G. S. Engel, W. S. Drisdell, F. N. Keutsch, E. J. Moeyr, and J. G. Anderson, "Ultrasensitive near-infrared integrated cavity output spectroscopy technique for detection of co at 1.57 ?m: new sensitivity limits for absorption measurements in passive optical cavities," *Appl. Opt*, vol. 45, pp. 9221–9229, 2006.

[13] D. S. Baer, J. B. Paul, M. Gupta, and A. O'Keefe, "Sensitive absorption measurements in the near-infrared region using off-axis integrated-cavity-output spectroscopy," *Appl. Phys. B*, vol. 75, pp. 261–265, 2002.

[14] J. B. Paul, L. Lapson, and J. G. Anderson, "Ultrasensitive absorption spectroscopy with a high-finesse optical cavity and off-axis alignment," *Appl. Opt.*, vol. 40, pp. 4904–4910, 2001.

[15] T. T. Groot, P. M. van Bodegom, F. J. M. Harren, and H. A. J. Meijer, "Quantification of methane oxidation in the rice rhizosphere 13c-labelled methane," *Biogeochemistry*, vol. 64, pp. 355–372, 2003.

[16] L. S. Rothman, I. E. Gordon, A. Barbe, D. C. Benner, P. F. Bernath, M. Birk, V. Boudon, L. R. Brown, A. Campargue, J.-P. Champion, K. Chance, L. H. Coudert, V. Dana, V. M. Devi, S. Fally, J.-M. Flaud, R. R. Gamache, A. Goldman, D. Jacquemart, I. Kleiner, N. Lacome, W. J. Lafferty, J.-Y. Mandin, S. T. Massie, S. N. Mikhailenko, C. E. Miller, N. Moazzen-Ahmadi, O. V. Naumenko, A. V. Nikitin, J. Orphal, V. I. Perevalov, A. Perrin, A. Predoi-Cross, C. P. Rinsland, M. Rotger, M. Simeckova, M. A. H. Smith, K. Sung, S. A. Tashkun, J. Tennyson, R. A. Toth, A. C. Vandaele, and J. V. Auwera, "The hitran 2008 molecular spectroscopic database," *J. Quantum Spectrosc. Radiat. Transf.*, vol. 110, pp. 533–572, 2009.

[17] F. J. M. Harren, R. Berkelmans, K. Kuiper, R. D. P. H. S. te Lintel Hekkert, P. Scheepers, and D. H. Parker *Appl. Phys. Lett.*, vol. 74, pp. 1761–1763, 1999.

Chapter 6

Real-time, subsecond, multicomponent breath analysis by Optical Parametric Oscillator based Off-Axis Integrated Cavity Output Spectroscopy

Abstract

Breath analysis is an attractive field of research, due to its high potential for non-invasive medical diagnostics. Among others, laser-based absorption spectroscopy is an excellent method for the detection of gases in exhaled breath, because it can combine a high sensitivity with a good selectivity, and a high temporal resolution. Here, we use a fast-scanning continuous wave, singly-resonant Optical Parametric Oscillator (wavelength range between 3 and 4 μm, linewidth 40 MHz, output power $>$ 1 W, scanning speed 100 THz/s) with Off-Axis Integrated Cavity Output Spectroscopy for rapid and sensitive trace gas detection. Real-time, low ppbv detection of ethane is demonstrated in exhaled human breath during free exhalations. Also, simultaneous, real-time multi-component gas detection of ethane, methane and water was performed in exhaled breath using a

This work has been published in:
D. D. Arslanov, K. Swinkels, S. M. Cristescu, and F. J. M. Harren, "Real-time, subsecond, multicomponent breath analysis by Optical Parametric Oscillator based Off-Axis Integrated Cavity Output Spectroscopy" Opt. Express, **19** 24078–24089 (2011).

wide spectral coverage over 17 cm^{-1} in 1 second. Furthermore, real time detection of acetone, a molecule with a wide absorption spectrum, was shown in exhaled breath, with a sub-second time resolution (0.4 s).

6.1 Introduction

Breathing is an important process that provides our body with oxygen but also removes carbon dioxide from the body. It is a complex process of gas exchange in the alveoli by diffusion of gasses over the lung capillaries. Our exhaled breath consist of 15-18% O_2, 4-6% CO_2, 5% H_2O, ppmv-levels of H_2 and CO, around 0.5-1 ppmv (parts-per-million by volume, 1×10^{-6}) NH_3, several hundreds of ppbv (parts-per-billion by volume, 1×10^{-9}) of acetone, methanol, ethanol, and many other volatile organic compounds (VOCs) at ppbv and pptv level (parts-per-trillion by volume, 1×10^{-12}) level [1]. The source of exhaled gases can be of exogenous origin via inspiration air or the skin, via ingested foods or beverages; it can be produced in the mouth, nose, sinuses and airways, or can come from the blood via the alveolar-capillary junction in the lungs [1]. In general, the amount and composition of exhaled VOCs vary per subject and within a subject over time. Especially, diseases or metabolic disorders will change the production of VOCs. Produced locally, they are spread over the entire body and reach the lungs via the blood circulation. Hence, breath analysis is an attractive and promising field for diagnostics and monitoring in medicine. It is non-invasive and safe, and allows easy sample collection, even from very sick, old people or neonates. It provides physicians and patients with real-time results, which is important for early disease diagnostics.

The last decade, a large amount of clinical and scientific studies are performed using breath analysis. Nowadays, a number of fundamental problems still needs attention in breath analysis; in particular with regard to preparation and storage of breath samples, proper realtime breath monitoring, and correlating disease with the exhaled VOCs [2–4]. There are more than thousand different gases found in exhaled breath [5], but only detectors for O_2, CO_2, CO, H_2, methane (CH_4) and nitric oxide (NO) are widely used in commercial devices. Yet, there are other known indicators that relate to a certain diseases or disorders. For example, acetone (C_3H_6O) is related to diabetes, dietary fat losses, congestive heart failure, brain seizure and lung cancer; ethane (C_2H_6) is related to lipid peroxidation and oxidative stress; methane is associated with intestinal problems and colonic fermentation [5, 6]. However, the detailed formation mechanism for some of these indicators is not well understood. Hence, it is important to quantify amount and timing of gaseous indicators in relation to a disease, detecting their sensitivity at trace gas concentration level.

In the past, several detection methods were used for trace gas measurements in biomedical applications, ranging from mass spectrometry [6], gas chromatography [6],

chemiluminescence [7], electronic nose [8], to different laser-based spectroscopic methods [5, 9–14] . As many molecular gases have strong absorption in the mid-IR wavelength region, it is advantageous to use laser absorption spectroscopy; it is an excellent method for highly sensitive and selective detection of VOCs. While a gas cell is filled with a sample gas, the wavelength of the laser is tuned over an absorption line of the gas under investigation. According to Lambert-Beer's law, the transmitted laser intensity, detected on a photodetector, depends on the absorption strength of the gas at that wavelength, the gas concentration and the path length within the sampling cell. As each molecule has its own specific absorption spectrum in the mid-IR wavelength region, it is possible to determine gas concentration and to distinguish selectively molecules in a complex gas mixture.

A disadvantage of the breath analysis is that the gas composition of exhaled breath varies within one exhalation. The actual exhaled breath consist of contributions from different parts of the respiratory system: nose, mouth, upper/lower trachea, or the alveolar-capillary junction; hence, the gas concentration in exhaled breath varies over time. High finesse optical cavity methods are often used for breath studies. However, they are not always fulfilling real-time analysis criterion [15–17], have a narrow wavelength tuning range [18], do not have a continuous coverage of the wavelength tuning range [19], or use a low power laser source [20]. In addition there is a spectroscopic problem, larger VOCs have many more ro-vibational transitions than simpler molecules such as CH_4. Their rotational lines are not resolved; therefore, the spectrum is broad and structureless. Thus, a tunable laser system over a wide wavelength range is needed to properly detect such VOCs.

Usually, laser spectroscopy deals with the detection of one molecule as function of time. Although, there are systems which allow measuring several gases simultaneously, they are often complex, expensive [21], and contain several laser sources [22], or have a relatively slow wavelength tuning scheme [23]. Here we aim to overcome these issues and built, based on Optical Parametric Oscillator spectroscopy, a sensitive and selective trace gas detector with a sub-second time resolution, and tunable over a wide wavelength range for simultaneous multicomponent detection.

In our recent work [13] we have shown that fast scanning continuous wave Singly-Resonant Optical Parametric Oscillator (SRO) incorporated with Off-Axis Integrated Cavity Output Spectroscopy (OA-ICOS) is a powerful tool for rapid and sensitive trace gas detection. A detection of 50 pptv of ethane (C_2H_6) measured in 0.25 s. was determined [13]. The noise equivalent detection limit of 25 pptv/$Hz^{1/2}$ is found to be almost in 20 times better than the one determined in [24] of 0.48 ppbv/$Hz^{1/2}$ for ethane when using OA-ICOS with an interband cascade laser. This definitely proves the suitability of our setup to perform human exhaled breath ethane measurements. The sensitivity of OA-ICOS is comparable to other spectroscopic techniques such as Cavity Ring Down Spectroscopy (CRDS) and Photoacoustic (PA) spectroscopy, known for their high-quality

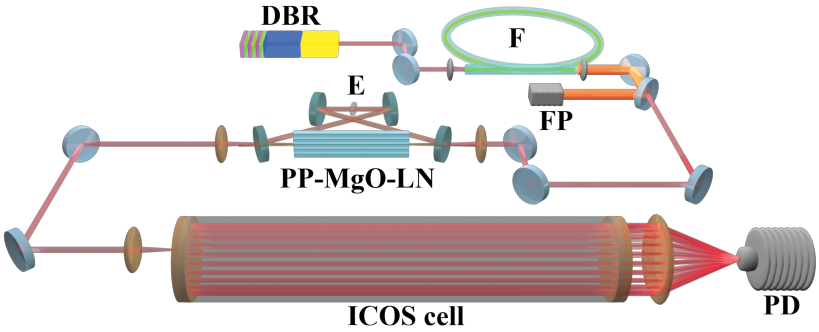

Figure 6.1: *Experimental setup of the Optical Parametric Oscillator pumped by a fiber amplified DBR laser incorporated with ICOS setup. DBR- Distributed Bragg Reflector diode laser, F double clad Yb-doped fiber, FP- fiber pump diode laser bar, PP − MgO − LN- MgO-doped periodically poled lithium niobate crystal, E- intra-cavity etalon, ICOScell- integrated cavity output spectroscopy cell, PD- photodetector.*

detection limits [5, 25, 26]. The advantage of Integrated Cavity Output Spectroscopy (ICOS) is that the recording time can be much shorter than for CRDS or PA, because it is not a resonant technique and there are no slow response elements (such as microphones). Here, the developed setup gives us the opportunity to evolve a real-time breath analysis system, measuring ethane during free exhalation; perform real-time multicomponent detection of water, ethane and methane with a time resolution of 0.1 s; and detect acetone with a time resolution of 0.4 s in exhaled human breath taking advantage of the fast, wide spectral coverage (17 cm^{-1} recorded in 1 s) of the OPO.

6.2 Experimental setup

6.2.1 Optical parametric oscillator Integrated Cavity Output Spectroscopy (ICOS)

The experimental setup of the SRO pumped by a fiber-amplified diode laser based ICOS is shown in Fig. 6.1 and was described earlier in detail [13]. Here only a short description is given. An 80 mW multisection Distributed Bragg Reflector (DBR) diode laser (Eagleyard Photonics) with an output wavelength of 1082 nm seeds a 30 m long double-clad Yb-doped fiber (F), which is pumped by a 25 W fiber-coupled 976 nm cw diode-laser bar (FP). Two isolators (not shown) are used to prevent feedback, while a quarter-wave plate and half-wave plates (not shown) are used for polarization control and for gauging of a total output power of up to 7.5 W. The gain section within the DBR laser is used to generate the output wavelength, while the phase and Bragg sections are used to tune the output wavelength by applying the currents through the resistors attached to these

sections. By synchronized tuning of the phase and the Bragg section of the DBR laser, 3 cm^{-1} wide mode-hop-free tuning ranges can be achieved at scanning rates of 1 kHz. Slower scanning rates will cover a wider wavelength range (e.g. 5 cm^{-1} at 100 Hz). The effective output linewidth of the DBR laser is 40 MHz. The cw SRO cavity consists of a four- irror bow-tie ring design. The pump beam is focused in a quasiphase matched 5% MgO-doped periodically poled lithium niobate crystal (PP-MgO-LN) with seven poling periods ranging from 28.5 to 31.5 μm. The crystal was placed in an oven capable of maintaining temperatures from 20°C to 200°C with a stability of 0.02°C. A 400 μm thick YAG intracavity etalon (E) was inserted into the SRO cavity for the frequency stabilization. For course wavelength generation, the appropriate crystal poling period and temperature are chosen, after that DBR laser tuning was used for the fast mode-hop-free tuning of the output wavelength of the OPO. The wavelength was monitored with a wavelength meter (WA-1000, Burleigh; not shown), whereas during experiments Fabry-Perot etalon fringe pattern was used to measure the accurate relative wavelength. Up to 1.2 W of idler output was produced, at a pump power of 7.5 W.

For OA-ICOS, the high-finesse optical cavity (calculated finesse value F = 15700) consists of a pair of highly reflective, 2 inch diameter, concave mirrors (R = 99.98% at 3.3 μm, ROC = 1 m, Nova-Wave Technology) mounted on a 60 cm long stainless steel tube (inner diameter 40 mm) with two inlets/outlets for gas exchange. The transmitted laser intensity was focused via a lens on the fast thermoelectrically cooled photodetector (PD) with a time response of 20 ns (HgCdZnTe, VIGO Systems PDI-2TE-4). ICOS is more robust technique than the CRDS and less technically demanding. Similar to CRDS, the laser light is used to excite high finesse cavity modes, but the technique can be used without limitations concerning ring-down time or mode matching between the laser frequency and the free spectral range (FSR) of the cavity. In contrast to cw CRDS, the laser light is not locked on each cavity mode but swept over the gas absorption line. Off-axis injection of the laser beam into the ICOS cell increases effectively the cavity length; hence, the FSR of the cavity collapses and laser light can be coupled into the cell at many cavity modes, simultaneously. In a successful off-axis alignment many cavity modes exist under every molecular transition line, which decreases the mode noise [9, 27, 28].

6.2.2 On-line breath measurements

Figure 6.2 shows the scheme of the experimental setup for real-time breath analysis. The ICOS cell was pumped by a vacuum pump with a capacity of up to 230 ml/s (Edwards, model ESDP 30). This pump speed was chosen for a sub-second refreshing time of the cell, taking into account the flow rate (exhaled breath, 14 l/min) and the cell volume (1 l, effective volume 200 ml at 200 mbar pressure. Using smaller cell volumes or lower pressures will result in lower pump speeds, but can also lead to reduced sensitivities.

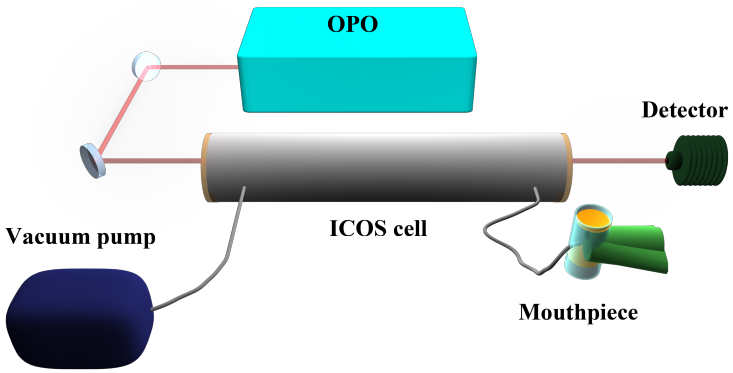

Figure 6.2: *Experimental setup for the real-time breath sampling. OPO- Optical Parametric Oscillator pumped by a fiber amplified diode laser, Vacuumpump- capacity 230 ml/s (Edwards, model ESDP 30), ICOScell- Integrated Cavity Output Spectroscopy cell, Mouthpiece- mouthpiece with a two-way non-rebreathing valve in T-shape configuration (Hans Rudolph inc.), Detector- HgCdZnTe photodetector (VIGO Systems PDI-2TE-4).*

Lab air was supplied as a background gas in the experiments in cases where high water, methane etc. concentrations did not influence the results. However, for precise measurements pure nitrogen gas was used. To deliver a gas sample into the cell a mouthpiece connected to a two-way non-rebreathing valve in T-shape configuration (Hans Rudolph inc.) was used. A small portion of the sample went to the conventional capnograph (Capnomac Ultima, Datex Ohmeda), which provided real-time carbon dioxide concentrations in exhaled breath.

6.3 Results and discussion

6.3.1 Real-time detection of ethane in exhaled breath

Rapid and sensitive trace gas detection was performed by measuring ethane in exhaled human breath. Figure 6.3(a) shows the 200 mbar broadened spectra for 1 ppbv ethane and 2% water using HITRAN 2008 database [29] in the wavelength range between 2970 cm^{-1} and 3005 cm^{-1}; the wavelength region around 2997 $cm^{-1}$was used for C_2H_6 detection, because it is free of H_2O interference. Figure 6.3(b) represents the same data in the range of 2996.4 cm^{-1} to 2997.6 cm^{-1}adding 5% carbon dioxide and 1.7 ppmv methane. The figure shows that ethane is spectroscopically well separated from the other gases, which are present at high concentrations in exhaled breath.

Although the absorption cross section of ethane is much higher than that of methane at 2996.9 cm^{-1}, methane is present in the atmosphere at a relatively high concentration

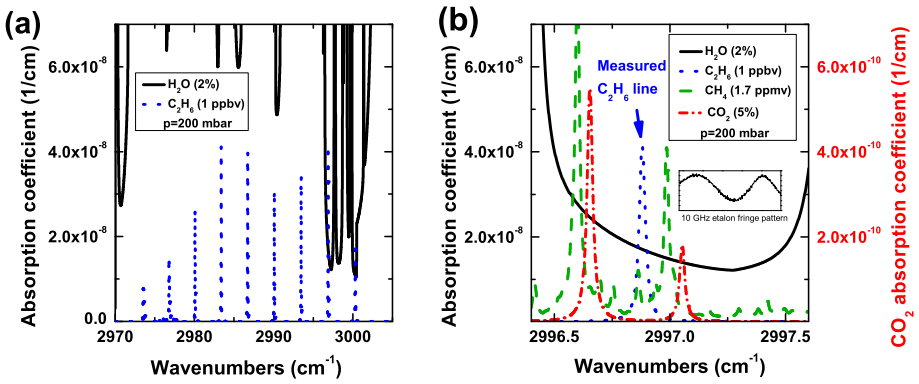

Figure 6.3: *Simulated spectra at a pressure of 200 mbar based on HITRAN 2008 database [29] for: (Panel a) 2% water (black solid line) and 1 ppbv ethane (blue dotted line) in the wavelength range 2970-3005 cm^{-1}; (Panel b) 2% water (black solid line, left vertical scale), 1 ppbv ethane (blue dotted line, left vertical scale), 1.7 ppmv methane (green dashed line, left vertical scale) and 5% carbon dioxide (red dot-dashed line, right vertical scale) in the wavelength range 2996.4-2997.6 cm^{-1}. Figure insertion shows etalon fringe pattern with free spectral range of 10 GHz for the fine wavelength tracking during long-term measurements.*

of 1.7 ppmv [30]; Fig. 6.3(b) indicates that absorption coefficients of 1 ppbv ethane and 1.7 ppmv methane are nearly equal at this wavelength. This shows that for precise measurements during long-term experiments the wavelength has to be controlled. However, the wavemeter (Wavemeter WA-1000 has a speed of 1 Hz) cannot follow the high scanning speeds, up to 100 THz/s, of the OPO [31]. Therefore, we measured the relative wavelength by tracking an etalon fringe pattern (see insertion in Fig. 6.3(b)); a 1.5 cm long, air-spaced etalon with a free spectral range of 10 GHz was used for this.

Real-time breath sampling of ethane was performed over the ethane absorption line at 2996.9 cm^{-1} (Fig. 6.3(b)) during free exhalation in multiple breaths. It is known that air contains ethane at a concentration level typically of between 1 and 10 ppbv [24]. Our lab air, which was used as background gas, contained ethane concentrations around 6 ppbv at the time of the measurements. Ethane data were taken at a laser scanning rate of 1 kHz over the absorption line and averaged over 256 scans. This resulted in a sampling time of 0.25 seconds. Figure 6.4(a) represents the dynamics of ethane (black solid line, left vertical scale) and carbon dioxide (red dotted line, right vertical scale) concentrations for a non-smoking subject. No difference was found in the ethane concentration between air and exhaled breath. Figure 6.4(b) shows similar measurements for a person half an hour after he smoked a cigarette. Here, the exhaled breath contained ethane at a concentration level of 11 ppbv, 5 ppbv higher than the background ethane concentration. That higher concentrations can be found is breath is seen in Fig. 6.5 , the exhaled breath of a smoker

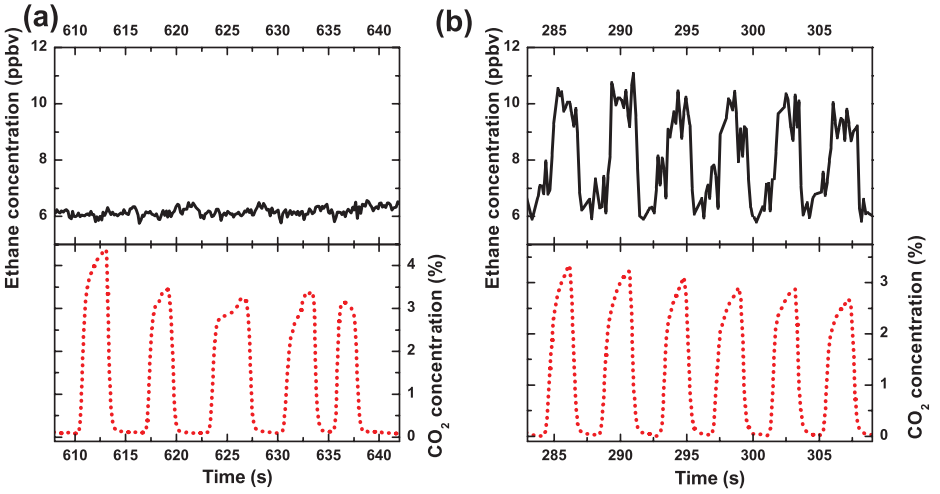

Figure 6.4: *Concentration dynamics of ethane during free exhalation in multiple breaths (black solid line, left vertical scale, measured with OPO based OA-ICOS) and carbon dioxide (red dotted line, right vertical scale, measured with capnograph (Capnomac Ultima, Datex Ohmeda): (Panel 4a) non-smoking subject, (Panel 4b) smoking subject half an hour after a cigarette was smoked.*

is showed over a period of 35 minutes, directly after smoking a sigarette; even after 40 minutes an elevated level of ethane is present in exhaled breath.

6.3.2 Real-time multi-component gas detection in exhaled breath

Using a spectral region within one mode-hop-free tuning range of the laser, containing absorption spectra of several gases, allows detection of multiple gases at high temporal resolution. Here, the spectroscopic range around 2997 cm^{-1} was used for simultaneous detection of ethane, methane and water in exhaled breath. Figure 6.6 represents the calculated spectra of these gases at this wavelength region. Experimentally, ethane (blue dotted line) was measured at the top of the 2996.9 cm^{-1} line, methane (green dashed line) at the top of the 2997 cm^{-1} and water (black solid line) at the top of the 2997.5 cm^{-1} line. Figure 6.7 shows the real-time measurements of concentration of C_2H_6 (blue dotted line), CH_4 (green dashed line), H_2O (black solid line) and CO_2 (red dash-dotted line) during free exhalation of three different subjects (panel a, b and c) at a time resolution of 0.13 s (256 scan averages at a 2 kHz repetition rate). Figure 6.7(a) shows the elevated level of ethane and methane in exhaled breath of the first subject, while Fig. 6.7(b) shows only the high level of methane for the second subject, and Fig. 6.7(c)- neither methane, nor ethane in exhaled breath of the third subject.

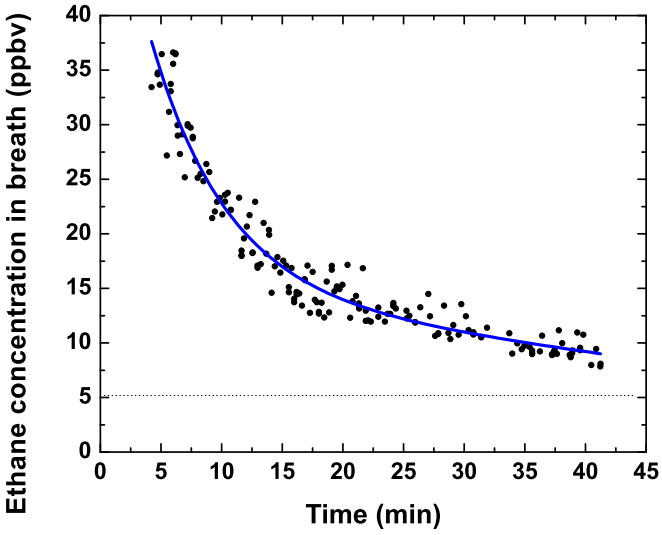

Figure 6.5: *Long-term measurements of ethane, exhaled by a smoking subject. Every dot corresponds to a concentration in a single, free exhalation. The blue solid line is an exponential fit of the experimental data. Dashed line at the bottom of the figure shows the level of ethane in air during measurements. Zero time corresponds to the moment when the last cigarette was smoked.*

6.3.3 Combining fast detection with a wide spectral coverage

Often, interesting absorption lines of different gases are found to be spectroscopically far from each other. Since the typical tuning range of narrowband laser sources is limited, a multi-component gas measurement is either not possible, or requires additional time to change the wavelength (e.g. by temperature), in order to detect another gas compound. In our setup, apart from a (maximum) 5 cm^{-1} mode-hop-free tuning range of the multi-section DBR laser, an overall 16.5 cm^{-1} tuning range, including mode hops, can be achieved [32]. By varying the current offsets of Bragg and phase section in the pump DBR diode laser mode hops in the pump laser can be avoided up to a tuning range of 5 cm^{-1}, a pump mode hop will induce a mode hop in the signal frequency and thus in the idler frequency. By scanning the pump laser at higher frequencies the total tuning range is considerably reduced to 2 cm^{-1}, the thermal expansion and thermal capacity in the phase and Bragg section is limiting this.

In contrast to the wide tuning range, with mode hops, shown earlier [32], in which a scan of 16.5 cm^{-1} was recorded in 2 min, we demonstrate here a quasi-mode-hope-free tuning over 17 cm^{-1} (2947-2964 cm^{-1}) in just 1 s (Fig. 6.8). The recorded spectrum consists of eight mode-hop-free regions of about 2 cm^{-1} width, which were merged

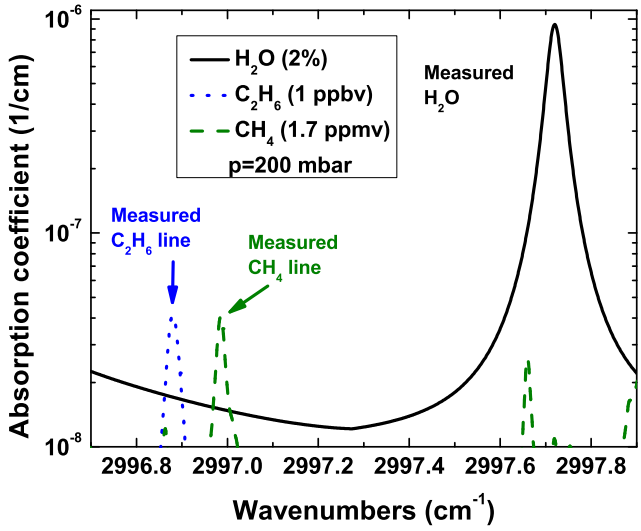

Figure 6.6: *Calculated spectra for water 2% (black solid line), ethane 1 ppbv (blue dotted line) and methane 1.7 ppmv (green dashed line) in the wavelength range between 2996.7 and 2997.9 cm^{-1} at a pressure of 200 mbar.*

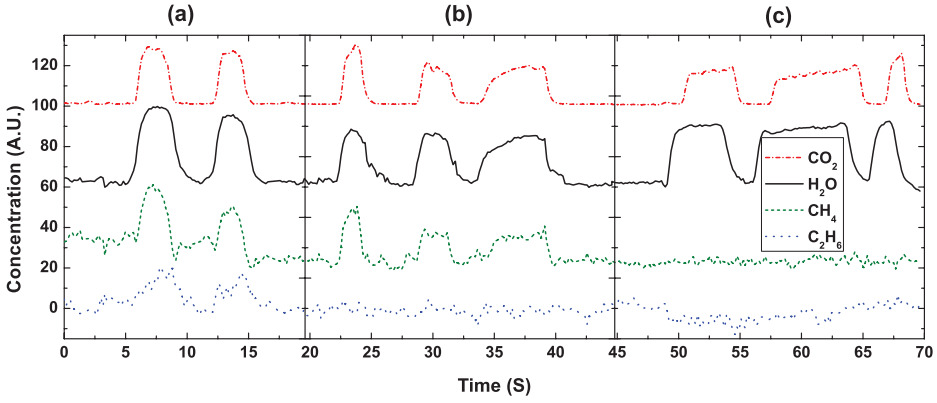

Figure 6.7: *Real-time multicomponent detection of water (black solid line), methane (green dashed line), carbon dioxide (red dash-dotted line) and ethane (blue dotted line) during free exhalation for three different persons: The first person (Panel 7a) shows elevated levels for both methane and ethane, while the second person (Panel 7b) shows only elevated level of methane, and person three (Panel 7c) shows neither elevated levels for methane nor ethane.*

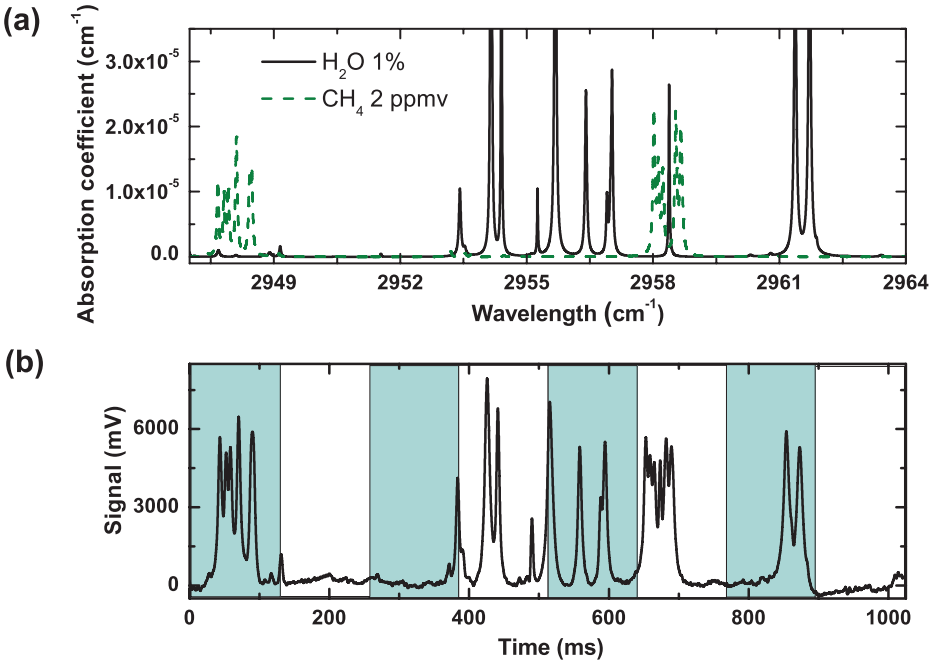

Figure 6.8: *(Panel a) Simulated spectra for 1% water (black solid line) and 2 ppmv methane (green dashed line) in the wavelength range between 2947 and 2964 cm^{-1}. (Panel b) A 17 cm long recorded spectrum of air in 1 s. The spectrum consists of eight mode-hop-free regions of about 2 cm^{-1} width. Each of eight mode-hop-free regions represents the result of 128 averages at a 1- kHz scanning rate and corresponds to certain current offsets for the Bragg and phase sections of the DBR laser. The recorded spectrum is found to be also in good agreement with the simulated spectrum shown on Fig. 6.8(a).*

together creating wide spectral coverage. Each of eight segments in Fig. 6.8(b) represents the result of a 128 averages recorded at a 1-kHz scanning rate of the laser each with a recording time of 0.13 s, and with a total recording time of 1 s for the complete 17 cm^{-1} wide spectrum. This spectrum (Fig. 6.8 b)) is found to be in good agreement with the simulated spectrum using the HITRAN 2008 database [29], for a mixture of 1% water and 2 ppmv methane (Fig. 6.8(a)).

6.3.4 Detection of acetone

It is generally known that larger molecules have broad absorption features, due to large amount of vibrational transitions and closely spaced rotational lines. It is, therefore, a challenge to measure larger VOCs with narrowband laser absorption spectroscopy.

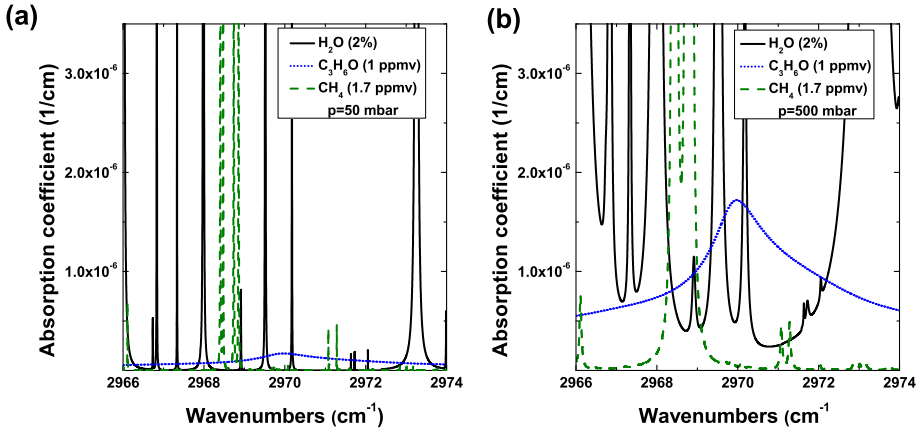

Figure 6.9: *Simulated spectra for 2% water (black solid line), 1 ppmv acetone (blue dotted line) and 1.7 ppmv methane (green dashed line) in the 2966-2974 cm^{-1} wavelength range for 50 mbar pressure (Panel a) and 500 mbar pressure (Panel b).*

On the other hand, broadband laser spectroscopy does not yield a high sensitivity and high spectral resolution and can, therefore, hardly applied for breath analysis. Here, we demonstrated that a wide spectrum can be recorded in 1 s time scale. This opens the possibility to detect larger molecules such as acetone with a high spectral and time resolution. Figure 6.9 shows the simulated spectra for water, methane and acetone in the 2969-2972 cm^{-1} wavelength region at 50 and 500 mbar, using the HITRAN 2008 [29] and PNNL [33] databases. Applying lower pressures in the detection cell will reduce the spectral interference of acetone with water, but consequently it reduces also the detection limit, because the absorption depends proportionally on the amount of acetone molecules present (i.e. pressure).

Figure 6.10 shows a real-time scan detecting acetone in exhaled breath in the wavelength range between 2967 cm^{-1} and 2973 cm^{-1}. Figure 6.10(a) represents spectra of lab air (upper blue line) and exhaled air (bottom red line). The result of subtraction of the exhaled breath spectrum from lab air is shown in Fig. 6.10(b), as the red line shows the fit with a Voigt profile. The wide absorption feature in the figure belongs to acetone, while other thinner lines are mostly water and methane lines. A scanning rate of the OPO of 1 kHz was used for these measurements. The total scan consists of three mode-hop-free regions. The data shown are the result of 128 scan averages for each of three mode-hop-free regions with a total recording time of 0.4 s.

The acetone concentration in the exhaled breath was measured to be 1 ppmv, based on performed calibration measurements (not shown), which leads to a detection limit of

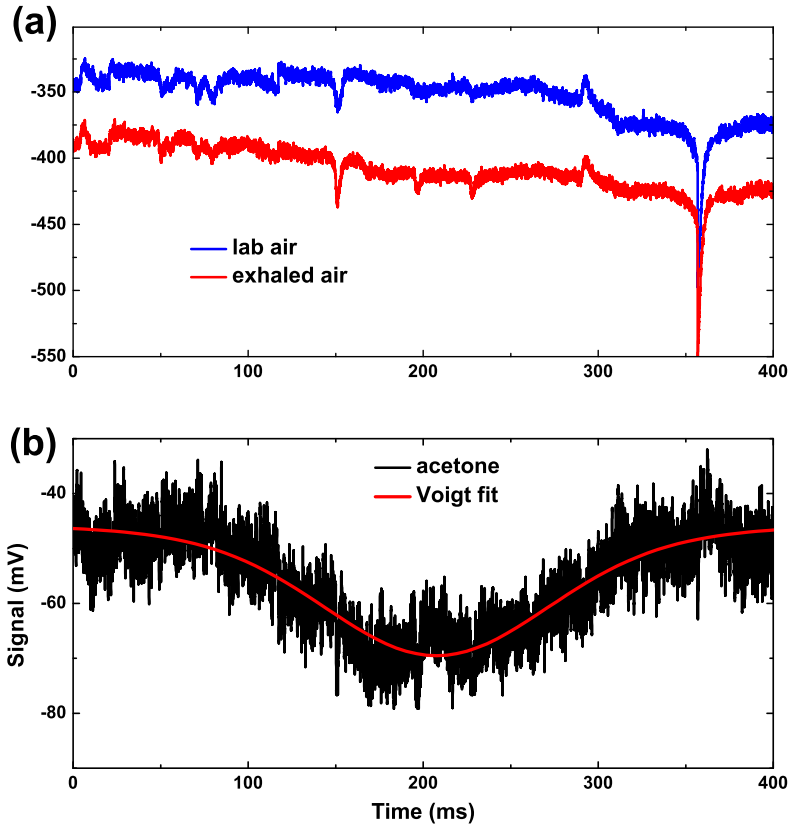

Figure 6.10: *Real-time measurements of acetone in exhaled human breath. Panel a: Upper blue line indicates a spectrum of lab air, the lower, red line shows exhaled human breath. Panel b: Black line represents the result of subtraction of both lines from panel a. The red curve is the fit with a Voigt profile of the spectrum.*

acetone of 100 ppbv. This detection limit can be improved by using a detector with better signal to noise ratio than the one we used during our experiments (HgCdZnTe, VIGO Systems PDI-2TE-4). Since typical adult exhaled breath concentrations are around 600 ppb [34], the equipment can be used for the real-time measurements of acetone in exhaled breath.

6.4 Conclusions

The cw OPO offers high power (>1 W), narrow linewidth and wide wavelength coverage in the wavelength range between 3 and 4 μm, where many molecules have strong

absorption lines. Compared with other sources of coherent radiation in the mid-IR, such as quantum cascade lasers and difference frequency generation (low output power of mW or even μW range), it is able to perform an excellent sensitivity for these gasses. This makes the OPO an attractive source for the laser-based absorption spectroscopy. In addition, OA-ICOS is a robust technique, insensitive for temperature fluctuations and mechanical vibrations and provides a sensitivity comparable to other techniques such as CRDS and PA. Furthermore, one of its biggest advantages is that the recording time depends only on the laser scanning speed, which can be as fast as 1 ms or less, for a single scan over a few cm^{-1}. Here, we have demonstrated that the combination of OPO and OA-ICOS is powerful for rapid and sensitive trace gas detection. It allowed real-time detection of ethane in exhaled human breath at lowpppbv level. Simultaneous multi-component gas detection of ethane, methane and water was performed in exhaled breath in real time at a time resolution of 0.1 s. Wide spectral coverage was recorded over 17 cm^{-1} in 1 second, which resulted in the detection of acetone in exhaled breath at sub-second time resolution (0.4 s). A noteworthy feature is the ability to perform real-time multicomponent trace gas detection in exhaled human breath even for larger VOCs, which is an important step forward in breath analysis.

Acknowledgements

This research was financially supported by the IOP Photonic Devices PD 55 "On-chip integrated NH3 human gas sensor" project. The authors would like to thank Cor Sikkens and Peter Claus (Radboud University Nijmegen, the Netherlands) for the technical help to complete the experiments.

References

[1] T. H. Risby and F. K. Tittel, “Current status of midinfrared quantum and interband cascade lasers for clinical breath analysis,” *Opt. Eng.*, vol. 49, pp. 11123–1–14, 2010.

[2] W. Miekisch, J. K. Schubert, and G. F. E. Noeldge-Schomburg, “Diagnostic potential of breath analysis-focus on volatile organic compounds,” *Clinica. Chimica. Acta.*, vol. 347, pp. 25–39, 2004.

[3] T. H. Risby, “Volatile organic compounds as markers in normal and diseased states,” in *Disease markers in exhaled breath: basic mechanisms and clinical applications* (N. Marczin and M. H. Yacoub, eds.), pp. 113–122, NATO ASI Series: IOS, 2002.

[4] T. H. Risby and S. F. Solga, “Current status of clinical breath analysis,” *Appl. Phys. B*, vol. 85, pp. 421–426, 2006.

[5] C. Wang and P. Sahay, “Breath analysis using laser spectroscopic techniques breath biomarkers, spectral fingerprints, and detection limits,” *Sensors*, vol. 9, pp. 8230–8262, 2009.

[6] B. Buszewski, M. Kesy, T. Ligor, and A. Amann, “Human exhaled air analytics: biomarkers of diseases,” *Biomed. Chromatogr.*, vol. 21, pp. 553–566, 2007.

[7] A. Artlich, B. Jonsson, M. Bhiladala, P. A. Lonnqvist, and L. E. Gustafsson, “Single breath analysis of ensogenous nitric oxide in the newborn,” *Biol.Neonate*, vol. 79, pp. 21–26, 2001.

[8] V. H. Tran, P. C. Hiang, M. Thurston, P. Jackson, C. Lewis, D. Yates, G. Bell, and P. S. Thomas, "Breath analysis of lung cancer patients using an electronic nose detection system," *IEEE Sens. J.*, vol. 10, pp. 1514–1518, 2010.

[9] G. Berden and R. Engeln, *Cavity Ring-Down Spectroscopy: Techniques and and Applications*. Wiley 2009.

[10] S. M. Cristescu, S. T. Persijn, S. te Lintel Hekkert, and F. J. M. Harren, "Laser-based systems for trace gas detection in life sciences," *Appl. Phys. B*, vol. 92, pp. 343–349, 2008.

[11] R. Lewicki, J. H. Doty, R. F. Curl, F. K. Tittel, and G. Wysocki, "Ultrasensitive detection of nitric oxide at 5.33 mum by using external cavity quantum cascade laser-based faraday rotation spectroscopy," *Proc. Natl. Acad. Sci. U.S.A.*, vol. 106, pp. 12587–12592, 2009.

[12] V. Spagnolo, A. A. Kosterev, L. Dong, R. Lewicki, and F. K. Tittel, "No trace gas sensor based on quartz-enhanced photoacoustic spectroscopy and external cavity quantum cascade laser," *Appl. Phys. B*, vol. 100, pp. 125–130, 2010.

[13] D. D. Arslanov, S. M. Cristescu, and F. J. M. Harren, "Optical parametric oscillator based off-axis integrated cavity output spectroscopy for rapid chemical sensing," *Opt. Lett.*, vol. 35, pp. 3300–3302, 2010.

[14] B. J. Orr and Y. He, "Rapidly swept continuous-wave cavity-ringdown spectroscopy," *Chem. Phys. Lett.*, vol. 512, pp. 1–20, 2011.

[15] E. R. Crosson, K. N. Ricci, B. A. Richman, F. C. Chilese, T. G. Owano, R. A. Provencal, M. W. Todd, J. Glasser, A. A. Kachanov, B. A. Paldus, T. G. Spence, and R. N. Zare, "Stable isotope ratios using cavity ring-down spectroscopy: Determination of 13c/12c for carbon dioxide in human breath," *Anal. Chem.*, vol. 74, pp. 2003–2007, 2002.

[16] M. L. Silva, D. M. Sonnenfroh, D. I. Rosen, M. G. Allen, and A. O'Keefe, "Integrated cavity output spectroscopy measurements of no levels in breath with a pulsed room-temperature qcl," *Appl. Phys. B*, vol. 81, pp. 705–710, 2005.

[17] J. Manne, O. Sukhorukov, W. Jager, and J. Tulip, "Pulsed quantum cascade laser-based cavity ring-down spectroscopy for ammonia detection in breath," *Appl. Opt.*, vol. 45, pp. 9230–9237, 2006.

[18] I. Ventrillard-Courtillot, T. Gonthiez, C. Clerici, and D. Romanini, "Multispecies breath analysis faster than a single respiratory cycle by optical-feedback cavity-enhanced absorption spectroscopy," *J. Biomed. Opt.*, vol. 14, pp. 064026–1–5, 2009.

[19] H. Dahnke, D. Kleine, P. Hering, and M. Murtz, "Real-time monitoring of ethane in human breath using mid-infrared cavity leak-out spectroscopy," *Appl. Phys. B*, vol. 72, pp. 971–975, 2001.

[20] D. Halmer, S. Thelen, P. Hering, and M. Murtz, "Online monitoring of ethane traces in exhaled breath with a difference frequency generation spectrometer," *Appl. Phys. B*, vol. 85, pp. 437–443, 2006.

[21] M. J. Thorpe, D. Balslev-Clausen, M. S. Kirchner, and J. Ye, "Cavity-enhanced optical frequency comb spectroscopy: application to human breath, analysis," *Opt. Exp.*, vol. 16, pp. 2387–2397, 2008.

[22] J. H. Shorter, D. D. Nelson, J. B. McManus, M. S. Zahniser, S. R. Sama, and D. K. Milton, "Clinical study of multiple breath biomarkers of asthma and copd (no, co2, co and n2o) by infrared laser spectroscopy," *J. Breath Res.*, vol. 5, pp. 037108–1–12, 2011.

[23] G. N. Rao and A. Karpf, "External cavity tunable quantum cascade lasers and their applications to trace gas monitoring," *Appl. Opt.*, vol. 50, pp. A100–A115, 2011.

[24] K. R. Parameswaran, D. I. Rosen, M. G. Allen, A. M. Ganz, and T. H. Risby, "Off-axis cavity output spectroscopy with a mid-infrared interband cascade laser for real-time breath ethane measurements," *Appl. Opt.*, vol. 48, pp. B73–B79, 2008.

[25] S. Persijn, F. Harren, and A. van der Veen, "Quantitative gas measurements using a versatile opo-based cavity ringdown spectrometer and the comparison with spectroscopic databases," *Appl. Phys. B*, vol. 100,

pp. 383–390, 2010.

[26] A. K. Y. Ngai, S. T. Persijn, G. von Basum, and F. J. M. Harren, "Automatically tunable continuous-wave optical parametric oscillator for high-resolution spectroscopy and sensitive trace-gas detection," *Appl. Phys. B*, vol. 85, pp. 173–180, 2006.

[27] J. B. Paul, L. Lapson, and J. G. Anderson, "Ultrasensitive absorption spectroscopy with a high-finesse optical cavity and off-axis alignment," *Appl. Opt.*, vol. 40, pp. 4904–4910, 2001.

[28] G. S. Engel, W. S. Drisdell, F. N. Keutsch, E. J. Moeyr, and J. G. Anderson, "Ultrasensitive near-infrared integrated cavity output spectroscopy technique for detection of co at 1.57 ?m: new sensitivity limits for absorption measurements in passive optical cavities," *Appl. Opt.*, vol. 45, pp. 9221–9229, 2006.

[29] L. S. Rothman, I. E. Gordon, A. Barbe, D. C. Benner, P. F. Bernath, M. Birk, V. Boudon, L. R. Brown, A. Campargue, J.-P. Champion, K. Chance, L. H. Coudert, V. Dana, V. M. Devi, S. Fally, J.-M. Flaud, R. R. Gamache, A. Goldman, D. Jacquemart, I. Kleiner, N. Lacome, W. J. Lafferty, J.-Y. Mandin, S. T. Massie, S. N. Mikhailenko, C. E. Miller, N. Moazzen-Ahmadi, O. V. Naumenko, A. V. Nikitin, J. Orphal, V. I. Perevalov, A. Perrin, A. Predoi-Cross, C. P. Rinsland, M. Rotger, M. Simeckova, M. A. H. Smith, K. Sung, S. A. Tashkun, J. Tennyson, R. A. Toth, A. C. Vandaele, and J. V. Auwera, "The hitran 2008 molecular spectroscopic database," *J. Quantum Spectrosc. Radiat. Transf.*, vol. 110, pp. 533–572, 2009.

[30] T. T. Groot, P. M. van Bodegom, F. J. M. Harren, and H. A. J. Meijer, "Quantification of methane oxidation in the rice rhizosphere 13c-labelled methane," *Biogeochemistry*, vol. 64, pp. 355–372, 2003.

[31] D. D. Arslanov, M. Spunei, A. K. Y. Ngai, S. M. Cristescu, I. D. Lindsay, S. T. Persijn, K. J. Boller, and F. J. M. Harren, "Rapid and sensitive trace gas detection with continuous wave optical parametric oscillator-based wavelength modulation spectroscopy," *Appl. Phys. B*, vol. 103, pp. 223–228, 2011.

[32] A. K. Y. Ngai, S. T. Persijn, I. D. Lindsay, A. A. Kosterev, P. Gross, C. J. Lee, S. M. Cristescu, F. K. Tittel, K. J. Boller, and F. J. M. Harren, "Continuous wave optical parametric oscillator for quartz-enhanced photoacoustic trace gas sensing," *Appl. Phys. B*, vol. 89, pp. 123–128, 2007.

[33] S. W. Sharpe, T. J. Johnson, R. L. Sams, P. M. Chu, G. C. Rhoderick, and P. A. Johnson, "Gas-phase databases for quantitative infrared spectroscopy," *Appl. Spectrosc.*, vol. 58, pp. 1452–1461, 2004.

[34] J. King, A. Kupferthaler, K. Unterkofler, H. Koc, S. Teschl, G. Teschl, W. Miekisch, J. Schubert, H. Hinterhuber, and A. Amann, "Isoprene and acetone concentration profiles during exercise on an ergometer," *J. Breath Res.*, vol. 3, 2009.

Chapter 7

Optical Parametric Oscillator based photoacoustic detection of Hydrogen Cyanide for bio-medical applications

Abstract

A versatile continuous wave optical parametric oscillator-based photoacoustic spectrometer was developed for long-term trace gas emission experiments on volatile compounds emitted by biological samples. The OPO-based spectrometer had (wavelength coverage 2.8 -3.8 μm, linewidth 8 MHz and an output power of 1 W) was successfully tested for the detection of HCN (hydrogen cyanide) emission from clover leaves, apple seeds and Pseudomonas bacteria next to its presence in exhaled human breath. For specific experiments the spectrometer operated continuously up to 10 days and showed a detection limit of 0.4 ppbv of HCN in 10 s, using the P_8 rotational line in the ν_3 vibrational band at 3287.25 cm^{-1}.

This work to be submitted to:

D. D. Arslanov, M. P. P. Castro, N. A. Creemers, M. Spunei, J. Mandon, S. M. Cristescu, P. Merkus, and F. J. M. Harren, "Optical Parametric Oscillator based photoacoustic detection of Hydrogen Cyanide for bio-medical applications" .

7.1 Introduction

Hydrogen cyanide (HCN) is a volatile compound that can be found both in the liquid and gaseous phase. This highly toxic gas is colorless and has a bitter -almond-like- odor. It is used in a number of industrial production processes, such as for adiponitrile production (for nylon), methyl methacrylate, pharmaceuticals, etc [1]. Hydrogen cyanide is produced in other industrial activities such as: electroplating, cleaning processes and metallurgy. Due to its toxicity an exposure limit is recommended 0.5-3.5 mg/kg for humans, 3.7 mg/kg for mice, 0.5-10.0 mg/kg for rats, 2.0 mg/kg for cattle, and 1.5 mg/kg for dogs [2, 3] nevertheless, the exposure limit value considered to be lethal for humans is 200 ppmv for 30 min and 600-700 ppmv for 5 min [4]. On the other hand, small amounts of HCN can be found from the human body due to biological processes. HCN in breath may originate from endogenous production, bacteria or ingestion of foods containing HCN [5]. In plant tissue HCN can be produced as a result of hydrolysis of cyanogenic compounds, but also through the biosynthesis of the plant hormone ethylene [6]. Peiser et al. were the first to demonstrate that cyanide is a co-product of ethylene biosynthesis [7]. More than 3000 plant species are able to produce HCN. The mechanism of production of HCN in most of species is generated by degradation of cyanogenic glycosides [8]. When the tissue is injured, the plant is able to synthesize some compounds which produce HCN. The cyanogenic glycosides when hydrolyzed by enzymes will produce sugars, fatty acids, aldehydes and hydrogen cyanide. Several cyanogenic plants are edible, such as clover and apple [9, 10]. However, the effect will only be toxic if ingested in large quantities of certain parts of the plant, such as seeds. In plant tissue, amounts of HCN larger than 20mg/100g are considered as a high risk.

HCN can be produced in significant amounts by specific bacteria [11]. This topic is still unexplored from a medical point of view but highly important. E.g., Pseudomonas Aeruginosa (PA) bacteria are dangerous for immune-compromised patients [12]. Infections with these bacteria are of particular significance in cystic fibrosis (CF) patients due to its association with increased morbidity and mortality [13, 14]. CF is the most common, fatal genetic disease affecting Caucasians [15] and is caused by a mutation in the gene coding for the Cystic Fibrosis Conductance Regulator (CFTR), a chloride channel [15, 16]. Due to this mutation the chloride efflux is impaired, which results in viscous, water deficient, mucus in the airways, impaired mucociliary clearance and an inability to effectively defend the airways from infections [17, 18]. As a result bacterial colonization and chronic airway infection mainly characterize the pathogenesis of CF lung disease [19].

It is therefore important, to detect bacterial infections in the airways as early as possible [20]. However, current diagnostic techniques lack sensitivity (cough swab), are very invasive (Broncho Alveolar Lavage (BAL) and commonly miss early infection, especially in young children. A sensitive and specific non-invasive technique for the di-

agnosis of PA infection would be extremely useful. An attractive, but hardly explored, avenue for non-invasive and fast medical diagnostics is breath analysis.

HCN seems to be a promising indicator for PA infections; a study of Enderbyet. al. showed concentrations of HCN higher in breath of PA colonized patients as compared to non-infected persons [21], but the results remain inconsistent and inconclusive [22, 23]. In the search for a non-invasive diagnostic biomarker for PA infections HCN production should be quantified and investigated to a larger extend.

There is a growing interest in the development of sensitive and selective methods to detect HCN [21, 24, 25]. Several studies have been conducted with different types of matrices such as water, soil, air exhaled breath and food [26–30]. A large number of different methods has been used to monitor HCN such as: colorimetry and spectrophotometry [31, 32], optical detection of cyanide following capillary electrophoresis (CE) [33, 34], fluorometry [35], chemiluminescence [36], potentiometry and amperometry [37, 38], mass spectrometry and gas chromatography [39], next to near infrared cavity ring-down spectroscopy (NI-CRDS) [2, 25]. Most of these methods are complex and involve a large amount of manipulations of samples, or the use of solvents. Furthermore, a number of these methods feature a slow response time (minutes) and it is difficult to perform continuous gas monitoring over days or weeks; in the most cases the detection limits are in ppmv volume mixing range, which is not sufficient to perform trace emission of low amounts of biological sample. Thus, the developing of more sensitive methods to measure ppbv (parts-per-billion volume) level of HCN appears to be very relevant.

Laser-based spectroscopic techniques can overcome most the drawbacks of the conventional methods; they have the advantage of high sensitivity, good selectivity and wide dynamic range. A high sensitivity is important to detect low concentrations; a high selectivity is essential to identify the gas in a multicomponent gas mixture. In addition, a wide dynamic range is required to monitor of a wide range of concentrations for numerous gas components using the same instrument.

Here, we use continuous wave Optical Parametric Oscillator (cw OPO) combined with sensitive photoacoustic detection to achieve the required sensitivity and selectivity for the detection of HCN at the low part per billion volume range. Nowadays mid-infrared singly-resonant Optical Parametric Oscillators (SROs) are considered as the most useful configurations for such sensitive gas sensing due to their high power (Watt level) and ease of tunability [40–42].

Amongst other laser spectroscopic methods photoacoustic spectroscopy (PAS) serves as a very sensitive, efficient, easy and robust method [43–45]. However, it cannot easily be used at sub second time scales, which limit its use for fast detection such as in real-time breath analysis. Nevertheless, due to the above mentioned advantages, it is preferably used in long-term experiments. In addition, PAS is cheap and can be used at any wavelength; this in contrast to other optical cavity enhanced approaches such cavity Ring Down or Cavity Enhanced spectroscopy [46, 47] in which the wavelength depen-

dence of the highly reflective mirror coatings limits the tunability of the system.

Combining OPOs with photoacoustic spectroscopy has another important advantage: photoacoustics utilize the high infrared power of the OPO, resulting in sensitive detection of gases, since the generation of the photoacoustic signal goes proportional with the laser power [42]. Many gases have strong fingerprint absorption spectra in the mid-infrared wavelength region and each molecular gas has its own uniquely recognizable absorption spectrum that makes OPO based absorption spectroscopy an excellent method for selective detection of volatile organic compounds (VOCs) in complex gas mixtures. OPO based photoacoustic spectroscopy was described earlier for sensitive trace gas measurements [48–51]. However, it has not been previously used for the detection of HCN in bio-medical applications. Here, we present a study on HCN in different matrices; first results from clover leaves to verify the potentiality such as sensitivity, selectivity and detection limits. After that, its emission from apple seeds and its presence in exhaled breath. Finally, its emission from Pseudomonas Aeruginosa bacteria during their growth over a period of 13 days. As such the long term stability of the set-up was tested.

7.2 Experimental set-up

A 1064 nm distributed Bragg reflector (DBR) diode laser (EM4, Bedford, MA, USA) in a 14-pin butterfly package design is used as oscillator for the fiber amplifier (see Fig. 7.1). The laser has a linewidth of 8 MHz and is therefore a sufficient source for Doppler-broadened spectroscopy of molecular gases. The laser has long-term stability better than 50 MHz over 4.5 hours (I_c= 250 mA, operating temperature 25°C), which was measured using a Bristol 621A wavemeter (see Fig. 7.2); the stability accuracy was limited by the wavemeter. The compact laser diode driver (Multiwave, San Jose, CA, USA) was modified to ensure faster wavelength scanning by changing the laser operating temperature. The temperature scans were performed by applying a saw-tooth current ramp on the thermo-electrical cooling of the laser. The maximum scanning range was set from 15 to 25 °C to comply with the guaranteed technical specifications of the laser. Under these conditions the maximum scanning wavelength range without any mode hops was between 9386.9 cm^{-1} and 9391.6 cm^{-1} (see Fig. 7.3). However, for this long scan the laser scanning speed was only 10 s per scan, which cannot compete with the fast scans for similar DBR lasers used as pump sources for OPOs [52]. Nevertheless, faster scans were possible in the current configuration using a shorter wavelength range. We recorded 1 cm^{-1} scanning range in 1 s at 9390 cm^{-1} and 0.5 cm^{-1} scanning range in 0.1 s. The scans were recorded with a 2.54 cm long Germanium etalon (FSR=1.48 GHz). The maximum output power of the DBR laser is 150 mW; to pump a singly-resonant OPO (SRO) a typical threshold is needed of 1.5-3.5 W [51]. Therefore, to pump our SRO we amplified our seed laser with a commercially available fiber amplifier unit (Nufern,

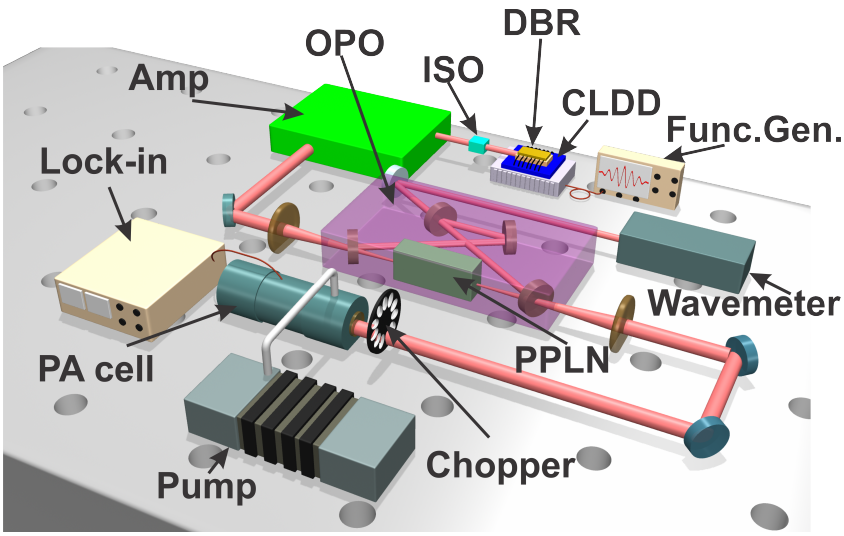

Figure 7.1: *Experimental setup of the OPO based photoacoustic detector for bio-medical applications: DBR- 1064 nm distributed bragg reflector laser; CLDD- compact laser diode driver; Func.Gen.- function generator to drive CLDD; ISO- 30 dB optical isolator at 1064 nm; Amp- fibre amplifier; OPO- singly-resonant optical parametric oscillator; PPLN- periodically polled lithium niobate crystal; PA cell- photoacoustic cell with Silcosteel coating.*

Model NUA-1064-PD-0010-C1). This amplifier has two amplification stages to allow a changing output power from 800 mW to 12 W. To prevent feedback in our seed laser an additional isolator (Thorlabs, Model 10-J-1064APC, 30 dB) was used.

The OPO unit itself is similar to the one described earlier [41] (see Fig. 7.1). Four mirrors (two plano-concave with radii of curvature of 20 cm and two plane mirrors) bow-tie ring design cavity configuration were used. The mirrors (diameter 25 mm, thickness 6.3 mm, QTF inc., Oldsmar, FL, USA) are highly reflective for the signal beam (>99.9% at 1450-1700 nm) and highly transparent for the pump (<10% at 1062-1085 nm) and idler beam (<10% at 2.9-4.0 μm). The periodically-poled lithium niobate crystal with 5% MgO doping (PP-MgO-LN, 7 periods from 28.5-31.5 μm, facets: 90°/89°; HC Photonics) was placed inside an oven, capable of maintaining temperature from room temperature up to 200°C; the oven was controlled by a temperature controller (Thorlabs, Model TC200). The complete cavity including PPLN oven were placed inside an aluminum box thermally stabilized at 30°C using a thermal bath (Tamson Holland) to gain long-term (days) wavelength and power stability.

The photoacoustic cell [48, 49] was designed as an acoustical resonator with a length of a 10 cm (diameter 5 mm) with two adjacent buffer volumes with a larger diameter. As such an acoustical standing wave in the open resonator is generated at a frequency

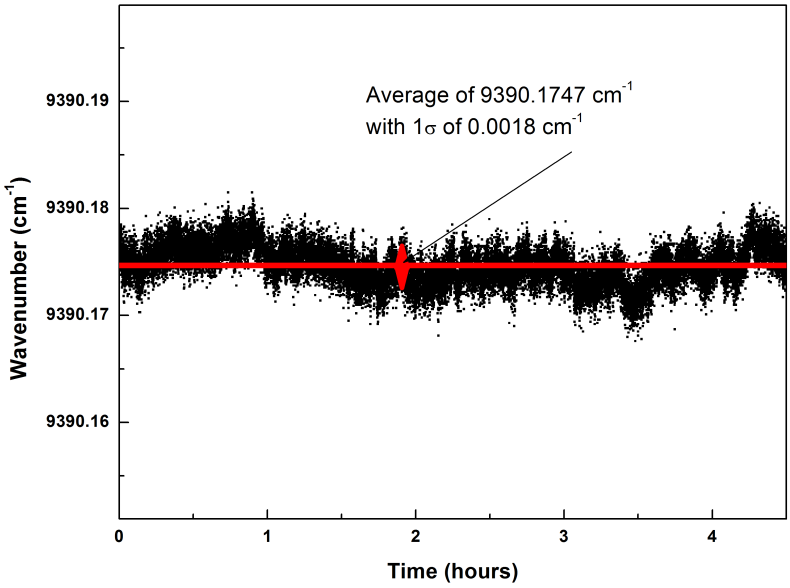

Figure 7.2: *Long-term frequency stability of the DBR seed laser at constant current of 250 mA and constant temperature of 25°C, which was < 50 MHz (0.0018 cm^{-1}) over 4.5 hours.*

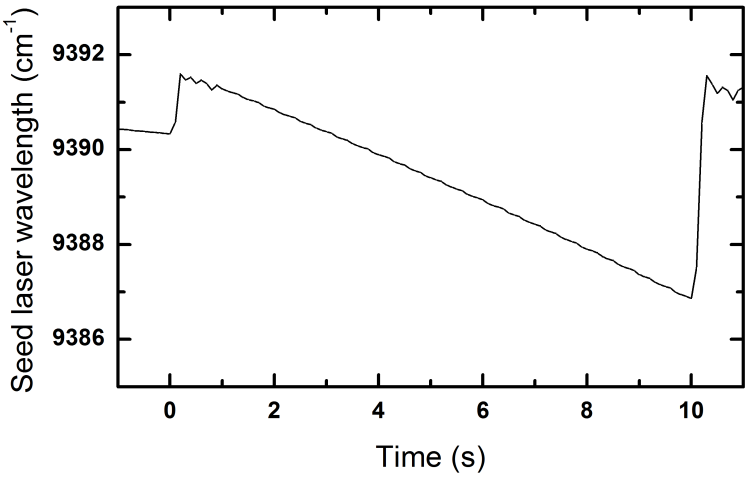

Figure 7.3: *Maximum wavelength, mode-hop-free scans of the seed DBR laser up to 4.7 cm^{-1} at around 9390 cm^{-1} recorded in 10 s.*

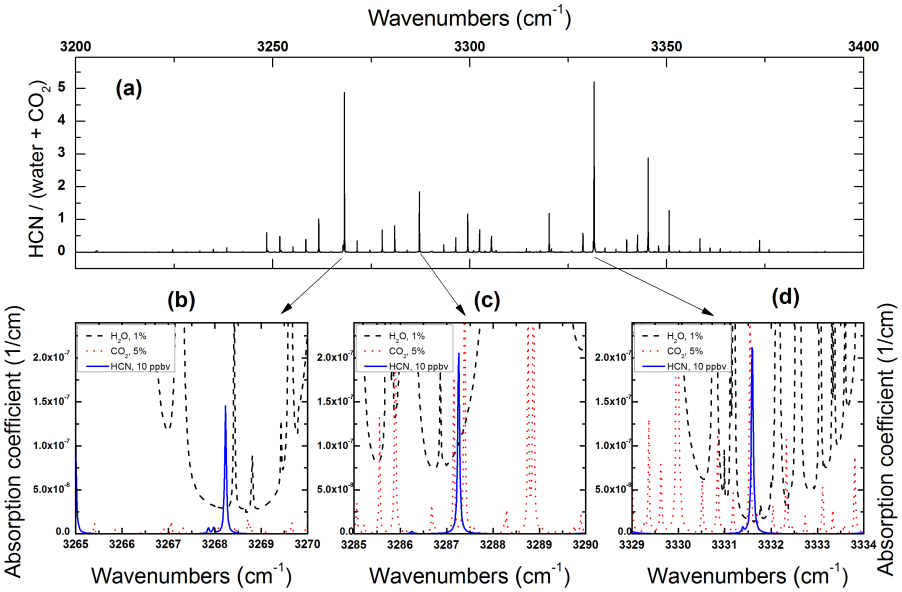

Figure 7.4: *(a)- Ratio between 10 ppbv of HCN and a sum of 1% of water and 5% of CO2 for a pressure of 200 mbar in the wavelength range of 3200 to 3400 cm^{-1}; (b), (c) and (d)- Simulated spectra at a pressure inside the photoacoustic cell of 200 mbar for 1% of water (black dashed line), 5% of CO2 (red dotted line) and 10 ppbv of HCN (blue solid line) for the wavelength ranges: (a) 3285 cm^{-1}–3290 cm^{-1}, (b) 3329 cm^{-1}–3334 cm^{-1}, (c) 3265 cm^{-1}–3270 cm^{-1}. Arrows connecting the figures relate the wavelength regions for the ratio calculation Fig. 7.4(a) with simulated spectra Fig. 7.4(b), Fig. 7.4(c) and Fig. 7.4(d).*

of 1610 Hz with a Q-value of ∼25. The stainless steel cell was coated with a Silcosteel coating to reduce adsorption of polar gases to the cell wall and reduce chemical reactions of gases with the cell material. The laser beam was modulated with a mechanical chopper and the enhanced photoacoustic signal was fed into a lock-in amplifier (dual phase lock-in amplifier Model 7220, EG&G Instruments).

To measure hydrogen cyanide we used the wavelength region around 3287 cm-1 (Fig. 7.4). When measuring biological samples such as plants, seeds, bacteria or human breath, only a limited amount of transition can be chosen. The P_8 line in the ν_3 band of HCN at the wavelength of 3287.247603 cm^{-1} [53] is found to be the best for the biological experiments. This transition interferes less with water absorption lines or absorption line of other gaseous compounds. To estimate the interference of HCN with water and CO2 the calculation of ratio between absorption coefficient per 1 cm pathlength of 10 ppbv of HCN and a sum of absorption coefficients of 1% of water and 5% of CO2 was made (see Fig. 7.4 , panel a). This helps to determine the best spectral regions for the

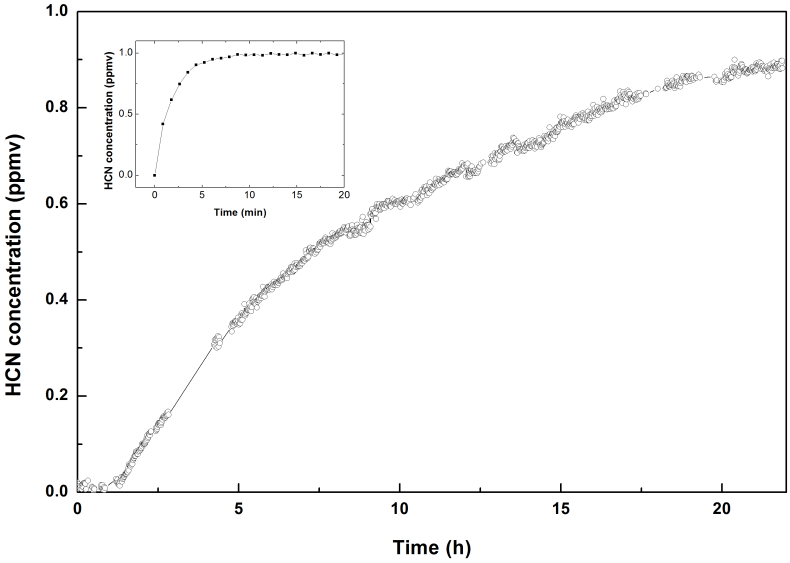

Figure 7.5: *Response time of 1 ppmv of HCN from calibration mixture cylinder when using non-coated reduction valve. 90% value (0.9 ppmv) is reached after 20 hours. Figure insertion shows the response time of optimized system.*

measurements of HCN from biological samples; a few of them are plotted in Fig. 7.4 panels b-d. Although, the absorption line around 3287.25 cm^{-1} (Fig. 7.4c) does not show the best ratio (see Fig. 7.4a), it was still chosen. This absorption line has less interference with CO_2 as compared to the transition at 3331.50 cm^{-1} (Fig. 7.4d) and is stronger than that at 3268 cm^{-1} (Fig. 7.4b).

To perform proper biological sampling we met several complications enabling stable and reliable, long-term measurements of HCN. Firstly, it is important to avoid any metal parts in the flow system from the sample to the detection; wall adsorption by HCN on metal parts will reduce initial gas concentrations and increase the response time. E.g., initially we had a metallic mass flow controller in the system to control the gas flow; as a result we observed a HCN response time of the gas flow system of many hours, instead of seconds for non-polar gases. This was demonstrated by applying 1 ppmv calibrated mixture of HCN into the system (Fig. 7.5). After this we replaced all the gas sampling lines and gas connectors (Polyfluor Plastics, Oosterhout, the Netherlands) and valves (Valco cheminert valves, Bester BV, Amstelveen, the Netherlands) by Teflon, the response time became as fast as tens of seconds for the flow rate of few l/h (estimated volume of the system was about 10 ml). Furthermore, we replaced the reduction valve of the high-pressure bottle containing the calibrated HCN mixture, by a specially coated

reduction valve.

In addition, we tried to de-humidify the sample gas using Nafion tubing; however, we observed gigantic losses of HCN, this is in contrast to the research described elsewhere [2]. Therefore, we did not incorporate Nafion tubing in our sampling system. High water concentration affect our HCN measurements in several ways: water adds a non-linear background on top of the HCN absorption line (see Fig. 7.4), this is important because the water concentration may change when analyzing biological samples over days. In addition, water vapor may condensate inside sampling tubes or inside the cell which will lead to the partial or full blocking of the flow system by water droplets. These effects were eliminated by: choosing the 3287 cm^{-1} HCN absorption line that has a reduced spectroscopic interference with water lines; by lowering the pressure inside the photoacoustic cell (about 400 mbar) to increase the spectral resolution; and by placing a cold trap (10 °C) in between sampling cuvettes and photoacoustic cell to reduce the relative humidity in the sampling flow below its dew point. A control experiment was carried out to ensure that the cold trap did not affect HCN measurements.

7.3 Results and discussion

The calibration measurements were carried out by recording the photoacoustic signal from five different concentration points ranging from 1000 ppbv to 100 ppbv. Different concentrations were prepared by diluting a calibrated mixture of 5 ppmv of HCN in nitrogen (5ppmv $\pm$ 5%, 10 l high pressure cylinder, the Linde group). Figure 7.6 shows the PA signal as a function of HCN concentration applied into the system. The red solid line is a linear fit of data with R-square value of 0.999 over a large dynamic range of concentrations. It allows to determine a detection limit of the spectrometer o 0.4$\pm$0.03 ppbv of HCN measured at 3287.25 cm^{-1} in 10 s.

7.3.1 HCN measurements from white clover leaves

To demonstrate HCN emission from cyanogenic plants ten white clover (Trifolium repens) leaves (total fresh weight 0.313 g) were collected from the greenhouse of Radboud University. They were cut into 2 mm wide pieces and placed into a small glass cuvette with a gas flow inlet and flow outlet. A second identical cuvette was set in a parallel to perform background measurements. As carrier gas flow a mixture of 21% of oxygen in nitrogen was used from a high pressure cylinder followed by a reduction valve and a flow controller (mass flow controllers Brooks Instr., Ede, the Netherlands). As such a constant flow rate of 5 l/h was maintained over the leaves for days. Electrically controlled 3 way Teflon valves (diaphragm isolated three way valves MTV-3-N1/4UG Takasago electric, Nagoya, Japan) were used to, either flow a sample gas is leaded into the photoacoustic

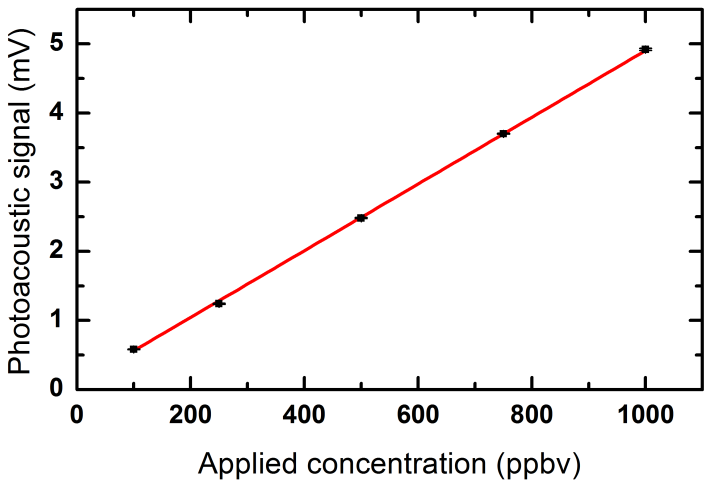

Figure 7.6: *HCN calibration measurements. Experimental points are the photoacoustic signal of five concentrations applied into the system. A detection limit of 0.4±0.03 ppbv was achieved.*

cell, or flow into the exhaust when the other sampling cell is monitored. In such a way identical flows and pressure conditions are maintained inside the sampling cuvettes during the whole experiment regardless which cuvette is measured. Figure 7.7 shows the sampling scheme and results for the clover leaves measurements. Initially, the photoacoustic cell was connected to the reference cuvette to measure background levels. After that the damaged clover leaves were placed inside the sampling cuvette and the system switched to the cuvette contained the clover. The HCN emission profile was monitored for 20 hours and was stopped due to dehydration of the clover leaves (see Fig. 7.7(b)). The insert of the Fig. 7.7(b) shows the fast increase of HCN concentration from zero level up to 4 ppbv within less than 10 min. The initial HCN decay curve due to cutting of the leaves -between 1 and 12 hours- is fitted an exponential curve (blue dashed line with value t= (15.7±0.8) hrs). However, the HCN concentration tended to drop significantly faster starting from 12 hours till zero level at 18 hours; the effect was found highly repeatable for various experiments. A reasonable explanation for this is dehydration of the leaves.

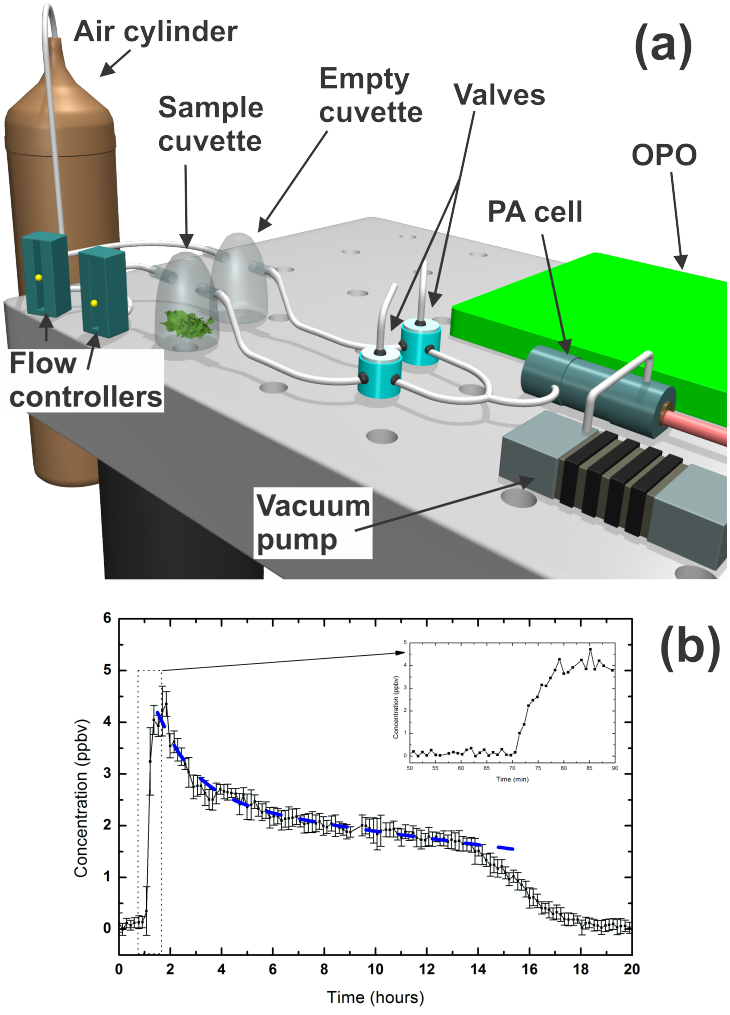

Figure 7.7: *(a) Artistic impression of the experimental scheme for the HCN detection from clover leaves: Air cylinder- high pressure cylinder of synthetic air, Flow controllers- mechanical mass flow controllers, Sample cuvette- glass cuvette with the sample to analyze; Empty cuvette- empty glass for reference comparison; Valves- diaphragm isolated three way valves; OPO- continuous wave optical parametric oscillator, PAS cell- photoacoustic cell with Silcosteel coating; Vacuum pump- diaphragm membrane vacuum pump. (b) Concentration dynamics of HCN emitted from ten cut clover leaves (fresh weight 313 mg. Blue dashed line represents an exponential fit with value t= (15.7±0.8) hrs. The insertion is a zoomed-in area of the dotted rectangle and it shows the response time of the system of few minutes. HCN dropped starting from 12 hours reaching zero level at 18 hours due to dehydration of leaves.*

7.3.2 Detection of HCN from apple seeds

The experiments were carried out using a pair of seeds from commercially available apples (cv. Jonagold) with the total weight of 0.1185 g. The seeds were crushed and quickly placed in the glass sampling cuvette. The experimental setup for HCN sampling from the apple seeds is similar to the one used for clover leaves, but now the sampling and reference cuvette contained water. The water was added to prevent quick dehydration of the sample. Figure 7.8(a) shows HCN emission from apple seeds (red solid dots) together with the records from reference cuvette (black empty circles). The sampling and reference cuvette were alternately sampled by computer-controlled switching every 25 minutes collecting 30 experimental data points per cuvette. A high HCN concentration of over 3.5 ppmv was observed during the first hours (flow rate of 5 l/h). Of every cycle the first 10-15 points are transition points, e.g. after the valve switched to the cuvette to take the measurements, there is still some gas of the previous cuvette in the system. Although, these points are not relevant for the concentration results, they help to estimate the response time of the system which was estimated to be of about 5 min. Figure 7.8(b) shows the averages of the last 10 points of every set for the sampling cuvette. The vertical scale of concentration is given in a logarithmic scale due to the large dynamic range. The blue solid line is the double exponential fit with the R^2=0.99916 of experimental data (fitting function is: $y = A_1 \times e^{(-x/t_1)} + A_2 \times e^{(-x/t_2)}$, where A_1=(5.4$\pm$1.2) ppmv, A_2=(400$\pm$45) ppbv, t_1=(1.38$\pm$0.03) hours and t_2=(5.5$\pm$0.3) hours). The second term $A_2 \times e^{(-x/t_2)}$ is introduced because water acts as a buffer volume for the released HCN and causes therefore long-term emission.

7.3.3 HCN from human breath

Breath analysis is a strongly growing field of research over the last decade. It is non-invasive, easy, safe, fast, and does not require a specific sample preparation, including laser-based breath analysis [47, 52, 54]. We were not able to carry out real-time breath analysis as described in Ref. [52] due to the slow photoacoustic response as described above, but we performed off-line analysis. Tedlar gas sampling bags (1 L Tedlar bags with 2 inlets/outlets) were used to collect and store human breath samples. Diaphragm membrane vacuum pump (MVP 015-4, Pfeiffer Vacuum, Asslar, Germany) with a restriction valve was used to deliver a breath sample from a bag to photoacoustic cell for analysis. Here, the pressure inside the photoacoustic cell was set at 500 mbar. A valve system was used to analyze the contents of the bags. Figure 7.9 depicts the results of HCN measurements of clean air, HCN in the lab air at the time of measurements, and HCN in the breath of two volunteers. The lab air contained 1.5 ppbv HCN while clean air does not show any presence HCN. The first volunteer (the first two peaks in the graph) has a slightly lower HCN concentration ($\sim$8 ppbv) as compared to the second subject

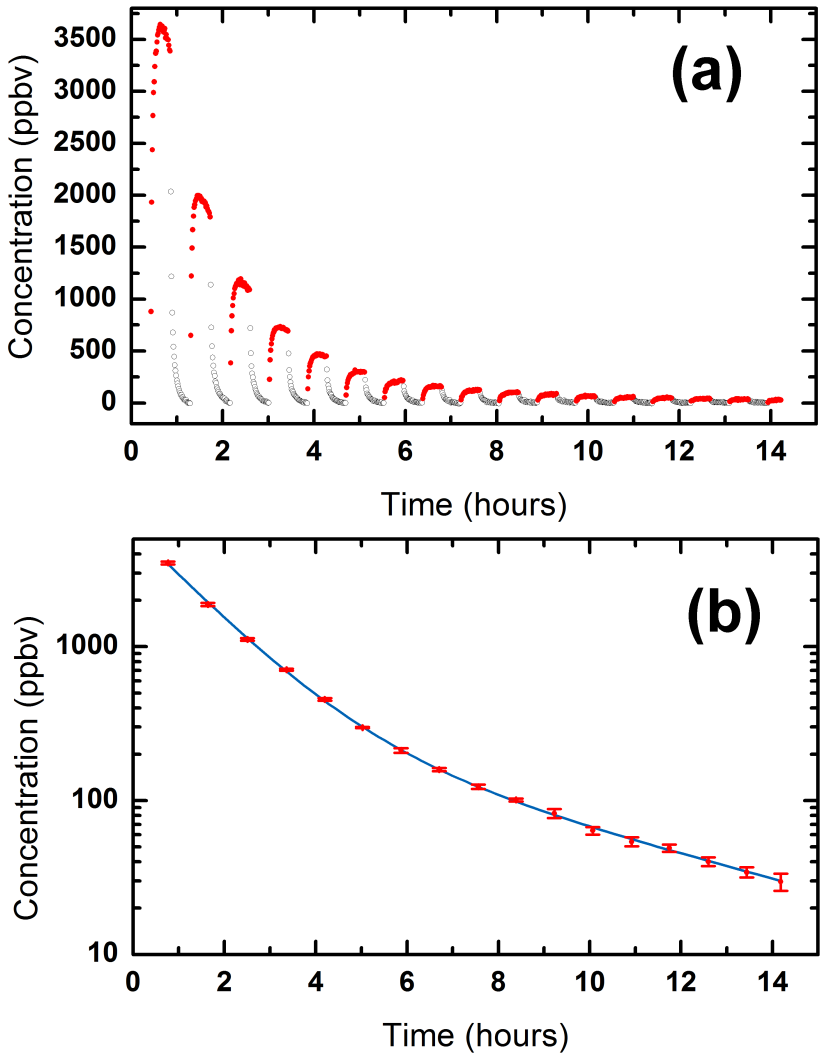

Figure 7.8: *(a) HCN concentration dynamics from crushed apple seeds (red solid dots) with the reference data (black empty circles) from empty cuvette. The valve system was switched between sampling and reference cuvette every 30 data points. (b) Averages of last ten data points of each set of data from sampling cuvette (see Fig. 7.8(a)) with double exponential fit (blue curve).*

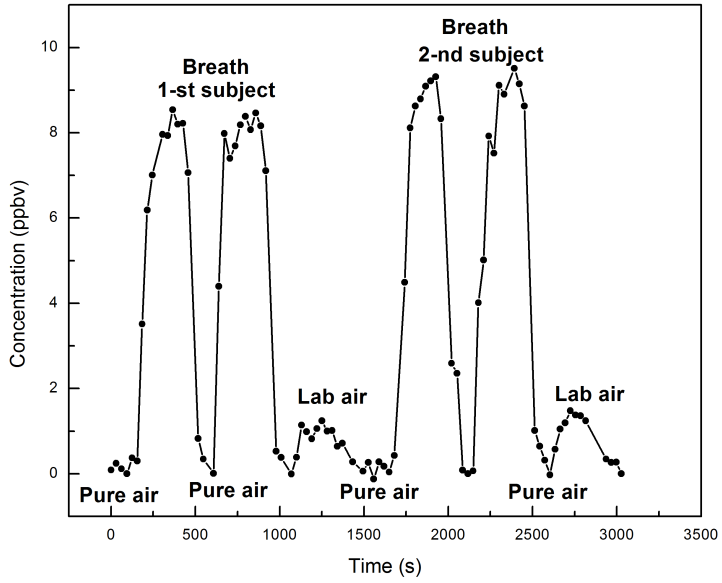

Figure 7.9: *HCN concentration from exhaled breath of two subjects repeated twice for every person. HCN value of about 1.5 ppbv was measured in the lab air and zero HCN level from synthetic air.*

($\sim$9 ppbv). The experiment also shows reproducibility when analyzing breath of the same person. Our results are in agreement with the data obtained by Stamyr et al. [25].

7.3.4 Detection of HCN produced by Pseudomonas bacteria

Pseudomonas bacteria (ATCC 10145, obtained from Oxoid BV, Badhoevedorp, the Netherlands) were cultured in liquid Brain Heart Infusion (BHI) broth and medium (obtained from Mediaproducts BV, Groningen, the Netherlands) and incubated at 37 °C, while constantly shaking at 70 rpm. 1 ml of a McFarland standard with an optical density of 0.5 (at 600 nm) was inoculated in 50 ml of liquid BHI medium in a 250 ml Erlenmeyer flask adapted for gas flow sampling; this resulted in an initial concentration of 2-5$\times 10^{-6}$ CFU (colony-forming units)/ml. The Erlenmeyer flasks have a glass stoppers fitted with two Teflon open/close valves acting as the inlet and outlet for gas sampling. Bacterial filters (FP 30/0.2 Ca-S, Whatman GmbH, Dassel, Germany) were placed on the inlet and outlet of the flasks to prevent contamination [55].

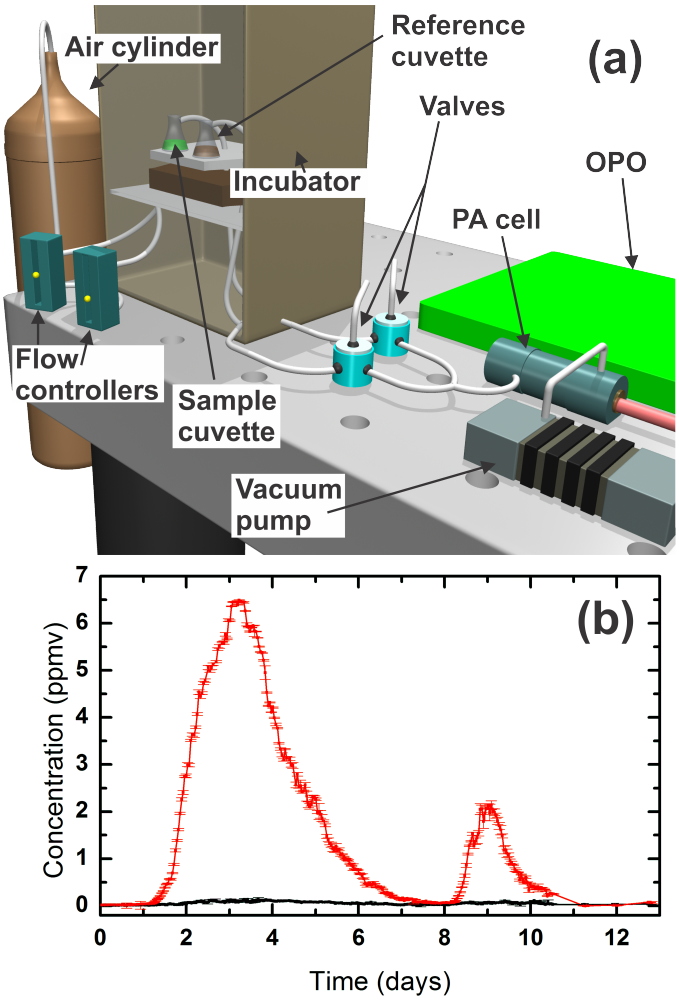

Figure 7.10: *(a) Artistic impression of the experimental scheme for the HCN detection from Pseudomonas bacteria: Air cylinder- high pressure cylinder of synthetic air; Flow controllers- mechanical mass flow controllers, Sample cuvette- glass cuvette with the sample to analyze; Empty cuvette- empty glass for reference comparison; Valves- diaphragm isolated three way valves, Incubator- environmental chamber set at 37 °C; OPO- continuous wave optical parametric oscillator pumped by, PAS cell- photoacoustic cell with Silcosteel coating. (b) Concentration dynamics of HCN emitted by Pseudomonas bacteria (red dots) with the data from the reference cuvette (black dots). Zero time corresponds to the bacteria inoculation. The maximum value of 6.5 ppmv was reached after 77 hours (∼3.2 days). New medium was added at 190 hours (∼7.9 days). After adding this new substrate HCN production started again after a lag-phase of 10 hours reaching pick of 2.1 ppmv.*

The bacteria were kept in an environmental chamber (Sanyo Versatile Enviromental Test Chamber, Osaka, Japan) at 37 °C and the headspace of the samples was constantly flushed with a mixture of 21% O2 in nitrogen controlled with flow controllers at a total flow rate of 3.4 l/h. From the headspace a flow of 3 l/h was lead to the photoacoustic cell. Overflow needle outlets were placed between the outlet of each cuvette and the selector valve to keep a constant air flow through the cuvette and to maintain a pressure inside the photoacoustic cell of 400 mbar. During the experiment the cuvettes were constantly shaken at 70 rpm on an orbital shaker (Sanyo,Osaka, Japan).

A blank, control measurement was provided by a cuvette containing only a medium with liquid BHI without Pseudomonas bacteria. In such a way potential HCN background production by the medium could be investigated. These sample and reference cuvettes were monitored sequentially. Figure 7.10(a) shows the artistic inpression of the experimental set-up; panel 7.10b shows the background HCN production by the medium (black dots) and Pseudomonas bacteria (red dots). Each data point and its error bar represent the mean of the last 10 points of each measurement cycle. No HCN production could be observed for the blank sample containing only medium (less than 10 ppbv). At time t=0 bacteria were inoculated in the medium. After 20 hours the bacteria start to produce exponentially HCN reaching concentrations as high as 6.5 ppmv after 77 hours. Then the production ceases; this production decrease is most likely caused by depletion of the medium. Bacteria run out of substrate and therefore stop producing HCN. This hypothesis was confirmed by adding 20 mL new medium at 190 hours ($\sim$7.9 days). After adding this new substrate HCN production started again after a lag-phase of 10 hours. However, absolute HCN production was not as high as at first time (2.1 ppmv in compare with 6.5 ppmv). Which specific substances in the medium are limiting the HCN production will be subject to further investigations.

7.4 Conclusion

The OPO based photoacoustic spectrometer for trace gas detection was successfully tested on the detection of hydrogen cyanide (HCN) from clover leaves, apple seeds, Pseudomonas bacteria and human exhaled breath. The OPO based detector showed good detection stability over a period of 13 days; the latter is a great advantage when measuring over long-term bio-medical samples. The detection limit achieved for this system was determined of 0.4 ppbv measured at 3287.25 cm^{-1} in 10 s. Our future plans include monitoring the HCN production of different types of Pseudomonas bacteria under different environmental conditions. This research will also extend to HCN detection in human exhaled breath and plant physiology experiments will be explored in more detail in the near future.

Acknowledgements The authors would like to thank Cor Sikkens and Peter Claus (Radboud University Nijmegen, the Netherlands) for their technical help in these experiments. Furthermore we would like to acknowledge the Microbiology department at Radboud University Nijmegen Medical Centre (Nijmegen, The Netherlands) for providing the microbiological materials. The research was financially supported by the Asthma Founds, (the Netherlands, project number 3.3.11.002), IOP Photonic devices, the Province of Gelderland and EFRO. Also M. P. P. Castro is grateful to Coordenação de Aperfeioamento de Pessoal de Nivel Superior - CAPES-Brazil for scholarship at Radboud University.

References

[1] http://www.atsdr.cdc.gov/toxprofiles/tp8-c1.pdf, pp. 6-7.

[2] F. M. Schmidt, M. Mietsala, O. Vaittinen, and L. Halonen, "Background levels and diurnal variations of hydrogen cyanide in breath and emitted from skin," *J. Breath Res.*, vol. 5, pp. 1–10, 2011.

[3] D. A. Jones, "Why are so many food plants cyanogenic?," *Phytochemistry*, vol. 47, no. 2, pp. 155–162, 1998.

[4] J. E. Tintinalli, G. D. Kelen, and J. S. Stapczynski, *Emergency Medicine: A Comprehensive Study Guide*. McGraw-Hill Professional, 2004.

[5] http://www.atsdr.cdc.gov/toxprofiles/tp8-c1.pdf, pp. 1-2.

[6] I. Siegien and R. Bogatek, "Cyanide action in plants - from toxic to regulatory," *Acta Physiol.*, vol. 28, pp. 483–497, 2006.

[7] G. D. Peiser, T. T. Wang, N. E. Hoffman, S. F. Yang, H. W. Liu, and C. T. Walsh, "Formation of cyanide from carbon-1 of 1-aminocyclopropane-1-carboxylic acid during its conversion to ethylene," *PNAS*, vol. 81, pp. 3059–3063, 1984.

[8] J. M. Miller and E. E. Conn, "Metabolism of hydrogen-cyanide by higher-plants," *Plant Physiol.*, vol. 65, pp. 1199–1202, 1980.

[9] K. Refsgaard, N. Bjarnholt, B. L. Moller, M. M. Saddik, and H. C. B. Hansen, "Dissipation of cyanogenic glucosides and cyanide in soil amended with white clover (Trifolium repens L.)," *Soil Biol. Biochem.*, vol. 42, no. 7, pp. 1108–1113, 2010.

[10] M. A. Hughes and E. E. Conn, "Cyanoglucoside Biosynthesis in White Clover (Trifolium-Repens)," *Phytochemistry*, vol. 15, no. 5, pp. 697–701, 1976.

[11] A.-S. Blier, J. Vieillard, E. Gerault, A. Dagorn, T. Varacavoudin, F. Le Derf, N. Orange, M. Feuilloley, and O. Lesouhaitier, "Quantification of Pseudomonas aeruginosa hydrogen cyanide production by a polarographic approach," *Journal of microbiological methods*, vol. 90, pp. 20–24, 2012.

[12] W. Lenney and F. Gilchrist, "Pseudomonas aeruginosa and cyanide production," *Eur. Respir. J.*, vol. 37, pp. 482–483, 2011.

[13] M. Rosenfeld, R. L. Gibson, S. McNamara, J. Emerson, J. L. Burns, R. Castile, P. Hiatt, K. McCoy, C. B. Wilson, and A. Inglis, "Early pulmonary infection, inflammation, and clinical outcomes in infants with cystic fibrosis," *Pediatr. Pulmonol.*, vol. 32, pp. 356–366, 2001.

[14] J. Emerson, M. Rosenfeld, S. McNamara, B. Ramsey, and R. L. Gibson, "Pseudomonas aeruginosa and other predictors of mortality and morbidity in young children with cystic fibrosis," *Pediatr. Pulmonol.*, vol. 34, pp. 91–100, 2002.

[15] P. M. Quinton, "Cystic fibrosis: a disease in electrolyte transport," *The FASEB Journal*, vol. 4, pp. 2709–2717, 1990.

[16] S. H. Cheng, R. J. Gregory, J. Marshall, S. Paul, D. W. Souza, G. A. White, C. R. O'Riordan, and A. E. Smith, "Defective intracellular transport and processing of cftr is the molecular basis of most cystic fibrosis," *Cell*, vol. 63, pp. 827–834, 1990.

[17] G. M. Roomans, "Pharmacological treatment of the ion transport defect in cystic fibrosis," *Expert opinion on investigational drugs*, vol. 10, pp. 1–19, 2001.

[18] R. C. Boucher, "Airway surface dehydration in cystic fibrosis: pathogenesis and therapy," *Annu.*, pp. 157–170, 2007.

[19] J. J. Smith, S. M. Travis, E. P. Greenberg, and M. J. Welsh, "Cystic fibrosis airway epithelia fail to kill bacteria because of abnormal airway surface fluid," *Cell*, vol. 85, pp. 229–236, 1996.

[20] B. Frederiksen, C. Koch, and N. Hoiby, "Antibiotic treatment of initial colonization with pseudomonas aeruginosa postpones chronic infection and prevents deterioration of pulmonary function in cystic fibrosis," *Pediatr. Pulmonol.*, vol. 23, pp. 330–335, 1997.

[21] B. Enderby, D. Smith, W. Carroll, and W. Lenney, "Hydrogen cyanide as a biomarker for pseudomonas aeruginosa in the breath of children with cystic fibrosis," *Pediatr. Pulmonol.*, vol. 44, pp. 142–147, 2009.

[22] M. D. Stutz, C. L. Gangell, L. J. Berry, L. Garratt, B. Sheil, and P. Sly, "Cyanide in bronchoalveolar lavage is not diagnostic for pseudomonas aeruginosa in children with cystic fibrosis," *Eur. Respir. J.*, vol. 37, pp. 553–558, 2011.

[23] S. U. Savelev, J. D. Perry, S. J. Bourke, H. Jary, R. Taylor, A. J. Fisher, P. A. Corris, M. Petrie, and A. De Soyza, "Volatile biomarkers of pseudomonas aeruginosa in cystic fibrosis and noncystic fibrosis bronchiectasis," pp. 610–613, 2011.

[24] M. M. Baum, J. A. Moss, S. H. Pastel, and G. A. Poskrebyshev, "Hydrogen cyanide exhaust emissions from in-use motor vehicles," *Environ. Sci. Technol.*, vol. 41, pp. 857–862, 2007.

[25] K. Stamyr, O. Vaittinen, J. Jaakola, J. Guss, M. Metsala, G. Johanson, and L. Halonen, "Background levels of hydrogen cyanide in human breath measured by infrared cavity ring down spectroscopy," *Biomarkers*, vol. 14, pp. 285–291, 2009.

[26] J. A. Ma and P. K. Dasgupta, "Recent developments in cyanide detection: A review," *Anal. Chem. Acta*, vol. 673, pp. 117–125, 2010.

[27] J. Q. Ren, W. H. Zhu, and H. Tian, "A highly sensitive and selective chemosensor for cyanide," *Talanta*, vol. 75, pp. 760–764, 2008.

[28] C. Mannel-Croise, B. Probst, and F. Zelder, "A straightforward method for the colorimetric detection of endogenous biological cyanide," *Anal. Chem.*, vol. 81, pp. 9493–9498, 2009.

[29] W. C. Blackledge, C. W. Blackledge, A. Griesel, S. B. Mahon, M. Brenner, R. B. Pilz, and G. R. Boss, "New facile method to measure cyanide in blood," *Anal. Chem.*, vol. 82, pp. 4216–4221, 2010.

[30] S. Jermak, B. Pranaityte, and A. Padarauskas, "Headspace single-drop microextraction with in-drop derivatization and capillary electrophoretic determination for free cyanide analysis," *Electrophoresis*, vol. 27, pp. 4538–4544, 2006.

[31] M. Tomasulo and F. M. Raymo, "Colorimetric detection of cyanide with a chromogenic oxazine," *Org. Lett.*, vol. 7, pp. 4633–4636, 2005.

[32] C. Mannel-Croise and F. Zelder, "Side chains of cobalt corrinoids control the sensitivity and selectivity in the colorimetric detection of cyanide," *Inorg. Chem.*, vol. 48, pp. 1272–1274, 2009.

[33] K. Papezova and Z. Glatz, "Determination of cyanide in microliter samples by capillary electrophoresis and in-capillary enzymatic reaction with rhodanese," *J. Chromatography A*, vol. 1120, pp. 268–272, 2006.

[34] L. Meng, X. Liu, B. Wang, G. Shen, Z. Wang, and M. Guo, "Simultaneous derivatization and extraction of free cyanide in biological samples with home-made hollow fiber-protected headspace liquid-phase microextraction followed by capillary electrophoresis with uv detection," *J. Chromatography B*, vol. 877, pp. 3645–3651, 2009.

[35] L. Shang and S. J. Dong, "Design of fluorescent assays for cyanide and hydrogen peroxide based on the inner filter effect of metal nanoparticles," *Anal. Chem.*, vol. 81, pp. 1465–1470, 2009.

[36] J. Lv, Z. J. Zhang, J. D. Li, and L. R. Luo, "A micro-chemiluminescence determination of cyanide in whole blood," *Forensic Sci. Int.*, vol. 148, pp. 15–19, 2005.

[37] A. Abbaspour, M. Asadi, A. Ghaffarinejad, and E. Safaei, "A selective modified carbon paste electrode for determination of cyanide using tetra-3,4-pyridinoporphyrazinatocobalt(ii)," *Talanta*, vol. 66, pp. 931–936, 2005.

[38] C. K. Zacharis, P. D. Tzanavaras, A. N. Voulgaropoulos, and B. Karlberg, "Amperometric determination of cyanides at the low ppb level by automated preconcentration based on gas diffusion coupled to sequential injection analysis," *Talanta*, vol. 77, pp. 1620–1626, 2009.

[39] P. Dumas, G. Gingras, and A. LeBlanc, "Isotope dilution-mass spectrometry determination of blood cyanide by headspace gas chromatography," *J. Anal. Toxicol*, vol. 29, pp. 71–75, 2005.

[40] I. Lindsay, B. Adhimoolam, P. Gross, M. Klein, and K. Boller, "110GHz rapid, continuous tuning from an optical parametric oscillator pumped by a fiber-amplified DBR diode laser," *Opt. Express*, vol. 13, no. 4, pp. 1234–1239, 2005.

[41] A. K. Y. Ngai, S. T. Persijn, G. Von Basum, and F. J. M. Harren, "Automatically tunable continuous-wave optical parametric oscillator for high-resolution spectroscopy and sensitive trace-gas detection," *Appl. Phys. B*, vol. 85, no. 2-3, pp. 173–180, 2006.

[42] A. K. Y. Ngai, S. T. Persijn, I. D. Lindsay, A. A. Kosterev, P. Gross, C. J. Lee, S. M. Cristescu, F. K. Tittel, K.-J. Boller, and F. J. M. Harren, "Continuous wave optical parametric oscillator for quartz-enhanced photoacoustic trace gas sensing," *Appl. Phys. B*, vol. 89, no. 1, pp. 123–128, 2007.

[43] M. Sigrist, A. Bohren, T. von Lerber, M. Nagele, and A. Romann, "Environmental applications of laser-based photoacoustic spectroscopy," *Anal. Sci.*, vol. 17, no. SI, pp. S511–S514, 2001.

[44] V. Koskinen, J. Fonsen, J. Kauppinen, and I. Kauppinen, "Extremely sensitive trace gas analysis with modern photoacoustic spectroscopy," *Vib. Spectrosc.*, vol. 42, no. 2, SI, pp. 239–242, 2006.

[45] S. M. Cristescu, S. T. Persijn, S. T. L. Hekkert, and F. J. M. Harren, "Laser-based systems for trace gas detection in life sciences," *Appl. Phys. B*, vol. 92, no. 3, pp. 343–349, 2008.

[46] M. W. Sigrist, R. Bartlome, D. Marinov, J. M. Rey, D. E. Vogler, and H. Waechter, "Trace gas monitoring with infrared laser-based detection schemes," *Appl. Phys. B*, vol. 90, no. 2, pp. 289–300, 2008.

[47] C. Wang and P. Sahay, "Breath analysis using laser spectroscopic techniques: Breath biomarkers, spectral fingerprints, and detection limits," *Sensors*, vol. 9, pp. 8230–8262, 2009.

[48] A. Miklos and P. Hess, "Application of acoustic resonators in photoacoustic trace gas analysis and metrology," *Rev. Sci. Instrum.*, vol. 72, pp. 1937–1955, 2001.

[49] M. W. Sigrist, "Trace gas monitoring by laser photoacoustic spectroscopy and related techniques plenary," *Rev. Sci. Instrum.*, vol. 74, pp. 486–490, 2003.

[50] M. van Herpen, S. Li, S. Bisson, S. te Lintel Hekkert, and F. Harren, "Tuning and stability of a continuous-wave mid-infrared high-power single resonant optical parametric oscillator," *Appl. Phys. B*, vol. 75, pp. 329–333, 2002.

[51] D. D. Arslanov, M. Spunei, J. Mandon, S. M. Cristescu, S. T. Persijn, and F. J. M. Harren, "Continuous-wave optical parametric oscillator based infrared spectroscopy for sensitive molecular gas sensing," *Laser and Photonics Rev.*, vol. DOI 10.1002/lpor.201100036, pp. 1–19, 2012.

[52] D. D. Arslanov, K. Swinkels, S. M. Cristescu, and F. J. M. Harren, "Real-time, subsecond, multicomponent breath analysis by optical parametric oscillator based off-axis integrated cavity output spectroscopy," *Opt. Express*, vol. 19, pp. 124078–24089, 2011.

[53] L. Rothman, I. Gordon, A. Barbe, D. Benner, P. Bernath, M. Birk, V. Boudon, L. Brown, A. Campargue, J.-P. Champion, K. Chance, L. Coudert, V. Dana, V. Devi, S. Fally, J.-M. Flaud, R. Gamache, A. Goldman, D. Jacquemart, I. Kleiner, N. Lacome, W. Lafferty, J.-Y. Mandin, S. Massie, S. Mikhailenko, C. Miller, N. Moazzen-Ahmadi, O. Naumenko, A. Nikitin, J. Orphal, V. Perevalov, A. Perrin, A. Predoi-Cross, C. Rinsland, M. Rotger, M. Šimečková, M. Smith, K. Sung, S. Tashkun, J. Tennyson, R. Toth, A. Vandaele, and J. V. Auwera, "The hitran 2008 molecular spectroscopic database," *Journal of Quantitative Spectroscopy and Radiative Transfer*, vol. 110, pp. 533 – 572, 2009.

[54] T. H. Risby and F. K. Tittel, "Current status of midinfrared quantum and interband cascade lasers for clinical breath analysis," *Opt. Eng.*, vol. 49, pp. 111123–, 2010.

[55] E. Crespo, S. M. Cristescu, H. de Ronde, S. Kuijper, A. H. J. Kolk, R. M. Anthony, and F. J. M. Harren, "Proton Transfer Reaction Mass Spectrometry detects rapid changes in volatile metabolite emission by Mycobacterium smegmatis after the addition of specific antimicrobial agents," *Journal of microbiological methods*, vol. 86, no. 1, pp. 8–15, 2011.

Summary

Gas phase spectroscopy is a well-established and widely known approach to detect and distinguish gases with a wide variety of applications within physics, chemistry, biology, environmental studies and medicine. For decades spectroscopic gas sensors are extensively exploited for fundamental research and industrial use. Nevertheless, there is a continuous progress in research and every year new papers are being published on the improvement of the sensitivity, selectivity and time resolution. Although the term 'spectroscopy of gases' is very general and is based on combinations of a large diversity of spectroscopic methods and detection techniques, laser absorption spectroscopy in the mid-infrared wavelength region serves as an attractive technology in the field of trace gas detection. Mid-infrared singly-resonant Optical Parametric Oscillators (OPOs) are considered to be the most useful configurations for such sensitive gas sensing. OPOs possess a high power output, ease and speed of tunability, besides a narrow linewidth, the first chapter of this thesis reports on the basic operating principles of OPOs and laser-based absorption spectroscopy.

Bio-medical trace gas sensing is a very promising and important field of research. Volatile organic compounds, emitted by plants and animals, contain information that helps to understand the physiology of biological species and their metabolism, as well as the interaction between plants and/or living organisms. In Chapter 2 the reader gets acquainted with the importance of trace gas detection for medicine and biology and its potential for the future. The restrictions of OPOs for field applications are also considered together with fundamental experiments.

All experiments described in this thesis carried out with the OPO, a coherent radiation source in the mid-infrared wavelength region. Chapter 3 reviews most applications of continuous wave OPOs. There are many possible detection schemes described in this chapter, each with its advantages and limitations. The choice for the appropriate detector needs careful consideration and should comply with the requirements of the specific application.

Chapter 4 reports on the use of the OPO in combination with Wavelength Modulation Spectroscopy (WMS) and a 76-m multipass cell. The setup was used to detect ethane

(C_2H_6) at wavelength of around 2997 cm^{-1} with a detection limit of 0.8 ppbv recorded in 1.3 s. The detector showed the ability of rapid (up to 100 THz/s) and broad mode-hop-free tunability (up to 5 cm^{-1}). Moreover, a broad continuous tuning over 35 cm-1 was demonstrated. These results clearly show the capability to multi-component detection of several gases simultaneously, which is a key feature in the field of bio-medical trace gas detection. In addition, a comparison between results using 1st, 2nd and 4th harmonic derivative signal from wavelength modulation is described, reporting similar signal-to-noise ratios. However, the signals are higher at the 1st harmonic and less time dependent at higher harmonics. Notwithstanding a good detection limit and a short acquisition time for the ethane measured, the sensitivity of WMS is limited due to the fringe patterns on the background signal that are induced by etalon effects between optical elements. The sensitivity could be further improved by use of cavity enhanced methods.

Chapter 5 deals with Integrated Cavity Output Spectroscopy in its off-axis configuration. Due to the extremely large effective path length inside the optical cavity created by pair of highly reflective mirrors, a detection limit of 50 pptv of ethane (C_2H_6) was achieved at the same ethane absorption line at the wavelength of around 2997 cm^{-1}, moreover in a much shorter time of 0.25 s. This resulted in a Noise Equivalent Absorption Sensitivity of $4.8\times10^{-11}cm^{-1}Hz^{-1/2}$. The signal-to-noise ratio dependences on the off-axis alignment parameter and scanning rate have been shown. In addition, the setup was also used to measure methane (CH_4) and water concentrations in exhaled human breath, in real time. The approach can be easily extended to multicomponent gas detection and for the real applications in life sciences.

In Chapter 6 the setup described in Chapter 5 was intensively used for real-time exhaled human breath analysis. Sub-second time resolution allowed resolving a single free exhalation with the sub-ppbv detection limit. The concentration dynamics of ethane were followed during free exhalation in multiple breath samples for non-smoking and smoking subjects over tens of minutes. Fast and sensitive detection combined with a wide spectral coverage allowed simultaneous detection of ethane, methane (CH_44) and water. Moreover a sub-second detection of larger molecules such as acetone was demonstrated in exhaled human breath. These experiments clearly demonstrated an important step forward in real-time, multicomponent breath analysis.

Another OPO configuration was built to enhance long-term wavelength and power stability. Chapter 7 reports on biological applications of Hydrogen Cyanide (HCN) measurements. An OPO based photoacoustic spectroscopic detector was built and successfully tested on HCN emission from clover leaves, apple seeds, exhaled human breath and *Pseudomonas* bacteria. HCN represents an important indicator of some processes in plants, bacteria or humans. However, it has not been studied very well yet due to its toxicity, high volatility and chemical reactivity. Most of the research carried out on HCN was performed using other than laser-based methods resulting in a poor sensitivity and slow time response. Our experiments showed a detection limit of 0.4 ppbv of HCN at

3287 cm^{-1}. Combined with a long-term continuous operation over a period of several weeks the setup proved itself to be sensitive and robust for a variety of applications.

Although, the laser spectroscopy and trace gas sensing for bio-medical applications are well-known and detailed studied for decades, they are not so often follow the same routes. This thesis provides noteworthy links between physics, biology and medicine. The methods and applications are incorporated with rapid and sensitive detectors, capable of multicomponent gas detection for various applications, including real-time breath analysis. Its potential can be also extended in terms of miniaturization and integration of photonic elements onto a chip. However, the diversity of the employed spectroscopic methods can satisfy the individual requirements for each application in Life Science since OPO based spectroscopy remains powerful and robust technique nowadays.

Samenvatting

Gasfasespectroscopie is een gerenommeerde en alom bekende techniek om gassen te detecteren en onderscheiden. Deze techniek heeft een grote verscheidenheid aan applicaties binnen de fysica, chemie, biologie, milieustudies en geneeskunde. Al tientallen jaren worden spectroscopische gas sensoren intensief gebruikt binnen fundamenteel onderzoek en de industrie. Desalniettemin, is er op dit gebied een continue progressie, elk jaar weer worden er nieuwe artikelen gepubliceerd met betrekking tot verbetering van sensitiviteit, selectiviteit en tijdsresolutie van de methode. Hoewel de term 'spectroscopie van gassen' erg algemeen is en gebaseerd op een combinatie van een diverse spectroscopische methoden en detectie technieken, is laser absorptie spectroscopie in het mid-infrarode golflengtegebied een aantrekkelijke technologie op het gebied van gassporen detectie. Mid-infrarood afzonderlijk-resonante Optische Parametrische Oscillatoren (OPO) worden beschouwd als de meest bruikbare configuraties voor sensitieve gas detectie. OPO hebben een hoog vermogen, grote gebruiksvriendelijkheid, zijn snel afstembaar en hebben bovendien een smalle lijnbreedte. Het eerste hoofdstuk van dit proefschrift geeft de basis principes van OPO en laser absorptie spectroscopie weer.

Biomedische gassporen detectie is een veelbelovend en belangrijk onderzoeksgebied. Vluchtige organische verbindingen, afgegeven door planten en dieren, bevatten informatie welke helpen om de fysiologie en het metabolisme van biologische soorten, alsmede de interactie tussen planten en/of andere levende organismen, beter te begrijpen. In hoofdstuk 2 maakt de lezer kennis met het belang van gassporen detectie binnen de geneeskunde en biologie en de toekomstige mogelijkheden hierbinnen. De beperkingen van OPO met betrekking tot toepasbaarheid in het veld worden beschouwd, maar ook enkele fundamentele experimenten komen aan bod.

Alle experimenten beschreven in dit proefschrift zijn uitgevoerd met de OPO, een coherente stralingsbron in het mid-infrarode golflengtegebied. Hoofdstuk 3 geeft een overzicht van de meeste applicaties van continue golf OPO. Verschillende mogelijke detectie schema's worden beschreven in dit hoofdstuk, elk met voordelen en beperkingen. De keuze voor een geschikte detector verdient zorgvuldige overweging en moet overeenkomen met de eisen van de specifieke applicatie.

Hoofdstuk 4 belicht het gebruik van de OPO in combinatie met Golflengte Modulatie Spectroscopie (WMS) en een 76-m multipass cel. De opstelling werd gebruikt om ethaan (C_2H_6) te detecteren bij een golflengte van ongeveer 2997 cm^{-1} met een detectielimiet van 0.8 ppbv opgenomen in 1.3 s. De detector toonde de mogelijkheid van snelle (tot 100 THz/s) en brede mod-hop-vrije mogelijkheid tot afstemmen (tot 5 cm^{-1}). Bovendien werd een brede, continue afstemming over 35 cm^{-1} aangetoond. Deze resultaten geven de mogelijkheid tot detectie van meercomponenten van meerdere gassen tegelijkertijd weer, wat een sleutelrol is op het gebied van biomedische gassporen detectie. Tevens is ook de vergelijking van resultaten met 1ste, 2de en 4de harmonische signaal afgeleide van de golflengte modulatie beschreven, welke eenzelfde signaal-ruis verhouding weergeeft. Echter, de signalen zijn hoger bij de 1ste harmonic en minder tijdsafhankelijk bij hogere harmonics. Desondanks werd een goede detectielimiet en een korte acquisitietijd voor ethaan gemeten. De sensitiviteit van WMS is gelimiteerd door fringe patronen op het achtergrondsignaal welke geïnduceerd werden door etalon tussen de optische elementen. De sensitiviteit zou verder verbeterd kunnen worden door het gebruik van cavity verbeterende methoden.

Hoofdstuk 5 houdt zich bezig met Integrated Cavity Output Spectroscopy (ICOS) in een off-axis configuratie. Door de extreem lange effectieve padlengte binnenin de optische cavity, gecreëerd met behulp van een paar hoogreflectieve spiegels, werd een detectielimiet van 50 pptv ethaan bereikt bij eenzelfde golflengte van ongeveer 2997 cm^{-1} in een bovendien veel kortere tijd van slechts 0.25 s. Dit resulteerde in een Ruis Equivalente Absorptie Sensitiviteit van 4.8×10^{-11} cm^{-1} $Hz^{-1/2}$. De signaal-ruis verhouding, als afhankelijke van de off-axis richtingsparameter en scansnelheid worden getoond. Daarnaast werd de opstelling ook gebruikt om methaan (CH_4) en water concentraties in humane, uitgeademde lucht, in real-time te samplen. Deze benadering kan makkelijk uitgebreid worden naar meercomponenten gas detectie en is goed toepasbaar binnen de levenswetenschappen.

In hoofdstuk 6 wordt de in hoofdstuk 5 beschreven opstelling intensief gebruikt voor de real-time analyse van humane uitademinglucht. Met behulp van een tijdsresolutie kleiner dan een seconde werd een detectie limiet onder ppbv niveau bereikt met één enkele vrije uitademing. De concentratie dynamiek van ethaan werd gevolgd in de vrije uitademing in meerdere ademsamples van niet-rokers en rokers gedurende tientallen minuten. Snelle en sensitieve detectie gecombineerd met een breed spectraal bereik stond gelijktijdige detectie van ethaan, methaan en water toe. Bovendien was het mogelijk grote moleculen, zoals aceton, te detecteren in de humane uitademinglucht. Deze experimenten tonen een belangrijke stap voorwaarts in real-time, meercomponenten ademanalyse.

Een andere OPO configuratie werd gebouwd om stabiliteit van zowel golflengte als vermogen op de lange termijn te bereiken. Hoofdstuk 7 behandelt de biologische applicatie van Waterstofcyanide (HCN) metingen. Een fotoakoestiek, spectroscopische detec-

tor op OPO gebaseerd werd gebouwd en succesvol getest voor detectie van HCN , geproduceerd door klaverbladeren, appelpitten, humane uitademinglucht en Pseudomonas bacteriën. HCN vertegenwoordigt een belangrijke indicator van enkele processen in planten, bacteriën en de mens. Echter, door zijn toxiciteit, hoge vluchtigheid en chemische reactiviteit is HCN tot op heden niet erg goed bestudeerd. Het meeste onderzoek naar HCN werd uitgevoerd met andere technieken dan op lasergebaseerde methoden, wat vaak resulteerde in een lage sensitiviteit en een trage reactietijd. Onze experimenten lieten een detectielimiet van 0.4 ppbv HCN bij een golflengte van 3287 cm^{-1} zien. Gecombineerd met een lange, continue werking over een periode van enkele weken bewees de opstelling zichzelf in zowel sensitiviteit als wel robuustheid voor een verscheidenheid aan applicaties.

Hoewel laserspectroscopie en gassporen detectie voor biomedische applicaties erg gebruikelijk en al tientallen jaren zeer goed bestudeerd zijn, worden ze niet vaak gecombineerd. Dit proefschrift biedt opmerkelijke koppelingen tussen fysica, biologie en geneeskunde. De methoden en applicaties gaan samen met snelle en sensitieve detectoren, die in staat zijn meercomponenten gas detectie uit te voeren binnen verscheidene toepassingen, waaronder real-time ademanalyse. Het potentieel kan worden uitgebreid in termen van miniaturisatie en integratie van fotonische elementen waardoor plaatsing op een chip mogelijk zal zijn. De diversiteit van de gebruikte, werkzame spectroscopische methoden kan voorzien in de individuele behoeften voor elke applicatie binnen de levenswetenschappen omdat de op OPO gebaseerde spectroscopie krachtig blijft en robuuste techniek vertegenwoordigd.

Curriculum Vitae

Name :
Denis Arslanov
Place of birth :
Nizhnevartovsk, Russia
Date of birth :
29 December 1984

Education :

2008–2012:
PhD student, Molecular and Laser Physics, Institute for Molecules and Materials, Radboud University Nijmegen, Heyendaalseweg 135, 6525AJ Nijmegen, the Netherlands.
Supervisor: Prof. dr. D. H. Parker.
Co-supervisors: Dr. F. J. M. Harren, Dr. S. M. Cristescu.
Subject: "Optical Parametric Oscillator based real-time trace gas analysis for bio-medical applications".

2007-2008:
Guest scientist at Faculty of Physics, Duisburg-Essen University, Lotharstrasse 1, 47048 Duisburg, Germany.
Supervisor: Prof. dr. D. von der Linde.
Co-supervisor: Dr. A. Tarasevitch.
Subject: "High-order harmonic generation from solids".

2001-2007:
Undergraduate student at M.V. Lomonosov Moscow State University, Faculty of Physics, Department of Nonlinear Optics, International Laser Center of M.V. Lomonosov Moscow State University.
Five and a half-year course providing graduation in physics with a specialization of Laser Physics and Nonlinear Optics.

List of Publications

[1] D. D. Arslanov, S. M. Cristescu, and F. J. M. Harren, "Optical parametric oscillator based off-axis integrated cavity output spectroscopy for rapid chemical sensing," Optics Letters **35**, 3300–3302 (2010).

[2] D. D. Arslanov, M. Spunei, A. K. Y. Ngai, S. M. Cristescu, I. D. Lindsay, S. T. Persijn, K. J. Boller, and F. J. M. Harren "Rapid and sensitive trace gas detection with continuous wave Optical Parametric Oscillator-based Wavelength Modulation Spectroscopy," Applied Physics B- Lasers and Optics **103**, 223–228 (2011).

[3] D. D. Arslanov, K. Swinkels, S. M. Cristescu, and F. J. M. Harren "Real-time, subsecond, multicomponent breath analysis by Optical Parametric Oscillator based Off-Axis Integrated Cavity Output Spectroscopy," Optics Express **19**, 124078–124089 (2011).

[4] D. D. Arslanov, M. Spunei, J. Mandon, S. M. Cristescu, S. T. Persijn, and F. J. M. Harren "Continuous-wave optical parametric oscillator based infrared spectroscopy for sensitive molecular gas sensing," Laser and Photonics Reviews, DOI 10.1002/lpor.201100036, (2012).

[5] D. D. Arslanov, M. P. P. Castro, N. A. Creemers, M. Spunei, J. Mandon, S. M. Cristescu, P. Merkus, and F. J. M. Harren, "Optical Parametric Oscillator based photoacoustic detection of Hydrogen Cyanide for bio-medical applications," to be submitted.